Master's Thesis

Hydration and mobility of trehalose in aqueous solution

Louise Revsbech Winther

1st of October 2011

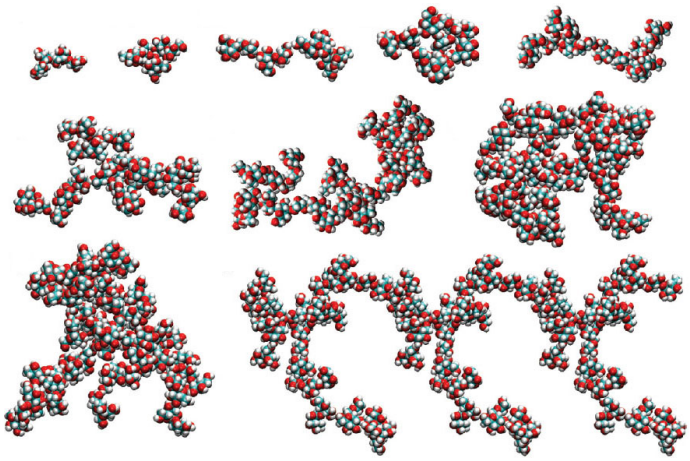

Niels Bohr Institute
Copenhagen University

Preface

The front page picture shows examples of trehalose clusters from the Molecular Dynamics study by Sapir et al. (2011) [77].

Supervisors
Prof. Bertil Halle, Lund University
Ph.D. student Johan Qvist, Lund University
Prof. Thomas Heimburg, Copenhagen University

Acknowledgements

I would first of all like to thank Johan Qvist for his patient and enormous help with all the experiments, which made the work more like a collaboration than anything else. Furthermore I would like to thank Bertil Halle for guiding and advising me through the past year. Finally I thank Peter Immerzeel for conducting the ion chromatography experiment on the deuterated trehalose.

Abstract

Trehalose is a naturally occuring dissaccharide composed of two glucose units. It is capable of stabilizing proteins and membranes during dessication and extreme heat very effectively compared to other sugars, and can act as a cryoprotectant. There are many theories for the reasons behind effects of trehalose, but it is still not well understood why it is such a potent bioprotectant. This study aimed to determine the effect of trehalose on water dynamics, to establish whether the potency of trehalose could be related to extraordinary effects on water dynamics.
The mobility of trehalose and water in trehalose-water solutions, was probed with ^{2}H and ^{17}O relaxation of deuterated trehalose dissolved in ^{17}O enriched water. The resulting concentration dependence of the rotational correlation time of trehalose, gave indications of trehalose self-association at least down to a concentration of 75 mM trehalose. The ^{17}O relaxation data showed that at low concentrations (< 0.25 M) and 20°C, the hydration water of trehalose only rotates 1.65 times slower than bulk water, which means that trehalose does not perturb water dynamics more than many other small molecules, such as small alcohols, peptides or many other sugars. But the hydration water dynamics becomes increasingly perturbed with concentration, in particular above 1 M trehalose a more steep increase is observed in the rotational correlation time of both hydration water and trehalose.

Resume

Trehalose er et naturligt forekommende disakkarid, der består af to glukose enheder. Det er i stand til at stabilisere proteiner og membraner under dehydrering og ekstrem varme, og er samtidig en cryoprotektant. Der er mange teorier for årsagen til virkningerne af trehalose, men der mangler stadig en detaljeret forståelse af hvorfor trehalose er så potent en bioprotektant. Dette studie forsøger at afgøre om de stabiliserende effekter af trehalose er relaterede til en ekstraordinær pertubation af vandmolekylers dynamik.
Mobiliteten af trehalose og vand i vandige trehalose opløsninger, blev bestemt ved hjælp af ^{2}H og ^{17}O relaksation af deutereret trehalose opløst i ^{17}O beriget vand. Dette gav koncentrationsafhængigheden af den rotationelle korrelationstid af trehalose, som viste indikationer af at trehalose aggregerer ved koncentrationer mindst ned til 75 mM. ^{17}O relaksations data viste at ved lave koncentrationer (< 0.25 M) og 20°C, roterer trehaloses hydreringsvand kun 1.65 gange langsommere end rent vand. Dette betyder at trehalose ikke pertuberer vandmolekylers dynamik mere end mange andre små molekyler. Men den rotationelle korrelationstid for hydreringsvandet vokser med trehalose koncentrationen, især omkring 1 M trehalose er der en mere skarp stigning i både den rotationelle korrelationstid af hydreringsvandet og af trehalose.

Contents

Chapter 1

Introduction

Trehalose is a non-reducing disaccharide composed of two glucose units linked together with an α,α-1,1-glycosidic linkage, see figure 1.1. It is present in a large variety of different organisms such as bacteria, fungi, yeast, insects, invertebrates and some plants, but not in mammals. [1],[2].

Until the 70-ties it was believed that the main role of trehalose was to serve as a carbon

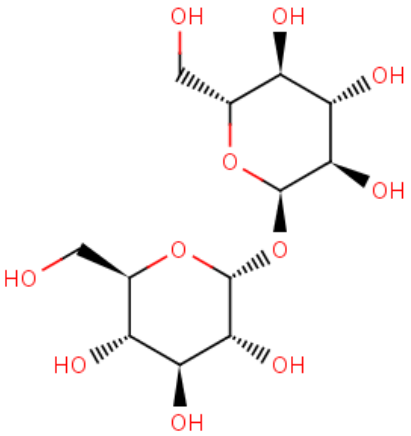

Figure 1.1: *The chemical structure of α,α-trehalose [3].*

source for these organisms [2]. Since then it has been realized that trehalose plays a variety of complex roles in biology (see table 1.1).

When exposed to stress conditions, such as extreme heat, cold, dessiccation (drying) and oxidation, many small organisms are capable of synthesizing small molecules that can counteract the harmful effects of these conditions. These stabilizing molecules can for example be amino acids are their derivatives (fx. TMAO), or different kinds of sugars such as the disaccharide trehalose. Experimental findings have shown that the trehalose level in yeast (*S. cerevisiae*) is correlated to cell survival under dehydration [4]. In *E. coli* trehalose is synthesized in response to high osmolarity[1] [7]. Studies of many other fungi,

[1] concentration of solute particles, fx. salt ions

Table 1.1: *Applications of trehalose in nature [1]*

	Source
Carbon/energy source	[1]
Osmoregulation	[7]
Dessication protection	[15]
Cryoprotection	[9]
Protection against heat	[16]
Structural component of cell wall	[8],[10]
Immunogenicity (in mycobacteria)	[11]
Growth regulator in plants	[12],[13]

prokaryotes and nematodes[2] show the same correlation between high levels of trehalose and increased stress tolerance [5].

In particular, organisms capable of surviving dehydration, also called anhydrobiotic organisms, generally contain high concentrations of trehalose (and sometimes also other sugars) - even up to 20% of the dry weight [2]. These include plants, yeast cells, some microscopic animals (fx. nematodes), and fungal spores [6], some of which may survive without water for up to centuries. This dehydration tolerance has been explained by the discovery that trehalose protects and stabilizes dry lipid membranes and protects protein structure during dehydration [14],[15].
Some anhydrobiotic organisms also produce trehalose during heat shock and the trehalose level has been correlated with thermotolerance. Trehalose has been shown to protect enzyme activity, reduce protein aggregation during heat shock [16], and increase the thermal stability of proteins [18]. It increases the stability of proteins by raising the temperature at which they unfold - also called the transition temperature T_m, by as much as 18°C for RNase A in 2M trehalose [18], thus making them less prone to unfolding by heat, and helping them retain their structure and function.
Trehalose not only protects against heat, but also against freezing, which means that it belongs to the group of molecules called cryoprotectants. If cells are frozen down without cryo-preservation, ice crystals will grow inside or outside the cells, and since this causes an expansion, this will cause the cell to break. Trehalose supresses ice crystal growth [64] and thereby enables cells to be frozen down.

Table 1.2: *Reported effects of trehalose* in vitro

	Source
Stabilization of dry membranes and proteins	[14],[15]
Prevention of ice crystal growth	[64]
Protein Stabilization	[18]

The large stabilizing effects of trehalose has made it very useful in both the food industry, pharmaceutics and cryopreservation of living tissue [1]. Because of the stabilizing effects on proteins, there is also ongoing research attempting to prevent disease related protein aggregation with trehalose. One example is the study by Tanaka et al., who found that trehalose alleviates the symptoms of Huntington's disease in mice [17].

Many other sugars such as fx. sucrose, maltose and glucose are also capable of stabilizing

[2] roundworms

membranes and proteins during dehydration and heat shock and act as a cryoprotectant, but they are less effective than trehalose [15], [24]. At the same time trehalose is non-reducing and hence does not interfere with any of the cellular chemical reactions. Thus it is not surprising that Mother Nature has chosen trehalose to be one of its primary bio-protectants. But why trehalose is so effective is still not fully understood at the molecular level. The exact mechanism behind the many amazing effects of trehalose mentioned above, has still to be discovered.
Many attempts have been made to explain the properties of trehalose, the most widely accepted are explained below.
The vitrification theory The ability of trehalose to form a glassy state is considered one of the most important properties of trehalose. Glasses are amorphous solids, so solids without a repetitive crystal pattern. They can be described as a liquid that has lost its ability to flow. The glass transition (the transition from liquid to glass) is a kinetic transition, where the translational mobility of the particles undergoes a dramatic slow down. There are many ways to obtain the glassy state: Fx. rapid cool down of a liquid melt, or solvent evaporation. Some substances would in this case form crystals, but good glass formers have a very low probability of germinating a crystal. So the substance chooses a low energy non-crystalline packing mode, even though it may not be as low energy as the crystalline packing mode [19]. Now the translational mobility is so slow, that it will take an extremely long time for the substance to relax to the lower energy crystal form, even though the latter is the equilibrium state.
Green and Angell (1989) [20] found that trehalose has a high glass transition temperature compared to other mono- and disaccharides, and thus proposed that this is the reason for its protective effects, also they showed that there is a correlation between the glass transition temperature and the efficiency of membrane preservation upon dehydration.
The glassy state has a very high viscosity, so it is envisioned that trehalose immobilizes macromolecules in a glassy matrix during dehydration thereby making them more stable when exposed to stress (the vitrification theory) [1]. Since trehalose has a higher glass transition temperature than the other small saccharides, the glass transition occurs at higher temperature and/or lower sugar concentration, see the phase diagram in figure 1.2, and trehalose would then be more effective. But the problem with the vitrification theory is that it does not explain why dextran, another carbohydrate has a much higher glass transition temperature than trehalose, but is less effective as a cryoprotectant [66]. Also Crowe et al. (1998) later found that even though glass formation is required for stabilization of dry biomaterials, it is in itself not sufficient. Both interaction and vitrification is required. [21].

Water replacement theory During dehydration the water-macromolecule hydrogen bonds are proposed to get replaced by sugar-macromolecule hydrogen bonds [14].

Preferential exclusion theory The most widely accepted explanation for the stabilizing effect of trehalose and other osmolytes on proteins, is that they are preferentially excluded from the surface of proteins. This heterogenous distribution of the cosolute is entropically unfavourable, and because the unfolded state has a larger surface accessible than the folded state, the folded state is less entropically unfavourable / more entropically favourable and the folded state is thus stabilized [22]. But it is not fully understood why trehalose and other stabilizing osmolytes are excluded from the surface of proteins, and there is no explanation for why trehalose is among some of the most potent stabilizers.

Water entrapment theory Belton et al. (1994) [23] found that trehalose in accordance with preferential exclusion does not interact directly with the protein surface and suggests

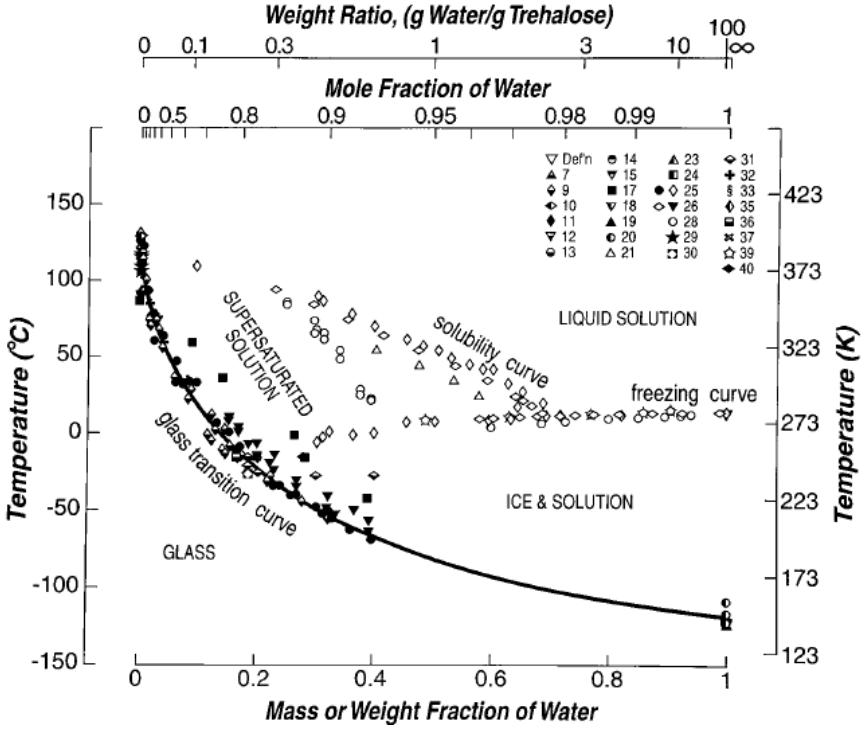

Figure 1.2: *The phase diagram of trehalose. Data from different sources collected by Chen et al. (2000) [63].*

that the first hydration shell of the protein is preserved at low water contents, and this entrapment would slow the protein dynamics.
According to Sola-Penna et al. (1998) [24] the exclusion of cosolvent from the protein hydration layer gives a competition between the cosolvent and the protein for water, thus decreasing the size of the protein solvation layer, which restricts its mobility and stabilizes it. Sola-Penna et al. claim that trehalose has a significantly larger hydrated volume (about 2.5 times) compared to other disaccharides, because less water must be added in the case of trehalose to get the same molar concentration. Because of the bigger size they believe that trehalose is more excluded from the solvation layer of the protein, thus preferential hydration will be attained at a lower concentration and result in a stronger stabilization.

Destructuring effect According to Branca et al. (1999) [73] trehalose destructures the tetrahedral hydrogen bond network of water and thereby inhibits ice crystal formation.

The experimental evidence for the hypotheses above is not completely consistent, some studies question their basis. None of the hypotheses above serve a complete description of the biopreservative mechanism of trehalose, because they only cover narrow temperature and hydration ranges.
But the fact that trehalose has been reported to stabilize a large variety of proteins and lipids and also affects pure water-sugar solutions by inhibiting ice crystal growth and changing the glass transition temperature of the solution, indicates that the effect of trehalose on macromolecules is non-specific.
Thus the best starting point to improve the understanding of the effects of trehalose would be to investigate its effect on water.
Several studies have been done on the hydration of sugars, and many of these found that

sugars strongly slow down the dynamics of the water molecules in their vicinity. Heyden et al. (2008) [49] used Terahertz spectroscopy to show that disaccarides slow down the water dynamics at distances up to 6.5 Å (trehalose), so significantly further than the first hydration shell (about 2.8 Å), a result I will return to at the end of this study. Magazu et al. (eg. in 2001, [94]) found that trehalose induces a stronger retardation of the dynamics of water in its vicinity compared to other disaccharides, with Quasi Elastic Neutron Scattering. Paolantoni et al. (2009) [25] found using Depolarized Light Scattering that the rearrangement dynamics of hydration water (in the first solvation shell) of trehalose was 5-6 times slower than in bulk water.
The slowing down of water by sugars has been claimed to be able to partly explain the stabilizing effect of trehalose in combination with preferential exclusion: If the sugars are excluded from the surface of proteins in aqueous solution, the stronger the sugars slow down their vicinal water layers, the more the hydration water belonging to the protein will be perturbed, if the concentration of sugar is large enough that the hydration shell of protein and sugar overlap. Thus the hydration water of the protein will be further slowed down and the protein stabilized [95] (water entrapment).

To determine if trehalose really has an extraordinary effect on the dynamics of water compared to other small molecules, this study measured the rotational correlation time of water molecules in trehalose-water solutions with different concentrations and at different temperatures by NMR relaxation of ^{17}O enriched water. The rotational correlation time gives the rotational mobility of the water molecules, and is strongly affected by perturbations of the local hydrogen-bond configuration. The mobility of trehalose molecules was followed simultaneously through the rotational correlation time measured on ^{2}H from ^{2}H-labelled trehalose, to fully understand the dynamics of the trehalose-water system.

Chapter 2

Theory

2.1 Molecular Diffusion

Molecular diffusion is the movement of particles due to their thermal energy. Unlike the more macroscopic concept of diffusion where the diffusion coefficient is defined as the proportionality constant of molar flux (due to diffusion) as a function of the concentration gradient: $J = D\nabla\phi$ (Fick's law), molecular diffusion does not require a concentration gradient, but is merely a consequence of thermal collisions.
The first big step towards understanding the movement of particles suspended in a liquid was made by the Scottish botanist Robert Brown in 1827 [26]. Brown saw pollen particles suspended in water moving around in zigzag paths under his microscope. This phenomena came to be known as Brownian motion. In 1905 Albert Einstein published the theoretical explanation of Brownian motion [27]. Einstein assumed random collisions with solvent molecules, and no collisions with other solute molecules, which means that the solutes perform what is called a random walk - each particle/solute molecule has a random path independent of the other particles/solute molecules. From these assumptions he derived a linear equation for the mean square displacement of a Brownian particle:

$$\langle|\vec{r}(t) - \vec{r}(0)|^2\rangle = 6D_t t \tag{2.1}$$

Where t is time and D_t is the translational diffusion coefficient.
The assumption that the solute molecule only experiences collisions with solvent molecules means that the relation is only true for solutions that are sufficiently dilute to make this reasonable.
The equation for the translational diffusion coefficient was derived from the drag force on a sphere moving through a liquid calculated by Stokes [28] and the force of diffusion from osmotic pressure.

$$D_t = \frac{RT}{N_A}\frac{1}{6\pi\eta R} = \frac{k_B T}{6\pi\eta R} \tag{2.2}$$

Where R is the radius of the spherical particle and η is the solvent viscosity. - This is equation is therefore called the Stokes-Einstein equation.
There is a more general form of Stokes-Einstein which can also be used for non-spherical particles:

$$D_t = \frac{k_B T}{f} \tag{2.3}$$

Where f is the frictional drag coefficient. In case of a sphere $f = 6\pi\eta R$, for non-spherical shapes such as cylinders and ellipsoids, f is more complex but still easy to calculate. In case of more complex shapes that can not be approximated with simple geometry it becomes extremely complicated to calculate f.

In 1906 Einstein also derived the equation for the rotational diffusion coefficient. Whereas translational diffusion controls the position of the particles in space, rotational diffusion controls the statistical distribution of particle orientations. Imagine a particle colliding with a solvent particle due to thermal motions. If the particles do not hit exactly each others center-of-mass (very unlikely that they do), the collision will not only make the two particle change their path and velocity (translational diffusion), but it will also make them rotate differently. For molecules diffusing in a liquid, the viscous drag is so high that each collision can only change the orientation of the molecule by a small amount [65]. Each collision will change the molecular orientation in a random direction, this motion is called rotational diffusion.

Analogously to translational diffusion, the mean square angular deviation at time t due to rotational diffusion about one axis can be calculated as (if the change in orientation is small) [30]:

$$\langle |\theta(t) - \theta(0)|^2 \rangle = 6D_r t \tag{2.4}$$

Where D_r is the rotational diffusion coefficient. Einstein derived an equation for the rotational diffusion coefficient by using the Stokes equation for viscous drag on a sphere subjected to a torque [29]:

$$D_r = \frac{RT}{N_A} \frac{1}{8\pi\eta R^3} = \frac{k_B T}{8\pi\eta R^3} = \frac{k_B T}{8\pi\eta R^3} \tag{2.5}$$

This equation is sometimes called the Stokes-Einstein-Debye equation since Debye derived a similar equation for rotational diffusion of polar molecules [31].
Parallel to translational diffusion, the general form of the Stokes-Einstein-Debye equation is:

$$D_r = \frac{k_B T}{f_r} \tag{2.6}$$

Where f_r is the frictional drag coefficient for rotational diffusion, in case of spheres $f_r = 8\pi\eta R^3$.
Comparison of the equations for rotational and translational diffusion shows that rotational diffusion is more sensitive to the particle radius R, and will therefore also be more sensitive to changes in the particle dimensions fx. due to aggregation.

Rotational diffusion can be measured by perturbing a quantity that is a function of molecular orientation and then measuring its relaxation back to equilibrium. In this study the quantity measured is the magnetization of either ^{2}H or ^{17}O. For the simple Brownian diffusion described above, the correlation function of the relaxing quantity will be given by a linear exponential function [31] [32] with a characteristic time constant τ_r called the rotational correlation time:

$$f(\hat{u}, t) = f(\hat{u}, 0) \exp(-t/\tau_r) \tag{2.7}$$

Where $\hat{u}$ is the molecular orientation. The rotational correlation time τ_c is also defined as [31]:

$$D_r \equiv \frac{1}{6\tau_c} \tag{2.8}$$

Thus :

$$\tau_c = \frac{1}{6D_r} = \frac{8\pi\eta R^3}{6k_B T} = \frac{V_h \eta}{k_B T} \tag{2.9}$$

The rotational correlation time is also the average time it takes a particle to change its orientation by 1 radian [65]

2.1.1 Diffusion in complex systems

The theoretical solutions of Brownian motion made by Einstein in the early 1900's were based on the assumption that the diffusing molecules do not interact with each other, only with the solvent molecules. This means that their motions are independent of each other, which greatly simplifies the model. This assumption can only hold for very dilute solutions. When the solutes begin to interact, the Stokes-Einstein and Stokes-Einstein-Debye relations break down. Diffusion and relaxation of many-body interacting systems is still an unresolved problem in condensed matter physics and statistical physics [31]. Glass-forming systems are an important class of many-body interacting systems, to which sugars belong (at the right concentrations and temperatures).
One of the characteristics of many-body interacting systems is that relaxation cannot be well described by a linear exponential function, but instead follows the Kohlrausch exponential function / a stretched exponential function [31]:

$$M(t) \propto \exp(-(t/\tau_c)^{1-n}) \tag{2.10}$$

Where $0 < (1-n) \leq 1$.

2.2 A short introduction to Nuclear Magnetic Resonance

2.2.1 The main idea

When nuclei are in put in an environment with a significant magnetic field, they acquire a set of possible energy states that depend on the nature of the nucleus and its chemical environment. The chemical nature of the sample can thus be determined by measuring the (separation of) these energy levels. This is basically what is done in an NMR experiment.

2.2.2 Spin theory

In order to understand the theory behind the NMR technique, we must start at something called angular momentum. In classical mechanics, angular momentum ($\vec{L}$) of a particle

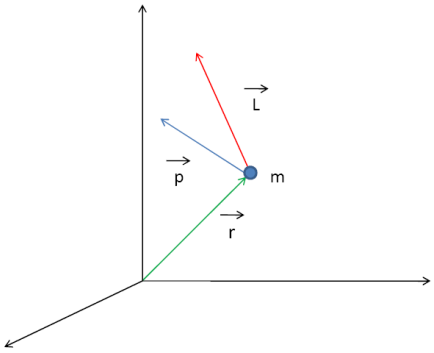

Figure 2.1: *Classical angular momentum.*

with mass m is defined as the cross product of the position vector ($\vec{r}$) and the momentum ($\vec{p}$) of the particle:

$$\vec{L} \equiv \vec{r} \times \vec{p} = \vec{r} \times m\vec{v} \tag{2.11}$$

Some nuclei have an intrinsic angular momentum, also called spin. Such nuclei are called magnetic. Whether a nucleus has a spin, is determined by the number of neutrons and protons and how their spins pair up. If the number of neutrons and protons are both equal, all spins pair up (in the up/down states) to give a total spin of zero.
To calculate the angular momentum of a nucleus, we have to employ quantum mechanics and it therefore becomes a bit more complicated. In quantum mechanics, angular momentum is quantized, both in size and direction.

The size can be written as:

$$|\vec{I}| = \hbar\sqrt{I(I+1)} \tag{2.12}$$

Where I is the spin quantum number which is nucleus specific and can take on the values:

$$I = 0, \frac{1}{2}, 1, \frac{3}{2}, 2, ... \tag{2.13}$$

Because also the direction is quantized, the z-component becomes quantized, and can be calculated as:

$$I_z = m\hbar \tag{2.14}$$

Where m is the magnetic quantum number and can take on integer values between +I and -I:

$$m = I, I-1, I-2, ..., -I \tag{2.15}$$

There are 2I+1 possible orientations of the spin, and therefore the same number of values of m.

The spin quantum number of the proton is I=1/2, thus the proton spin has 2 possible orientations as seen in figure 2.2, with $I_z = \pm\hbar/2$.

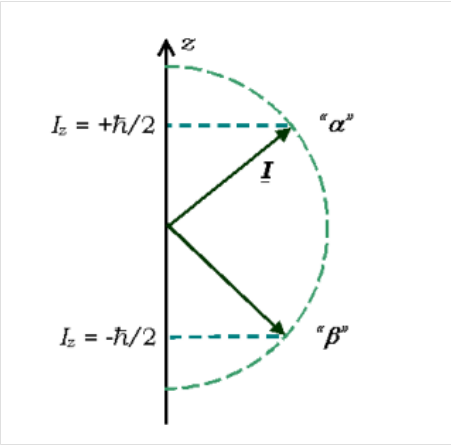

Figure 2.2: *Angular momentum of the proton [33].*

2.2.3 Magnetic moment

The nuclear angular momentum gives rise to a magnetic moment μ:

$$\vec{\mu} = \gamma \vec{I} \tag{2.16}$$

Where γ is a proportionality constant called the gyromagnetic ratio, and depends on the nucleus type.

To get a more intuitive picture of the reason for this link between angular momentum and magnetic moment, it can be helpful to think about the classical analogy: A small current loop, see figure 2.3.

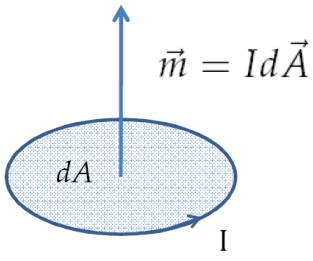

Figure 2.3: *Magnetic moment of a small current loop.*

Charges are moving around in the the wire, and therefore have angular momentum, but their movement also produces a magnetic field located in the direction of the large arrow in fig. 2.3, since generally moving charges/changing electrical fields produce magnetic fields. This small local magnetic field is described as a magnetic dipole moment.

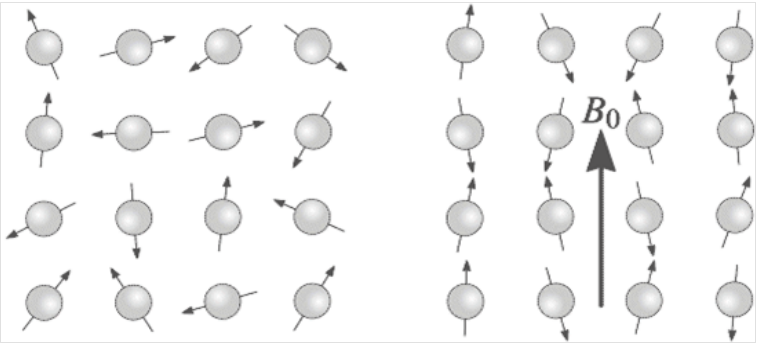

Figure 2.4: *Left: No external B field, all magnetic moments are randomly oriented, so the bulk magnetization sums up to 0. Right: External B field present: The magnetic moments tend to align with the B field. [35]*

2.2.4 Effect of external B-field

Magnetic fields also called B-fields can be described with vectors (or field lines) as not only their strength but also their direction is important to their effect.

If the sample is placed in an environment with no magnetic field, the magnetic moments in the sample will be oriented randomly. If instead an external magnetic field is created, the magnetic moments will tend to align with the B field. See figure 2.4.

The spinning nuclei will precess around the B field vector if they are not perfectly aligned. This is due to the fact that magnetic fields exert a torque on magnetic moments given by the cross product:

$$\vec{N} = \vec{\mu} \times \vec{B} \tag{2.17}$$

At the same time we have that the magnetic moment is proportional to the angular momentum, therefore we get that:

$$\vec{\mu} = \gamma \vec{L} \Rightarrow \vec{N} = \gamma \vec{L} \times \vec{B} \tag{2.18}$$

Thus $\vec{N} \perp \vec{L}$.

Classical mechanics gives the following relation:

$$\vec{N} = \frac{d\vec{L}}{dt} \tag{2.19}$$

Therefore we get that the new increment of angular momentum after time dt is perpendicular to the angular momentum at t=0:

$$\Delta\vec{L} \perp \vec{L} \tag{2.20}$$

Thus the angular momentum vector will not change length, but orientation, in such a manner that it will circle around the B-vector.

The energy of magnetic moments in a B-field

Magnetic moments become potential energy when they experience an external magnetic field. In general, electrodynamics states that the energy of a magnetic moment in a B field is given by the dot product:

$$E = -\vec{\mu} \bullet \vec{B} = -|\vec{\mu}||\vec{B}| \cos\theta \tag{2.21}$$

- the energy thus depends on the angle between the two vectors. The smaller the angle, the smaller the energy, therefore the magnetic moments tend to align with B.

If we define the z-axis so it is parallel to the B-field vector, the energy can be rewritten into the form:

$$E = \mu_z B \tag{2.22}$$

Since the magnetic moment is proportional to the angular momentum, we also know that:

$$\mu_z = \gamma I_z \tag{2.23}$$

And as explained previously:

$$I_z = m\hbar \tag{2.24}$$

Combining the three previous equations gives:

$$E_m = \gamma m \hbar B \tag{2.25}$$

Since m (the magnetic quantum number) is quantized, it is clear that the energy also becomes quantized. So there are only 2I+1 allowed energy levels. According to quantum mechanics, the allowed energy level transitions have to obey the following selection rule:

$$\Delta m = \pm 1 \tag{2.26}$$

Thus the energy of an allowed energy level transition becomes (see fig. 2.5):

$$\Delta E = \gamma \hbar B \tag{2.27}$$

The frequency of an electromagnetic wave with the right energy to give a transition is then:

$$\Delta E = \gamma \hbar B = h\nu \Leftrightarrow \tag{2.28}$$

$$\nu = \frac{\gamma B}{2\pi} \tag{2.29}$$

This is called the Larmor frequency, and is also the same as the precession frequency.

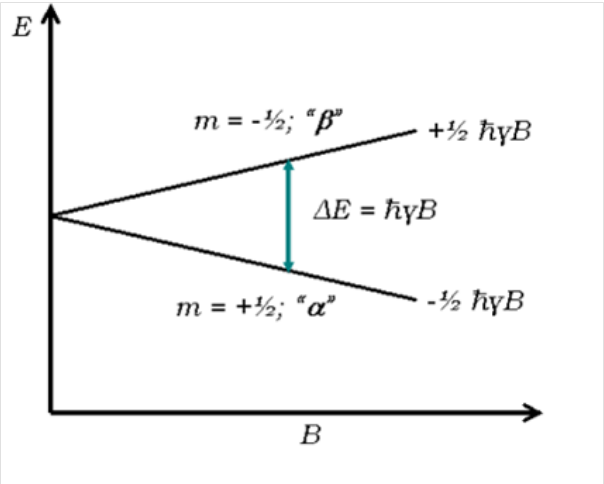

Figure 2.5: *The energy levels of a proton in a magnetic field and their dependence on magnetic field strength B [33].*

Populations

Magnetic nuclei are distributed among the 2I+1 available energy states as a Boltzmann distribution. Protons have only two available states, therefore the distribution can be described as:

$$\frac{n_{upper}}{n_{lower}} = exp\left(\frac{-\Delta E}{kT}\right) \tag{2.30}$$

Where n_{upper} and n_{lower} are the populations in the upper and lower energy state. But alignment of the magnetic moments is disrupted by thermal motion, because the energy of the thermal motion is larger than the energy difference between the energy levels of the nuclear magnetic moments: $\Delta E < kT$. So the difference between the populations in the two energy states becomes very small. This gives a very small total (bulk) magnetization of the sample, which makes the NMR signal hard to detect. But as shown in equation 2.27 and figure 2.5, ΔE and therefore also the difference in populations can be increased by increasing B. This is exactly the reason why extremely strong magnets are needed in NMR.

2.2.5 Nuclear shielding

The external magnetic field induces a "current" in the electron orbitals, which in turn produces a small magnetic field opposing the external magnetic field now called B_0, see figure 2.6.

Now the new total B field can be written as:

$$B = B_0 - B_{induced} \equiv B_0(1-\sigma) \tag{2.31}$$

Where σ is defined as the shielding constant.

The new Larmor frequency becomes:

$$\nu = \frac{\gamma B_0(1-\sigma)}{2\pi} \tag{2.32}$$

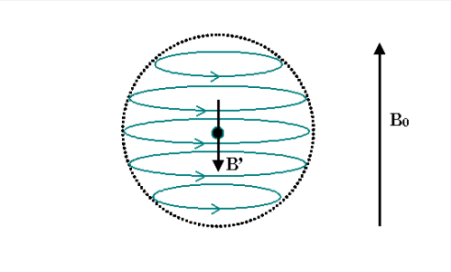

Figure 2.6: *Induced current in the electron orbitals weakens the local B field = shields the nucleus from the external B field [33].*

The larger the electron density, the larger induced current, the stronger shielding/larger shielding constant and the smaller Larmor frequency. The Larmor frequency thus gives a clue about the chemistry of the sample, since the electron density is determined by the atom type and its chemical environment. But there is a problem with the Larmor frequency: It depends on the size of the external B field (B_0), and therefore also the magnet used in the specific experiment, which makes it hard to compare results from different labs. In order to circumvent this problem, another variable called the chemical shift, is introduced.
Chemical shift is defined as:

$$\delta = 10^6 \frac{\nu - \nu_{ref}}{\nu_{ref}} \tag{2.33}$$

Here the dependence on B is divided out as the sample Larmor frequency is compared to the Larmor frequency of a known reference molecule ν_{ref}. A typical used reference compound in proton NMR is TMS (tetramethyl-silane), because it has a very low Larmor frequency, so the chemical shift of most other compounds becomes positive. The electron density around each nucleus in a molecule and thus also the chemical shift depends on (among others)
- the type of nucleus
- different types of bonds to other atoms (covalent bonds, H-bonds, etc.)
- ring currents (from aromatic rings)
Thus we can determine not only the type of nucleus, but also molecular structures (with more advanced analysis), with help from chemical shifts.

Examples of chemical shifts of protons in different chemical environments are seen in figure 2.7. The chemical shifts of H depends a lot on what atoms it is bound to.

2.2.6 Spin-spin coupling

The nuclear spin of a specific nucleus (A) can interact with the spin of other nuclei up to 3 chemical bonds away. The interaction depends on the orientation of the neighbouring spins and can either increase or decrease the Larmor frequency of nucleus A. Since the orientation of the neighbour spins follow some distribution, the interaction leads to a splitting of the NMR signal of nucleus A into multiple peaks, this phenomena is called coupling. It can be avoided with a technique called decoupling, that randomizes the orientation of the spins responsible for the coupling.

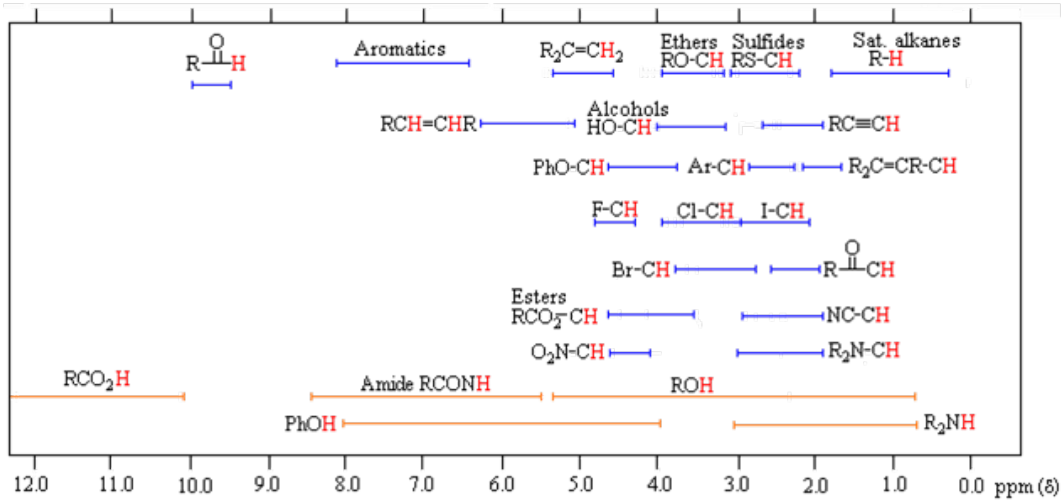

Figure 2.7: *Proton chemical shifts. For samples in $CDCl_3$ solution. The δ scale is relative to TMS at $\delta = 0$. [34]*

2.2.7 Detection

A while after the external B field is applied to a sample, the magnetic moments reach an equilibrium, where the sum of the magnetization vectors show a small net alignment with the external B-field, this is called the bulk magnetization and is represented as M in figure 2.8.

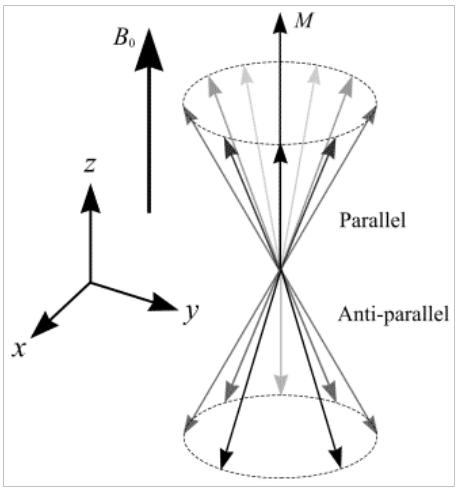

Figure 2.8: *Bulk magnetization in equilibrium. M is the total (bulk) magnetization. [35]*

In order to detect this small net alignment, the bulk magnetization vector must be flipped away from the z-axis, to get a detectable xy-component. The z-component cannot be detected, because it is overshadowed by the magnetic field from the orbiting electrons, which is parallel to the z-axis. The magnetization vector can be flipped by irradiating the sample with electromagnetic pulses of the right energy (radiofrequency) to cause the magnetic moments to experience energy level transitions, so with a frequency equal to the

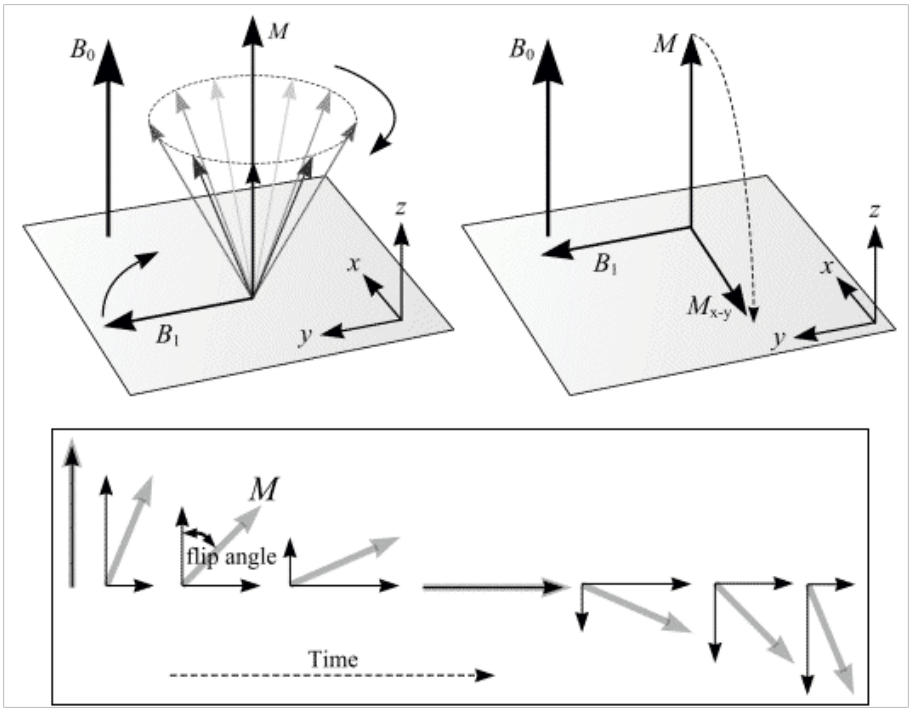

Figure 2.9: *The effect of a Radiofrequency pulse. [35]*

Larmor frequency. This is the same as changing their orientations. The longer the pulse, the more energy is transferred to the magnetic moments for transitions, the more will be flipped, and the further the bulk magnetization vector M will be flipped away from the z-axis.

The flip angle is proportional to the pulse length and the strength of the B field produced by the electromagnetic pulse B_1:

$$\beta = \gamma B_1 t_p \tag{2.34}$$

A pulse that is long enough to flip M into the xy-plane, is called a 90 degrees pulse and gives the strongest signal, for reasons that will soon become clear. What happens after a 90 degrees pulse can be seen in figure 2.10. The bulk magnetization vector still precesses

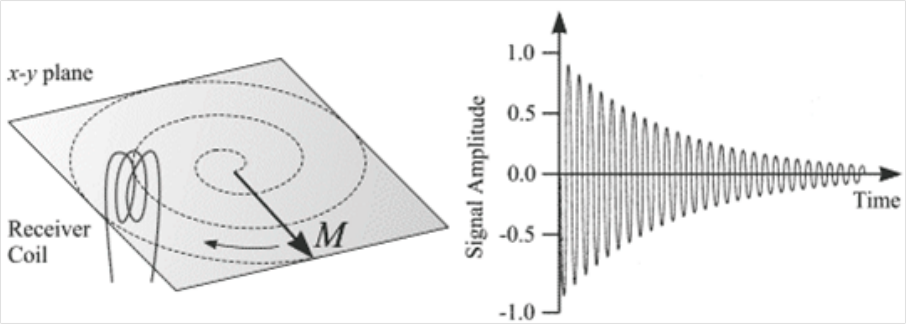

Figure 2.10: *Signal detection in an NMR experiment. Left: The magnetization vector after a 90 degrees pulse, slowly relaxing back to its equilibrium position. Right: The signal measured in the receiver coil.[35]*

about the z axis, it slowly precesses back towards the z-axis and thus the xy-component decreases. During the relaxation back to equilibrium, the xy-component of the magnetization vector is detected by a receiver coil placed in the xy-plane. The both oscillating and decaying magnetization induces an oscillating and decaying current in the receiver coil, this signal is called the Free Induction Decay (FID).

The basic pulse sequence

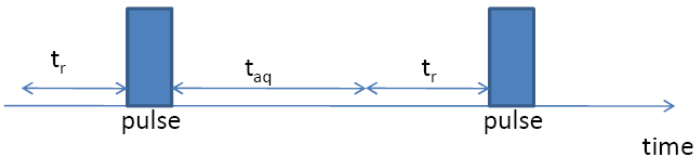

Figure 2.11: *The basic pulse sequence for an NMR experiment.*

The basic pulse sequence of an NMR experiment can be seen in figure 2.11 and is made of
- a relaxation delay to let the magnetization relax completely back to equilibrium
- short RF pulse ($< 20\ \mu s$)
- aqcuisition time: recording the FID

Many consecutive pulse sequences are made and the FIDs added together to improve the signal-noise ratio.

Data analysis

The measured signal (FID) is a function of time, but we want it as a function of frequency so we can separate the contributions to the signal from different Larmor frequencies (= different atoms). This is done by Fourier transforming the FID:

$$f(\omega) = \int_{-\infty}^{\infty} f(t) \cdot exp(-i\omega t)dt = \int_{-\infty}^{\infty} f(t) \cdot [cos(\omega t) - i \cdot sin(\omega t)]dt \tag{2.35}$$

Result: Defined peaks at the Larmor frequencies of the nuclei present in sample, so we can determine the composition of the sample.

2.2.8 NMR Relaxation

The relaxation of the z-component of the magnetization vector back to equilibrium with its surroundings, is called longitudinal relaxation or spin-lattice relaxation. In the relaxation process energy is transferred to the surroundings. For spin 1/2 nuclei such as H, the relaxation is driven by interaction between the magnetic dipole moment of the nuclei and the local (fluctuating) magnetic field. But for nuclei with spin quantum numbers larger than 1/2, this is no longer the major relaxation mechanism. Nuclei with I>1/2 cannot only be described by a magnetic dipole moment, their charge distribution must be described by

an electric quadrupole. For these nuclei the interaction between the electric quadrupole moment and the electric field gradient is much stronger than the interaction between the magnetic moment and the local B field. Thus it is predominantly the interaction between the electric quadrupoles and the electric field gradient that drives the relaxation [36]. More precisely, it is the fluctuation of the electric field gradient due to molecular motions that causes relaxation.
For reasons that will soon become clear, this study was on the longitudinal relaxation of ^{2}H and ^{17}O, which have spins of 1 and 5/2 respectively. Thus they both relax through quadrupolar relaxation.

Generally the relaxation of the magnetization vector follows the exponential decay:

$$M(t) = B(1 - A\exp(-t/T_1)) = B(1 - A\exp(-R_1 t)) \tag{2.36}$$

Where the decay constant T_1 is called the longitudinal relaxation time. The longitudinal relaxation rate is defined as:

$$R_1 = \frac{1}{T_1} \tag{2.37}$$

^{2}H relaxation

Spin 1 nuclei like ^{2}H always relax exponentially (if the solution is isotropic)[36]. Spin relaxation rates can mostly be expressed as a linear combination of spectral densities. For quadrupolar relaxation in inversion recovery experiments, the longitudinal relaxation rate is given by [55]:

$$R_1 = \omega_Q^2(0.2j(\omega_0) + 0.8j(2\omega_0)) \tag{2.38}$$

ω_0 is the Larmor frequency. The quadrupole frequency ω_Q is here defined as [36]:

$$\omega_Q^2 = C_Q\chi^2(1 + \eta^2/3) \tag{2.39}$$

χ is the quadrupole coupling constant and η the asymmetry parameter of the electric field gradient tensor. When I = 1, $C_Q = 3\pi^2/2$ [36].

$j(\omega)$ is the reduced spectral density function and is defined as the Fourier transform of the reduced time correlation function of the fluctuating quadrupole coupling, $g(t)$.

$$g(t) \overset{FT}{\rightarrow} j(\omega) \tag{2.40}$$

So $g(t)$ describes the fluctuation of the quadrupole coupling with time, whereas its fourier transform $j(\omega)$ describes the frequency of the fluctuations. If the fluctuations have a frequency equal to the Larmor frequency of the nucleus in question, they will cause the nucleus to relax. This is the reason why $j(\omega)$ is evaluated at the Larmor frequency ω_0 in the equation for R_1 / describing how fast relaxation occurs.

The spectral density is here defined as the fourier transformation of the correlation function including a prefactor of $1/2$.

$$j(\omega) = \frac{1}{2}\int_{-\infty}^{\infty} dt\exp(-i\omega t)g(t) = \frac{1}{2}\int_{-\infty}^{\infty} dt\,(\cos(\omega t) - i\sin(\omega t))\,g(t) \tag{2.41}$$

The correlation function is even in t while the sine function is odd in t so their product is odd in t. Thus the last term in the integral integrates to zero and:

$$j(\omega) = \frac{1}{2}\int_{-\infty}^{\infty} dt \cos(\omega) g(t) \tag{2.42}$$

Now the convenience of including the prefactor becomes clear, since the spectral density can now be reduced to:

$$j(\omega) = \int_{0}^{\infty} dt \cos(\omega t) g(t) \tag{2.43}$$

This integration gives [55]:

$$j(\omega_0) = \frac{\tau_c}{1+\omega_0^2\tau_c^2} \tag{2.44}$$

Recall the expression for the longitudinal relaxation rate in eq. 2.38:

$$R_1 = \omega_Q^2(0.2j(\omega_0) + 0.8j(2\omega_0)) \tag{2.45}$$

Inserting the expression for $j(\omega_0)$ into this equation for R_1 gives:

$$R_1 = \omega_Q^2\left(\frac{0.2\tau_c}{1+\omega_0^2\tau_c^2} + \frac{0.8\tau_c}{1+4\omega_0^2\tau_c^2}\right) \tag{2.46}$$

- the equation must be multiplied by an order parameter S^2 because the trehalose molecule is not perfectly rigid, so the end result becomes:

$$R_1 = S^2\omega_Q^2\left(\frac{0.2\tau_c}{1+\omega_0^2\tau_c^2} + \frac{0.8\tau_c}{1+4\omega_0^2\tau_c^2}\right) \tag{2.47}$$

The relaxation rate as a function of correlation time is plotted in figure 2.12.

The rotational correlation time decreases with increasing temperature, because the rotation is caused by thermal movement. As figure 2.12 shows, at long correlation times ($\omega_0\tau_c > 1$) or low temperatures the relaxation rate decreases with increasing τ_c and decreasing temperature. But at high temperatures or $\omega_0\tau_c < 1$ the magnetization starts to relax slower with decreasing τ_c and increasing temperature, which is a bit counter-intuitive.

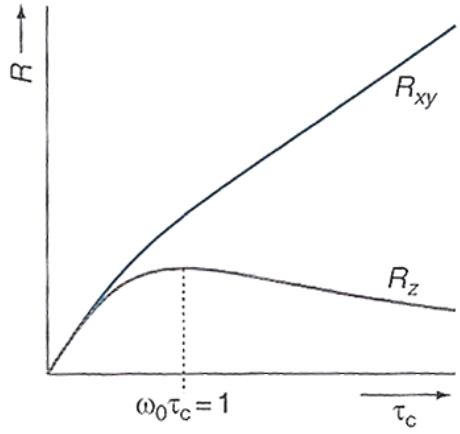

Figure 2.12: *The longitudinal relaxation rate $R_1 = R_z$ as a function of rotational correlation time τ_c [65].*

^{17}O relaxation

For molecules small enough that τ_c is so small/the molecule rotates so fast that $\omega_0\tau_c \ll 1$ - also defined as extreme narrowing, the relaxation rate in eq. 2.46 reduces to:

$$R_1 = \omega_Q^2 \tau_c \tag{2.48}$$

This is the case for ^{17}O in water [55].
The nuclear quadrupole frequency for ^{17}O in water is set to [47]:

$$\omega_Q^2 = \frac{12}{125}\pi^2\chi_o^2\left(1 + \frac{\eta_o^2}{3}\right) \tag{2.49}$$

In extreme narrowing ^{17}O will also relax exponentially [36].

As we shall see later, trehalose does not rotate fast enough to fulfill this for ^{2}H relaxation, and the rotational correlation time for ^{2}H has to be calculated from eq. 2.46.

Chapter 3

Methods

In order to measure the mobility of water and trehalose molecules in trehalose-water mixtures and how they affect each other, inversion recovery experiments were done on deuterated trehalose dissolved in ^{17}O enriched water, to selectively determine the mobilities of the two species in the same sample. ^{2}H relaxation experiments gives the mobility of trehalose, since most of the ^{2}H in the sample was bound in trehalose. ^{17}O relaxation gives the mobility of water only since all of the ^{17}O atoms are bound in water. To get a more detailed view of the interplay between water and trehalose, the temperature and trehalose concentration was varied.
The first experiments were done measuring the longitudinal relaxation times of ^{2}H and ^{17}O in pure trehalose-water samples with trehalose concentrations varying from 0-1.5 M and a constant temperature of $20^{\circ}C$. This was repeated for a large temperature interval $20^{\circ}C$ to $-37^{\circ}C$ with 0-0.250 M trehalose-water samples emulsified to prevent freezing at the lower temperatures.

3.1 Deuteration of trehalose

Koch and Stuart (1977) [37] published a protocol that uses Raney Nickel, a catalyst consisting of solid fine grains of Nickel-Aluminium alloy, to label carbohydrates with ^{2}H. Raney Nickel is a hydrogen exchange catalyst, but when washed in D_2O the hydrogen at the active sites are exchanged with ^{2}H. It can then be used to exchange hydrogen atoms that are bound to a carbon atom which also has a hydroxyl group directly bound to it (carbon-bound hydrogen geminal to a hydroxyl group) with ^{2}H, see figure 3.1. Hydrogen atoms bound to carbons with no hydroxyl group are not exchanged, because the hydroxyl group acts to stabilize an intermediate transition state.

Koch and Stuart (1977) boiled the catalyst with carbohydrate dissolved in D_2O under reflux for 10h. The experiment has a risk of creating isomers, but isomerization is slower than deuteration [39], so we tried to avoid this by shortening the boiling time.

The first two attempts to deuterate trehalose was done by boiling trehalose dissolved in D_2O with Raney-Nickel under reflux for 6 and 5 h respectively, and the nickel ions were removed by leaving a dialysis tube with the chelator Chelex 100 in the sample for several days. We got quite high deuteration levels, perhaps the activity of the catalyst improved

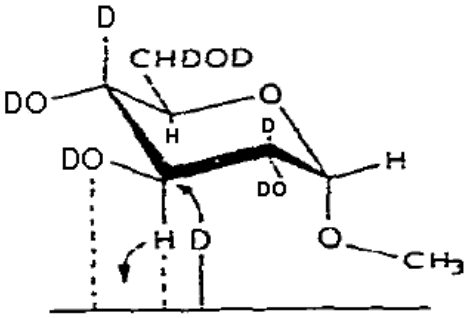

Figure 3.1: *Catalysis of ^2H labelling of carbohydrates by Raney Nickel. The horisontal line represents the active surface of the catalyst. [38]*

over the years. But we could not get the samples to crystallize, it had a strong tendency to become a viscous syrup instead, which we suspected could be due to byproducts from the deuteration experiment or other kinds of impurities.
When the food industry produces candy they add what is called interfering agents to prevent crystallization. This can be other kinds of sugar, interfering with the formation of a homogeneous crystal lattice, acid, which breaks up sugar into mono-saccharides, or fats and proteins can be added to coat the small crystals to prevent them from growing [41].
Extreme heating of the catalyst could possibly create other kinds of sugars or even break down the disaccaride into smaller units. We thus suspected that the crystallization problems were caused by byproducts. Several articles mention the importance of temperature control to prevent overheating in this kind of experiments to avoid decomposition and isomerization (eq. [40]). Therefore the heater was exchanged with a water bath to control the temperature and the sample was pumped through a Chelex 100 column to ensure better purification. Then we started getting crystals. We cannot be certain whether this is due to an improved crystallization protocol or less byproducts/impurities.

3.1.1 Final deuteration protocol

After a number of attempts we found a protocol that gave nice trehalose crystals with a reasonable degree of deuteration. We did not carry on to fully optimize the protocol, since we got enough deuterated trehalose crystals for our later experiments.

Pre-exchange of trehalose In order to ensure that the trehalose solution contained as little H_2O as possible during the experiment, the crystalline H_2O was removed and the labile hydrogen atoms from the hydroxyl groups on 15 g D-Trehalose Dihydrate from Sigma Aldrich was pre-exchanged for ^{2}H by dissolving it in $\sim$ 80 ml D_2O (>99.9%) and leaving it overnight in a 50^oC oven to evaporate.
Pre-exchange of Raney Nickel The Raney Nickel catalyst is dissolved in H_2O when bought, and needs to be washed in D_2O to exchange the hydrogen atoms bound to the catalytic surface of the Raney Nickel grains with ^{2}H, so we can get a catalytic reaction with ^{2}H.

52 ml sedimented Raney Nickel was washed 3 times in an equal volume of D_2O and left overnight in D_2O.

Deuteration The dried trehalose was redissolved in D_2O and mixed with the washed Raney Nickel while adding extra D_2O until a volume of about 300 ml was reached.
The sample was lowered into a 97^oC water bath and a reflux system was connected to the beaker to prevent the sample from drying out (can cause fire). The solution was not boiling at any time.
The deuteration level was followed by taking out NMR samples every 1-2 h. After 11 h the reaction was stopped, by taking the reaction mixture out of the heated water bath and letting it cool down in a cold water bath.

The deuteration level could possibly be improved by stirring the sample during the experiment, since the Raney Nickel grains sediment very fast and stay on the bottom of the beaker if no stirring is done. This may be the reason why we got a higher deuteration level when the sample was boiled, as boiling gives a fair degree of mixing.

3.1.2 Purification protocol

After the reaction product had cooled down, it was filtered through 2 layers of filter paper, and then filtered with 0.2 μm syringe filters. Finally 40 μl 1% Sodium Azide was added to prevent bacterial growth.
To get rid of metal ions, in particular Nickel ions from the catalyst, we used Chelex 100 as chelator. Chelex 100 is very basic and must thus be rinsed in acid. It was rinsed 3 times in 0.5M Sodium acetate pH 4.7 and thereafter rinsed 5 times in MilliQ water. The resulting pH of the Chelex was around 7-8.
A 1x10 cm Chelex column was then set up and the filtered deuterated trehalose sample was slowly pumped through the column which was regenerated after every 50 ml sample to get rid of bound metal ions and regenerate its capacity. The regeneration protocol was [45]:

- The column was washed with two bed volumes (1 bed volume = volume of Chelex) 1 M HCl
- Then flushed out the acid with at least 5 bed volumes MilliQ
- Washed with 2 bed volumes of 1 M NaOH
- Finally flushed with water for 5-10 min

Hereafter the sample was again filtered with 0.2 μm syringe filters.

3.1.3 Crystallization

We crystallized the trehalose sample to concentrate and further purify it. First the sample was dried in a 50^oC oven, which eventually gave an extremely viscous transparent syrup. After drying the sample long enough (i.e. up to a few days) it turned into a rubber-like

syrup, that was a static thin layer glued to the bottom of the beaker. To exchange bound D_2O and the labile ^{2}H from the hydroxyl groups on trehalose with hydrogen the syrup was dissolved in MilliQ H_2O and left to redry at 50^oC.
Chi et al. (2001) [42] and Chi et al. (2010) [43] found that trehalose crystallizes well in a 1:4 (v/v) water-ethanol mixture. After many crystallization trials, it was found that the weight of the dried out trehalose syrup could be used to determine how large a volume of water-ethanol mixture should be added to get optimal crystals. In principle we should be able to calculate the amount of trehalose in the sample from the amount of non-deuterated trehalose added to the deuteration experiment, but there will be a loss of trehalose along the way, some will stay with the Raney Nickel sand, some will be lost in the Chelex column and so on. Thus it is more precise to use the dry syrup weight. The water content of the rubber syrup may vary slightly, but not enough to create problems. The optimal syrup weight to volume water-ethanol mixture was found to be around 0.1 g/ml. The rubber/syrup weight was determined as the difference between the weight of the glass beaker before and after.
Surprisingly the nicest crystals were not grown by dissolving the syrup in the calculated volume with gentle heating, but instead really nice crystals grew when the calculated volume was just added to the dry syrup and then left untouched to let it dissolve slowly by itself (with parafilm).
After 1-2 days the crystals were loosened from the bottom of the beaker with very short and gentle heating, and the contents was poured into a funnel coated with filter paper connected to an air pump. The crystals were then washed gently under suction with small amounts of water-ethanol mixture and dried in a 50^oC oven. In order to remove the last D_2O from the crystals, they were crushed into powder and dried under vacuum for a couple of days.

3.2 Characterization of the product

To test that no byproducts had been made in the deuteration experiment, the product was examined with ion chromatography. This experiment was done by Peter Immerzeel, Department of Biochemistry, Lund University.
First the product was hydrolysed with acid, to separate it into mono saccharides, since standards for all kinds of monosugars were available in the laboratory. The sample was hydrolysed in 4% H_2SO_4 for 3 h and neutralized with $Ba(OH)_2$.
This solution was pumped through a CarboPac PA10 column from Dionex, which is an anion exchange column capable of separating different (di- and) monosaccharides. The column is kept basic with NaOH, which means that the hydroxyl groups in the sugars act as weak acids and become slightly deprotonated and therefore slightly negative, which results in attraction to the positively charged column. Depending on the number of hydroxyl groups the sugars interact more or less strongly with the column. But also the orientation of the hydroxyl groups affect the interaction with the column, since often only one "face" or "side" of the sugar interacts with the column resins at a time, the interaction will depend on how the hydroxyl groups are distributed or how the charge is distributed on the sugar surface. The location of the hydroxyl groups is what we are worried might have been changed in the deuteration experiment and what distinguishes different mono saccharides from each other.
The eluate was monitored using PAD detection (pulsed amperometric detection), a tech-

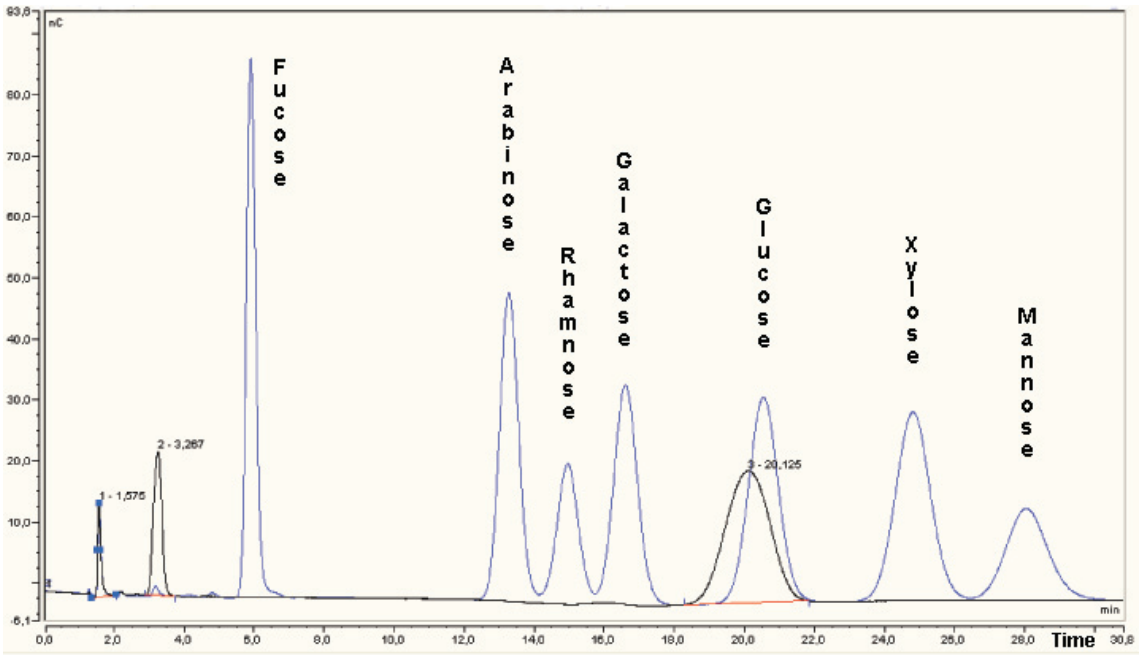

Figure 3.2: *Black line: Chromatogram of the hydrolysed deuteration product from batch 3 (out of 5) sent through an anion exchange column. The number next to the peak number is the peak area. Blue line: References. The experiments were done by Peter Immerzeel.*

nique capable of measuring ions in solution. The chromatogram of our sample together with a series of references is plotted in figure 3.2.

Since trehalose consists of two glucose units, the hydrolysed sample should be pure glucose, if no byproducts are present. The chromatogram shows a peak which shares the same elution time as the glucose reference peak, but also expands further to the left than the reference peak, which is likely because of some effect caused by the fact that some of the hydrogens have been exchanged for deuterium. It does not look like the solution contained any other kinds of monosaccharides, as the recorded peak is well separated from all other reference peaks.

The chromatogram also shows two small peaks that elute fast, which means that they are very small compounds. The first and smallest peak may be left over Nickel ions that were not removed with Chelex. The second peak is possibly ethanol from the crystallization process. The chromatography was done on crystals from batch 3 which had only been dried shortly in a $50^{\circ}C$ oven, but in the last trehalose batch (5th), which is the batch that was used in all experiments, we dried the crystals much more extensively by crushing them and leaving them in vacuum for a few days, thus most of the ethanol seen in the chromatogram should have evaporated in the last batch. This was confirmed by the fact that both proton and carbon 13 NMR spectra of the last batch show no signs of ethanol or anything else than trehalose.

3.2.1 Effect on ^{17}O R_1 in H_2O from Ni(II)

By Johan Qvist

Despite the use of chelating columns there will always be some Nickel remaining from the catalyst in our samples. Due to the two unpaired electrons of Nickel(II) this could significantly affect our ^{17}O R_1 due to paramagnetic relaxation enhancement.

We sent a small fraction of our most highly concentrated trehalose sample (1.5 M) for analysis to ALS, but diluted 200 times due to the large volume needed for their analysis. The analysis gave a concentration of 3.77 $\mu g/l$ corresponding to 754 $\mu g/l$ in the undiluted sample. With the atomic weight of 58.69 g/mol this corresponds to a concentration of 12.9 μM. As the concentration of Ni(II) is directly correlated to the concentration of trehalose we would have a lower concentration in the other samples.

Because of the low concentration we can safely use the dilute regime approximation, the relaxation rate of ^{17}O in water is then given by:

$$R_1 = (1 - f_{\mathrm{Ni}})R_1^0 + \frac{f_{\mathrm{Ni}}}{\tau_{\mathrm{Ni}} + T_{1,\mathrm{Ni}}} \tag{3.1}$$

Where R_1^0 is the relaxation of bulk water, f_{Ni} is the fraction of water molecules affected by the nickel ion, τ_{Ni} is the lifetime of the associated state and $T_{1,\mathrm{Ni}}$ is the longitudinal relaxation time for the water ^{17}O in this state.

f_{Ni} can be estimated, for our 1.5 M sample, as $6 \cdot 12.9 \cdot 10^{-6}/55.5 = 1.39 \cdot 10^{-6}$ as each Nickel coordinates 6 water molecules and the bulk concentration of water is 55.5 M. τ_{Ni} is given by Bechtold et al. [59] as 31.85 μs at 298K (at lower temperature the lifetime will be longer and the effect smaller). As an upper bound for the paramagnetic relaxation enhancement we can use $T_{1,\mathrm{Ni}} = 0$.

Using the above equation to calculate the contribution to the relaxation rate we get:

$$\frac{f_{\mathrm{Ni}}}{\tau_{\mathrm{Ni}} + T_{1,\mathrm{Ni}}} = \frac{1.39 \cdot 10^{-6}}{31.85 \cdot 10^{-6} + 0} = 0.0436 s^{-1} \tag{3.2}$$

For ^{17}O in pure water we have $T_1 \approx 0.3 - 7ms$, depending on temperature, corresponding to $R_1 \approx 140 - 3300 s^{-1}$ almost four orders of magnitude larger. The paramagnetic relaxation enhancement from the small amount of Nickel present is clearly negligible at all temperatures and concentrations studied.

3.3 Measurement of deuteration level

The deuteration level of the deuterated trehalose was measured by ^1H-NMR. The sample was taken shortly after the deuteration experiment and filtered with 0.2μm syringe filters. Since the sample was dissolved in D_2O, the proton signal from the sample would stem

only from the non-deuterated hydrogen positions in trehalose. Comparing the signal intensity from partially deuterated positions (I_{peak}) to a position that is known not to become deuterated (I_{ref}), the deuteration level of hydrogen position i could be determined as:

$$D_i = \frac{N_{D,i}}{N_{H,ref}} = 1 - \frac{N_{H,i}}{N_{H,ref}} = \left(1 - \frac{I_{peak,i}}{I_{ref}}\right) \tag{3.3}$$

Where $N_{D,i}$ is the no. of trehalose molecules with a ^{2}H on position i. $N_{H,i}$ is the same but for ^{1}H. And $N_{H,ref}$ is the no. of trehalose molecules with a ^{1}H on the reference position, and equals the total no. of trehalose molecules.
The signal intensities are determined as the area of the peaks.
We used a Varian NMR spectrometer with a resonance frequency of 600 MHz. Shimmed on the D_2O in the sample, so on the lock signal. Placed the carrier (the frequency we send and listen at) in the middle of the spectrum to be recorded. The other variables were set to:
Temperature: 25°C
Delay time, d1 = 5 s
Acquisition time, at = 2 s
Number of transients, nt = 1

The proton peaks were assigned using the 2D [1H,13C]-HSQC spectrum for trehalose from the BRMB database and the carbon peak assignment from Asano et al. [44].

3.4 Emulsion preparation

The trehalose samples used for relaxation experiments at varying temperatures were emulsified to prevent freezing at subzero temperatures. By mixing the trehalose-water sample with oil and detergent, tiny droplets of trehalose solution are created. This means that not all of the droplets will contain an impurity that can seed the crystallization of water, thus it is possible to go to very low temperatures without freezing the sample.
The deuterated trehalose was dissolved in Ultra pure H_2O from Fluka Analytical with 0.5% H_2O^{17}. All samples were centrifuged at 13000 rpm for 10 min and the supernatant was extracted to get rid of dust.
Approximately 106.5 mg Span 65 (a detergent) was mixed with 5 ml heptane and heated to 45-50^oC in a water bath to dissolve. The trehalose sample for emulsification was also preheated and equal volumes of both solutions were transferred to preheated (50^oC) glass syringes. The two syringes were connected with a small ($<$ 1mm) nozzle (plastic tube) and the contents were pushed back and forth between the two syringes 70 times. The result was a milky white emulsion. All samples were kept at 5^oC until used for measurements.

3.5 Sample preparation and concentration determination

The first round of trehalose-water samples were made from dilution of a concentrated trehalose stock solution with a concentration of about 1.5 M. This solution had been made by

weighing off some amount of deuterated trehalose and adding ^{17}O enriched water until a specific sample volume was reached. When we later wanted to add more samples a new stock solution of about 1.3 M deuterated trehalose in ^{17}O enriched water was made and diluted to the wanted concentrations. All added water was Ultra pure H_2O from Fluka Analytical with 0.5% H_2O^{17}, the ^{17}O source was a 21% ^{17}O solution from Icon Services Inc.

Our problem with determining the concentration of the resulting samples, is that although we know the deuteration level, we do not know the exact molar mass of the used trehalose, since we do not know the amount of water bound in the crystals, nor the amount of labile deuterons left (O-D). We tried to dry the trehalose by crushing the crystals into powder and leaving it overnight in a vacuum chamber (up to several times). But the molar mass measured by ^{13}C NMR still seemed to be too large: 377 and 350 g/mol for the first and second sample series respectively (the second time we dried the powder again). From the deuteration level we calculated a molar mass of 345.03-345.84 g/mol. Anhydrous trehalose probably also sucks up moisture from the air quite fast. Thus we decided to use ^{13}C NMR to determine concentrations.
In order to determine the sample concentrations, natural abundance of ^{13}C in our trehalose samples was compared to natural abundance of ^{13}C in a reference sample of known concentration. The used reference was 911.44 mM Isobutanol, because the ^{13}C NMR peaks from isobutanol are not overlapping with any of the peaks from trehalose.
Since the concentration of ^{13}C nuclei is very low, many measurements are needed in order to capture a nice signal to noise ratio, but ^{13}C takes a long time to relax back to its ground state after having been "excited", thus the delay time after each experiment needs to be very long. This means that it would take several days to do enough measurements to get a satisfactory signal-noise ratio, unless the relaxation time is decreased. This can be done by adding a paramagnetic substance, in this case $MnCl_2$ was chosen. The manganese ions are paramagnetic due to an unpaired electron, and this creates a substantial local magnetic field which can affect the dipole moments of neighboring ^{13}C atom and get them to relax [65]. But the paramagnetic substance also broadens the NMR peaks, thus there is a limit to how much manganese should be added.
The 1.5M and 1.3M samples were measured by mixing 300μl original sample with 300μl 911.44mM isobutanol, the rest of the samples contained 400μl original sample and 200μl 911.44mM isobutanol. 3μl 1 M $MnCl_2$ was added to all samples.
Normally ^{13}C NMR spectra cannot be used for concentration determination, since the integrated peak areas are not proportional to concentration. The reason is that first of all ^{13}C has a very long relaxation time, but as explained this can be circumvented with addition of paramagnetic species. The other problem is what is called the NOE effect. In order to avoid splitting of the carbon peaks, which lowers the sensitivity, the hydrogen in the sample must be decoupled. But in order to decouple hydrogen, a block of pulses with the Larmor frequency of Hydrogen and different phases is transmitted to "randomize" the orientation of the Hydrogen spin, so the effect on the orientation of the neighboring ^{13}C spin evens out to zero. At the same time energy is transferred from the now excited hydrogens to the neighboring carbon atoms, thus enhancing the carbon signal (NOE effect). But the problem is that not the same amount of energy is tranferred to all carbons, so the signal intensity is no longer proportional to concentration.
If decoupling is done during signal acquisition and not during the relaxation period, and the relaxation period is sufficiently long, the NOE enhancement of signals will decay during the relaxation time and be negligible during acquisition. Therefore the peak intensities will approach proportionality [51]. This decoupling technique is called inverse gated de-

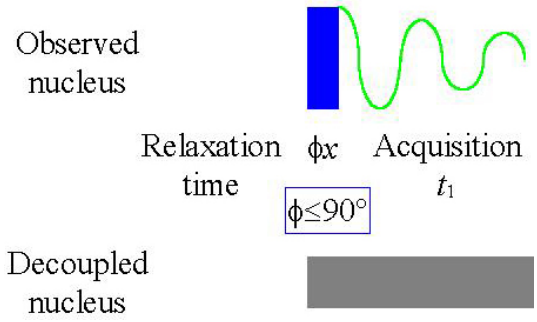

Figure 3.3: *Inverse Gated Decoupling [52].*

coupling, see fig. 3.3.

Thus normal 1D ^{13}C spectra were recorded with a Varian 600 MHz spectrometer with Inverse Gated Decoupling using the Waltz 16 pulse (decoupling) sequence. The spectra were recorded at $4°C$ to further enhance the relaxation rate.

Most of the experiments were done with a delay time of 7 s and a number of transients (= no. of subsequent experiments/pulse sequences/spectra recorded) of about 8192, but we later found out that this delay time was not long enough for the carbon atoms to have relaxed completely back to the ground state at low trehalose concentrations which is likely the reason for the higher concentration uncertainty seen at low concentrations. Therefore the last measurement, which was the 250 mM trehalose sample, the stock solution used for emulsions, was done with a delay time d1= 15 s and extra transients nt = 16384.
Besides that the other parameters for all measurements were:
Pulse width = 16.8 μs
Temperature = $4°C$
Acquisition time = 0.8 s

3.6 Relaxation experiments

A common experiment used to determine the longitudinal relaxation time (T_1) is the inversion recovery experiment. The pulse sequence consists of first a 180° pulse, a relaxation delay, then a 90° pulse followed by data acquisition. Many consecutive pulse sequences/experiments are done, and the relaxation delay (d2) between the two pulses is varied for each experiment, see figure 3.4.
The 180° pulse moves the magnetization vector from its equilibrium position along the +z axis down, to point in the opposite direction along -z. After the relaxation delay d2, the spins will have relaxed by a certain amount back towards their equilibrium position, depending on the length of the relaxation time, thus decreasing the magnetization vector along -z, while their xy-components are randomly distributed, so they sum up to 0. The leftover magnetization in the -z direction can be determined by now applying a 90° pulse, which moves it into the xy-plane, so it can be measured, because the pulse is coherent/has a narrow distribution of phases, so all spins are turned around the same axis.

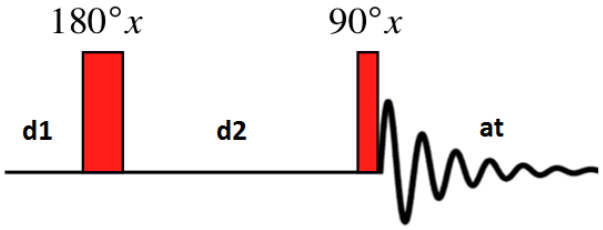

Figure 3.4: *Inversion recovery pulse sequence.*

A Varian 600 MHz NMR spectrometer was used to do inversion recovery experiments on ^{2}H and ^{17}O in trehalose samples consisting of deuterated trehalose dissolved in ^{17}O enriched water (0.5%). Trehalose concentration and temperature was varied one at a time, and in the ^{17}O relaxation experiments a water reference was also used (0 M trehalose, 0.5% ^{17}O).
The first delay time d1 was kept at 150 ms for both ^{17}O and ^{2}H relaxation. The acquisition time for ^{2}H experiments was about 400 ms and for ^{17}O about 40 ms (is varied slightly to include the entire FID). The initial T_1 guess was made from a small set of inversion recovery experiments. Then an array of 30-40 different delay times (d2) in the range 0 to 5 times the T_1 guess given, was created. The array was randomized to also randomize variations in variables that may change systematically with time. The number of experiments for each value of d2 was set to at least 64, but much higher numbers were used at the low concentrations and temperatures.

It was attempted to keep the temperature constant by first predrying the air and controlling the temperature of the air supplied to the NMR spectrometer with a temperature controller.
The probe temperature was measured 3 times at each temperature with a Thermocouple type T (Copper-Constantan). The construction of Thermocouplers is based on the fact that conductors generate a voltage when they experience a temperature gradient, and the voltage acquired depends on the conductor material. Thus leaving one end of two different conductors in an ice-water bath and the other in the (warmer) probe creates a voltage difference between the two conductors which can be measured with a voltmeter, see figure 3.5. The measurement can be used to calculate the temperature gradient, and since the reference temperature is kept constant at $0°C$ due to the ice-water bath, the probe temperature can be calculated.

The resulting standard deviation in the temperature measurements was kept below $0.1°C$ at 20, 10 and 0 $°C$. At lower temperatures down to -35 $°C$ the standard deviation was in the range 0.1-0.2$°C$, whereas the lowest temperature -37$°C$ had a standard deviation of $0.3°C$.

In figure 3.6 the relaxation rates for trehalose-water samples are compared to the relaxation rates for trehalose emulsions. The figure shows that there is no significant difference in the data, thus justifying the use of trehalose emulsions.

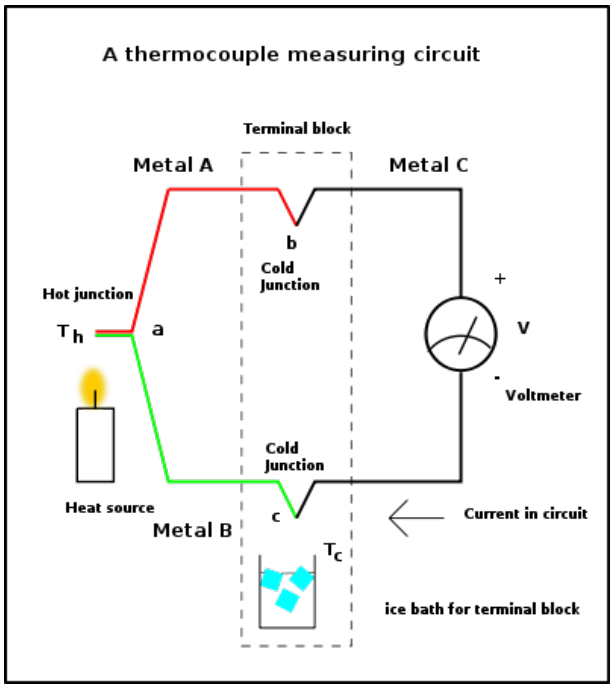

Figure 3.5: *The basic construction of a thermocouple. [67]*

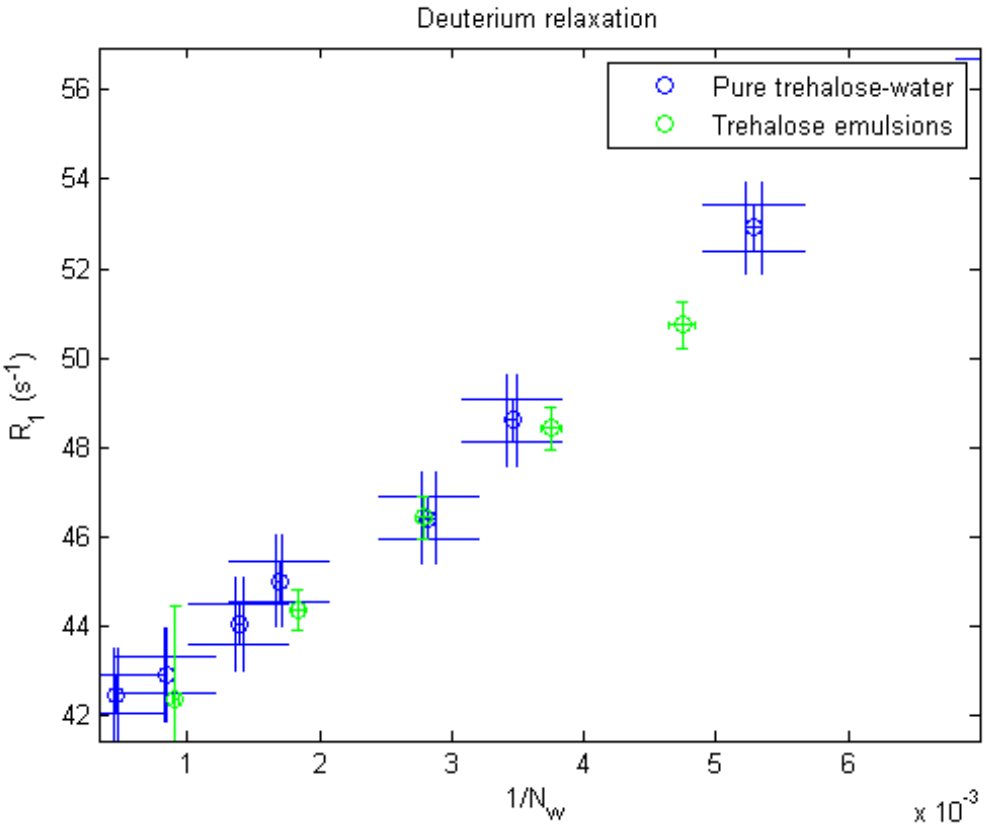

Figure 3.6: *The relaxation rate for deuterium at 20°C (pure trehalose-water: 19.99 ± 0.0727 °C, trehalose emulsions: 20.03 ± 0.0351 °C).*

3.6.1 Data analysis on relaxation data

For each sample 30-40 different delay times were applied giving 30-40 FIDs for each sample. The data was apodized (multiplying by) using cos^2 functions to weight the beginning of the FID (the strong part of the signal) most. After Fourier transformation of the FIDs the resulting spectra were baseline corrected, by fitting a second order polynomial to the non-peak areas of the spectra. The oxygen data was not apodized, and first order baseline correction was used.

The deuterium relaxation experiments showed 2 peaks: One large peak from trehalose and a smaller peak from deuterium in water, see figure 3.7.

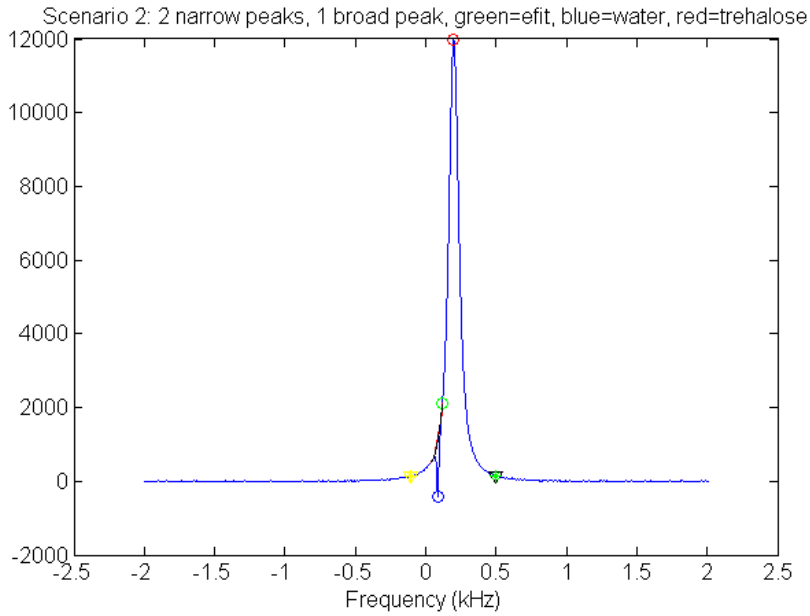

Figure 3.7: *One of the relaxation experiments on 1.47 M trehalose at* 20^oC.

The water bound ^{2}H concentration should be the highest in the most concentrated trehalose sample, since there could be left-over labile ^{2}H or small amounts of D_2O bound in the trehalose powder from the deuteration experiment, that have not been removed when the product was washed in H_2O or when subsequently dried. Therefore the concentration of water bound deuterium in the 1.47 M trehalose sample was determined from the ratio of the maximal absolute area of the two peaks: $c_{water-D} = c_{trehalose} A_{water-D} / A_{trehalose}$. The peak area of water is not strictly proportional to concentration here since the relaxation time of water bound ^{2}H is very long (about 400 ms) compared to the relaxation time of trehalose bound ^{2}H and to the delay times in the relaxation experiments probing ^{2}H (0-40 ms), and therefore it will not have relaxed completely in any of the experiments. But since the relaxation time of water bound ^{2}H is so much longer, it has relaxed so little in the experiments with short delay times, that the experiment almost corresponds to a regular $(-)90^\circ$ pulse and the (negative) peak area will be close to proportional to concentration. The resulting ^{2}H concentration in the water is 0.0326 M, which corresponds to 0.03% of the hydrogen atoms in a liter of water. This is about twice the natural abundance of ^{2}H, which means that there is a bit of labile deuterium or D_2O in the deuterated trehalose

powder, but it would not make a large improvement to repeat all the experiments with more thorough washing of the deuteration product.

But depending on the size of the trehalose peaks, which depends on the delay time, the water peak can constitute a substantial fraction of the total area, thus we decided to remove the water peaks computationally, see figure 3.7. This was in general (with some modifications in special cases) done by first finding the location of the trehalose and water peak by determining where the slope of the curve changed sign. Then the integration borders (triangles) where set (manually for each concentration) and the right border of the water peak (green circle) was determined as the location of the minimum of the curve slope in between the two peaks, or a reasonable distance from this minimum. The left border of the water peak was determined in various ways depending on the appearance of the plot, but often it was located as a third peak. The water peak was deleted from the data and a small piece of the left over curve on either side of the hole was fitted to a second order polynomial (black line). Finally the corrected peak was integrated.
The integral of the peak intensity with respect to frequency gives the total amount of magnetization measured in the frequency interval given by the peak. (The same reason why the peak integral is proportional to concentration). Thus the integral of a peak measured after a certain delay time d2, is the magnetization that is left along -z after a "relaxation time" of d2.
As explained in the Theory section the relaxation of the magnetization vector of both ^{2}H and ^{17}O follow an exponential decay according to:

$$M(t) = B\,(1 - A\exp(-R_1 t)) \tag{3.4}$$

- where the time t is the delay time d2.
This equation was fitted to the array of measured magnetizations after different delay times d2, in order to get the relaxation rate R_1.

Chapter 4

Results

4.1 Deuteration level

The measured 1D H NMR spectrum of the deuterated trehalose produced is plotted in figure 4.1. The proton peaks were assigned using the 2D [1H,13C]-HSQC spectrum from the BRMB database and the carbon peak assignment from Asano et al. [44]. The protons are numbered by the number in the glucose ring of the Carbon atom they are attached to, see fig. 4.2. Carbon atom number 6 has two H attached: $H6_1$ and $H6_2$. H1 and H5 did not get deuterated at all in the deuteration experiment, since the Carbons they are bound to, do not have an OH group attached also.

The assignment is shown in table 4.1 (from high ppm to low ppm) together with the integrated peak area normalized with the peak area of the non-deuterated H1 peak, and the deuteration level.

Table 4.1: *Deuteration level of deuterated trehalose*

Proton	Integrated area	Deuteration degree (%)
H1	1.00	0
$H6_1$	2.52	24*
H3		24*
H5		0
$H6_2$	0.78	22
H2	0.49	51
H4	0.44	56

*: The average deuteration degree of the $H6_1$ and H3, since their peaks are hard to separate.
In total, the 5 positions per glucose ring that can be deuterated are 35 % deuterated.

4.2 Concentration measurements

One of the recorded ^{13}C spectra can be seen in figure 4.3. The two peaks to the far right are isobutanol peaks, whereas the rest of the peaks to the left are from trehalose. Phasing

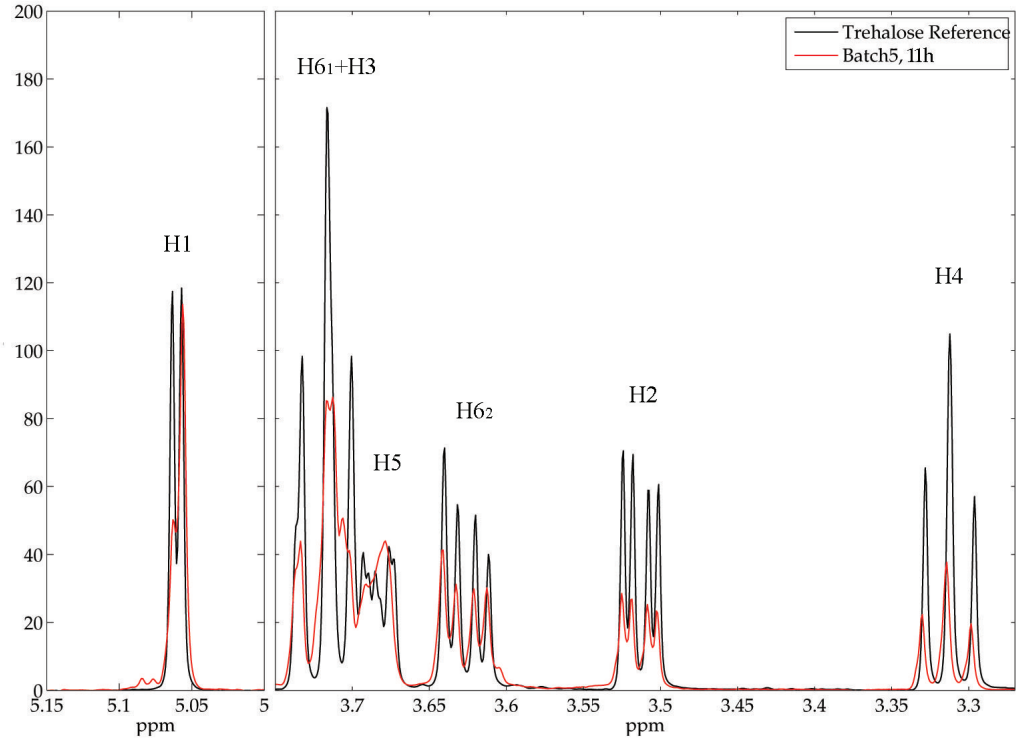

Figure 4.1: *Comparison of the proton NMR spectrum of normal trehalose (black line) and deuterated trehalose (red line).*

and baseline correction of the measured spectrum was unfortunately quite difficult, the baseline was very different and more curved on the left than on the right side, which probably contributed quite a lot to the uncertainty.
Comparing the ^{13}C spectrum in figure 4.3 to the ^{13}C spectrum of non-deuterated trehalose in figure 4.4, furthermore confirms that the deuteration product is indeed trehalose and nothing else. The reason why the peaks are split in the ^{13}C spectrum for deuterated trehalose, is that only H and not ^{2}H was decoupled.
As explained in Methods, the ^{13}C NMR experiments were designed such that the area of the peaks in the ^{13}C NMR spectra are proportional to the concentration of trehalose. Thus the trehalose concentration can be calculated from the integrated area of the isobutanol peaks for which the concentration is known:

$$c_{tre,eff} = c_{isobut,eff} \frac{A_{tre}}{A_{isobut}} / 2 \tag{4.1}$$

$$c_{isobut,eff} = c_{isobut} \frac{V_{isobut}}{V_{tot}} \tag{4.2}$$

$$c_{tre} = c_{tre,eff} \frac{V_{tot}}{V_{tre}} \Rightarrow \tag{4.3}$$

$$c_{trehalose} = \frac{V_{total}}{V_{trehalose}} \frac{A_{trehalose}}{A_{isobutanol}} \frac{V_{isobutanol}}{V_{total}} \cdot c_{isobutanol} / 2 \tag{4.4}$$

Where $c_{tre,eff}$ and $c_{isobut,eff}$ are the effective concentrations in the sample. To get the original sample concentrations before they were diluted in the sample for ^{13}C measurements, the effective concentrations are multiplied by their dilution factors. The trehalose concentration is divided by two because trehalose consists of two identical glucose rings, so for every trehalose molecule, two identical carbon atoms have been measured.
Only the two left-most trehalose peaks in the ^{13}C spectrum in fig. 4.3 and both the isobutanol peaks were used in the calculations. So a combination of the 2 trehalose and 2 isobutanol peaks gave 4 different area ratios, and the concentration given is an average of this.

The results can be seen in table 4.2.

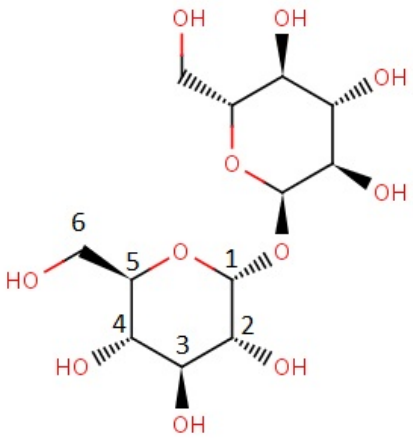

Figure 4.2: *The chemical structure of α,α-trehalose, incl. carbon numbering [3].*

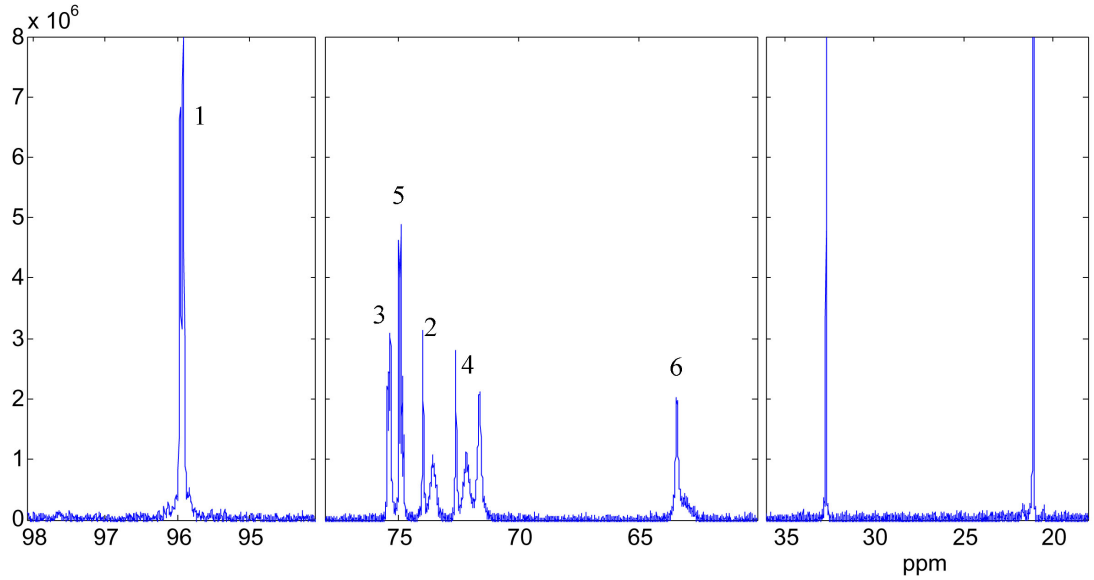

Figure 4.3: *^{13}C NMR spectrum for 250 mM deuterated trehalose with isobutanol as reference standard. The two peaks to the right are from isobutanol, the rest is from trehalose, which are assigned to a carbon number. Only the two left-most trehalose peaks were used in concentration calculations.*

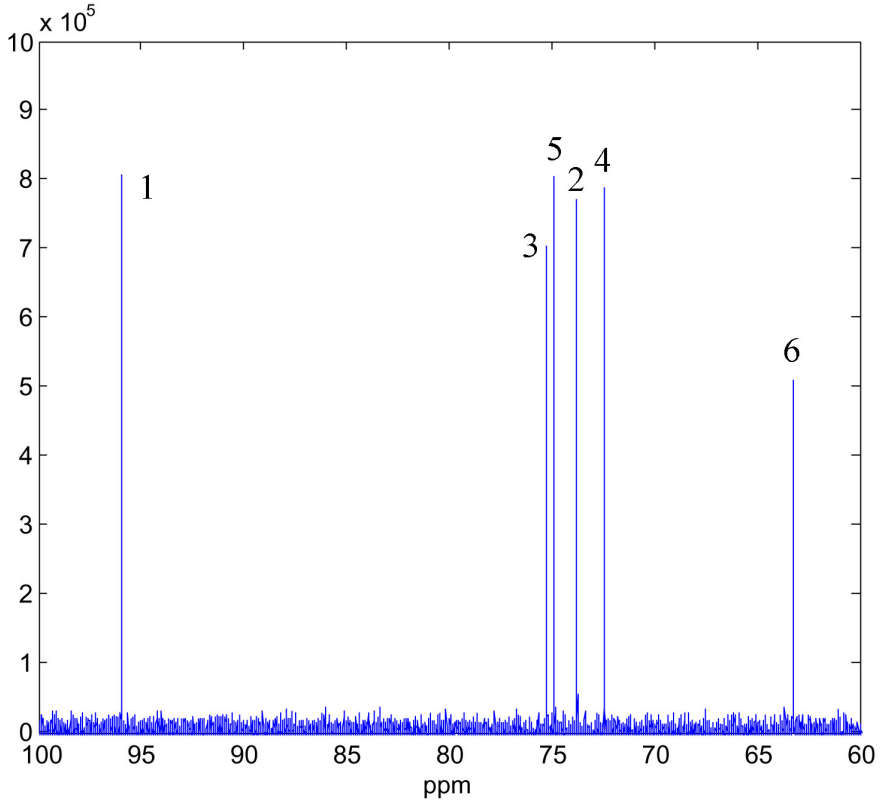

Figure 4.4: *^{13}C NMR spectrum for non-deuterated trehalose incl. Carbon assignments, only for comparison.*

Table 4.2: *^{13}C NMR concentration measurements*

Estim. c (M)	Measured c (M)	Rel. error on measurement	σ on measurement (M)
1.6	1.4732	0.009165	0.013503
0.8	0.7462865	0.0405	0.03024
0.3	0.28183	0.02495	0.0070326
0.7	0.6370635	0.00698	0.004445
0.5	0.458959	0.002689	0.001234
0.4	0.34674	0.03242	0.011243

Estim. c (M)	Measured c (M)	Rel. error on measurement	σ on measurement (M)
1.3	1.314559	0.01869	0.02457
0.15	0.147502	0.0102	0.001475

Estim. c (M)	Measured c (M)	Rel. error on measurement	σ on measurement (M)
0.250	0.249269	0.0206	0.0051227

The first table is from the first dilution series from the 1.5 M sample, the second table from the second dilution series from the 1.3 M sample, made independently from the other series. The third table is the stock solution used for all trehalose emulsion samples.
Since the error in the concentration measurements becomes quite high at low concentrations, it might be more reliable to just calculate the concentrations as a dilution series of the measured concentration of the stock solutions. The concentrations in table 4.3 were calculated from the measured concentration of the 1.5 M stock solution using the known dilution factor. The second dilution/sample series was calculated using the measured concentration for the 1.3 M sample. The difference between calculated and measured concentration is shown in the same table (4.3).

Table 4.3: *Comparison of measured concentrations to concentrations calculated from dilution series of the stock solution concentration.*

Estim. conc.	c_{calc}	$\delta = c_{meas} - c_{calc}$	$(c_{meas} - c_{calc})/c_{meas}$	$\lvert\delta\rvert - \sigma_{meas}$
0.05	0.0460	-	-	-
0.1	0.0921	-	-	-
0.2	0.1842	-	-	-
0.3	0.2762	0.0056	0.0199	-0.0014
0.4	0.3683	-0.0216	-0.0622	0.0103
0.5	0.4604	-0.0014	-0.0031	1.82e-4
0.6	0.5525	-	-	-
0.7	0.6445	-0.0075	-0.0117	0.0030
0.8	0.7366	0.0097	0.0130	-0.0206
1.6	1.4732	-	-	-
0.025	0.0253	-	-	-
0.075	0.0758	-	-	-
0.15	0.1517	-0.0042	-0.0283	0.0027
1.0	1.0112	-	-	-
1.3	1.3146	-	-	-

The table shows that the calculated concentrations for the 0.3M, 0.5M and 0.8M were within the standard deviation of the measured concentration, the 0.4 M within 2 standard deviations and the 0.15M and 0.7M within 1.5 standard deviations.

The concentrations used from here on were therefore chosen to be the concentrations calculated as 3 dilution series from the measured 1.5 M, 1.3 M and 0.25 M samples. The error in each concentration was then calculated as sum of squares of the error in the determined stock solution concentration from the ^{13}C experiment and a pipetting error. The latter was determined by weighing pipetted volumes (from the pipette used in the experiments) of pure water 30 times. This gave a pipetting error of 0.5%.

$$\frac{\sigma_c}{c} = \sqrt{\sigma_{C13}^2 + \sigma_{pipette}} \tag{4.5}$$

Dilution series from 1.5 M:

$$\frac{\sigma_c}{c} = \sqrt{0.0092^2 + 0.005^2} = 0.0104 \tag{4.6}$$

Dilution series from 1.3 M:

$$\frac{\sigma_c}{c} = \sqrt{0.0187^2 + 0.005^2} = 0.0193 \tag{4.7}$$

When more and more trehalose molecules are added to an aqueous solution, more and more water molecules will so to speak be "excluded" from a given volume of the solution, and because a trehalose molecule is a lot larger than a water molecule this effect is significant, especially at relatively high trehalose concentrations. Molar concentration does not report on this effect, it gives no clue as to how many water molecules are actually present in the sample. And this is a problem since the relaxation experiments depend on the fraction of water molecules bound or otherwise interacting with trehalose molecules, which again depends on the ratio of number of trehalose molecules to the number of water molecules.
It is therefore useful to convert molar concentration into the solute to water ratio N_w, in particular when plotting ^{17}O relaxation rates, to circumvent these problems and this conversion will also greatly simplify later calculations:

$$N_w = \frac{n_w}{n_s} \tag{4.8}$$

n_s = moles solute molecules, n_w = moles water molecules.

$$c_s = \frac{n_s}{V} = \frac{n_s}{n_w V_w^p + n_s V_s^p(0)} = \frac{1}{N_w V_w^p + V_s^p(0)} \tag{4.9}$$

Where c_s is the solute concentration. V_w^p is the partial molar volume of pure water. And $V_s^p(0)$ is the apparent partial molar volume for the solute at infinitely low concentration. Any volume change in water by the addition of trehalose to the solution, is taken into account by the apparent partial molar volume of trehalose, by setting the apparent partial molar volume of water equal to that of pure bulk water, and because the apparent partial molar volume of a solute is defined as differential of the total solution volume: dV/dn_s. So the apparent partial molar volume would be the total volume change of an infinitely large solution, if 1 molar solute is added.
But it has been assumed in eq. 4.9 that $V_s^p(0)$ can be assumed to be constant, so that the volume changes of the solute with increasing concentration or changes in temperature are negligible.

According to Banipal et al. [50], the partial molar volume of mono- and disaccharides increases linearly with concentration:

$$V^p_{tre}(c) = V^p_{tre}(0) + S_v \cdot c_{tre} \tag{4.10}$$

Where $V^p_{tre}(0)$ is the partial molar volume of trehalose at infinite dilution and S_v a proportionality constant.

The parameters from Banipal et al. [50] were used:
$V^p_{tre}(0)$=207.61 $\pm$ 0.06 cm^3/mol at 25° C.
S_v=1.60 $(cm^3 \cdot l)/mol^2$

The highest concentration used in these experiments is 1.5 M and this gives only a 1.2% increase in the partial molar volume of trehalose and a 0.5% change in N_w. This is at first not accounted for in the calculation of N_w, instead it is included in the error bars of N_w. The error in volume from the measurement of 0.06 cm^3/mol is only 0.03% of the volume and thus negligible compared to the error from concentration variations.
For the measurements at 20°C the partial molar volume was temperature corrected from 25°C to 20°C according to Banipal et al.:

$$V^p_{tre} = (207.61 - 0.76) cm^3/mol = 206.85 cm^3/mol \tag{4.11}$$

The temperature dependence is another story that I will get back to later, since it is only relevant for the emulsions.

Equation 4.9 can be rewritten to give:

$$N_w = \frac{1 - c_s V^p_s(0)}{c_s V^p_w} \tag{4.12}$$

The error in N_w caused by concentration errors is calculated for each concentration:

$$\sigma_{Nw(c)} = \frac{\partial N_w}{\partial c}\sigma_c = \sigma_c \frac{1}{c^2 V^p_w} \tag{4.13}$$

The error in N_w caused by errors in partial molar volume of solute:

$$\sigma_{Nw(V)} = \frac{\partial N_w}{\partial V^0_s}\sigma_{Vs} = -\frac{1}{V^p_w}\sigma_{Vs} \tag{4.14}$$

So the total error in N_w becomes:

$$\sigma_{Nw} = \sqrt{\left(\sigma_c \frac{1}{c^2 V^p_w}\right)^2 + \left(\frac{1}{V^p_w}\sigma_{Vs}\right)^2} \tag{4.15}$$

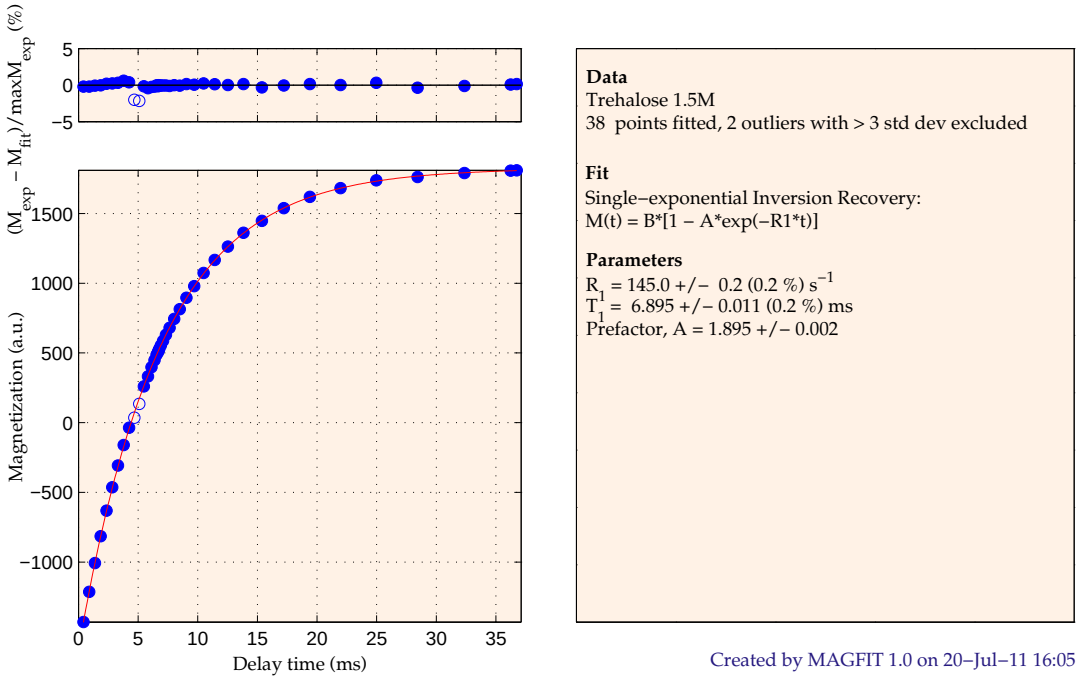

Figure 4.5: *^2H relaxation in 1.47 M deuterated trehalose at 20°C.*

4.3 Relaxation fits and R_1 error estimates

Figure 4.5 shows one example of the single exponential fit of the measured magnetization of ^{2}H as a function of delay time d2 in order to get the relaxation rate R_1.

The fitting of the single exponential function to the data gives very small standard deviations in R_1 and T_1: They were highest for ^{2}H: 0.1%-0.2%, except for 0.025-0.15 M where the standard deviation is higher: 0.4-0.7%.
It looks like there is a trend in the residuals (not shown), which may be due the fact that the relaxation follows a Kohlrausch exponential function instead, because of trehalose-trehalose interactions. But the very low fitting errors show that fitting a single exponential function to the data as is perfectly justified.

4.3.1 Emulsified trehalose-water solutions

The relaxation rates measured for the trehalose-water emulsions at various temperatures can be seen in the tables in Appendix A.

The relative error in T_1 is the same as the relative error in R_1:

$$\sigma_{R_1} = \frac{dR_1}{dT_1}\sigma_{T_1} = \frac{1}{T_1^2}\sigma_{T_1} = R_1\frac{\sigma_{T_1}}{T_1} \tag{4.16}$$

^2H R_1 errors for emulsion data: The tables in Appendix A show that the errors in T_1 and thus also in R_1 in the ^{2}H relaxation experiments are about 2 % for $-37^\circ C$ and the rest around 1%, because this is the order of the deviation between repeated experiments. The errors were then set to 2 % for $-37^\circ C$ and $-35^\circ C$ (the low temperature readings are more uncertain because of the higher risk of freezing) and 5% for 50mM at all temperatures. The error in the rest of the measurements were set to 1%.
^{17}O R_1 errors for emulsion data: The table shows that R_1 error at $-37^\circ C$ and $-35^\circ C$ should be set to 2% and the rest to 1%.

4.3.2 Trehalose-water samples at constant temperature

R_1 errors for trehalose-water solutions: The trehalose-water samples were measured at $20^\circ C$ and since the R_1 errors from the emulsion data seemed to be around 1% for both atomic species at this temperature, the error was also set to 1% here.

4.4 ^{2}H relaxation

The concentration dependence of the relaxation rate of ^{2}H is shown in figure 4.6.

The fact that the relaxation rate of trehalose is not constant at the lower concentrations is unexpected since the relaxation rate for one trehalose molecule should be independent

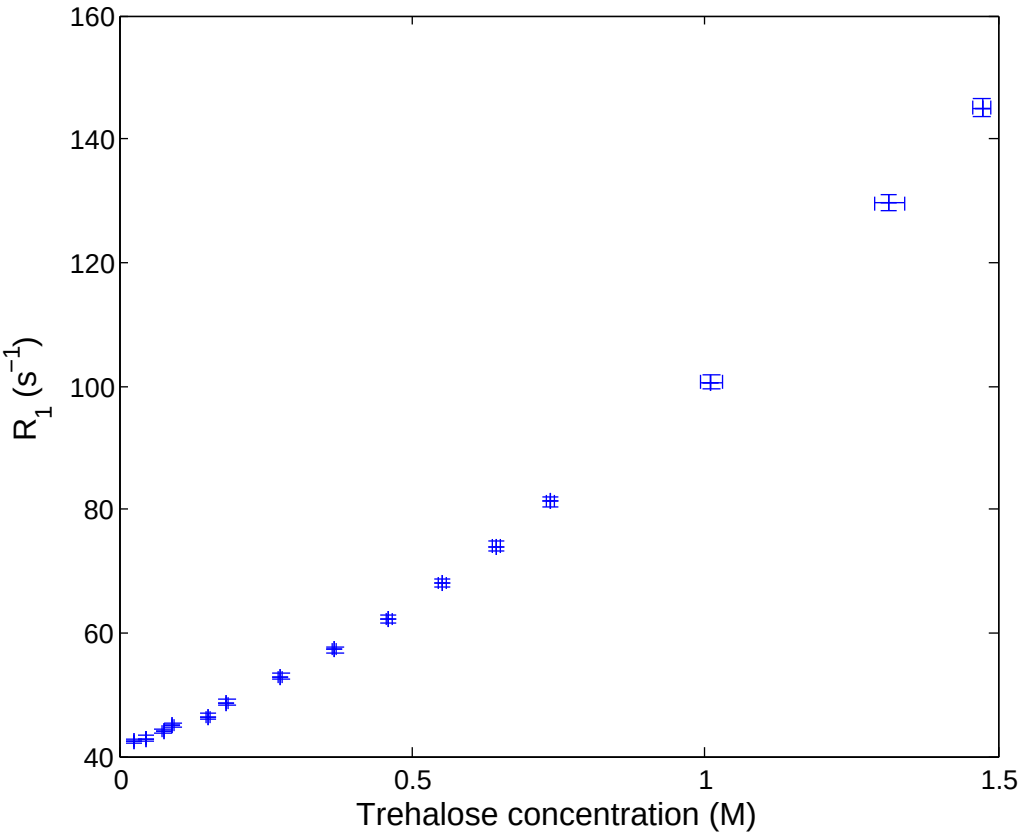

Figure 4.6: *The relaxation rate for ^2H at 19.99 ± 0.0727 °C.*

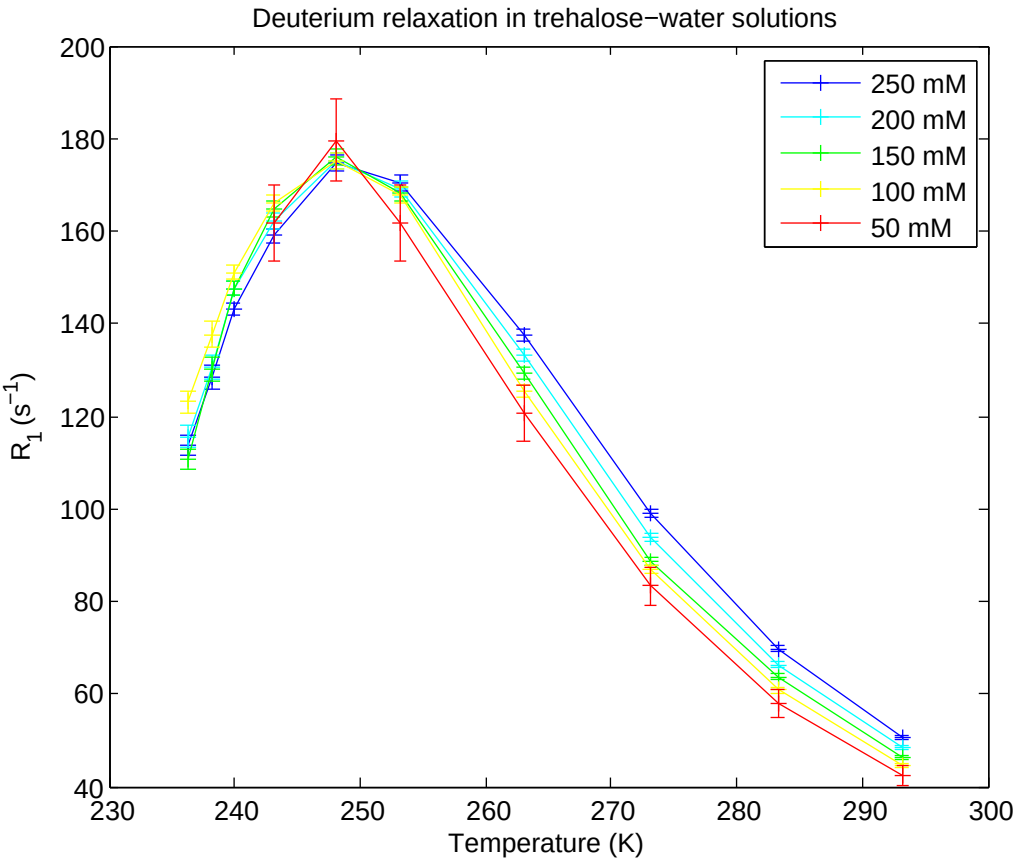

Figure 4.7: *^{2}H relaxation rate as function of temperature.*

of how many other there are present. The trehalose molecules must therefore somehow interact even at the lowest concentrations measured. Whether this effect is on the order of hydrodynamic and thermal interactions is calculated in a later section.

4.4.1 Calculation of τ_c for emulsified trehalose samples at varying temperature

The temperature dependence of ^{2}H relaxation rate in deuterated trehalose can be seen in figure 4.7. The relaxation rate is here split into two domains by a maximum in R_1: slow motion regime at low temperatures and a fast motion regime at high temperatures.

This behavior can be explained by the temperature dependence of the correlation time, decreasing the temperature increases the rotational correlation time. And the following correlation between relaxation rate and correlation time gives the curve shape seen in figure 4.7 (see Theory section):

$$R_1 = \omega_Q^2 S^2 \left(\frac{0.2\tau_c}{1+\omega_0^2\tau_c^2} + \frac{0.8\tau_c}{1+4\omega_0^2\tau_c^2} \right) \tag{4.17}$$

S^2 is an order parameter that needs to be included since the trehalose molecule is not perfectly rigid.
The Larmor frequency of ^{2}H ω_0 can be found from the "frequency of the used spectrometer", here 600 MHz. The frequency that is associated with an NMR spectrometer is really the Larmor frequency of a proton in the spectrometer or in a B-field of the same size as that produced by the spectrometer. As was explained in the theory section, the Larmor frequency of an atom is proportional to the B-field and the gyromagnetic ratio:

$$\omega_{0,p} = \gamma_p B = 600MHz \tag{4.18}$$

Thus the Larmor frequency of ^{2}H in the same spectrometer can be calculated as:

$$\omega_{0,d} = \frac{\gamma_d}{\gamma_p}\omega_{0,p} = \left((4.1066/26.752)\cdot 600\cdot 10^6 Hz\right)\cdot 2\pi = 5.7871\cdot 10^8 rad/s \tag{4.19}$$

According to Ludwig et al. (1995) [47] ω_Q for ^{2}H can be calculated as:

$$\omega_Q^2 \equiv \frac{3}{2}\pi^2\chi_D^2\left(1+\frac{\eta_D^2}{3}\right) \tag{4.20}$$

Bose-Basu et al. (2000) [46] measured quadrupolar coupling constants χ_D for carbon bound ^{2}H in glucose by measuring the longitudinal relaxation times of ^{13}C and ^{2}H labelled glucose, and got values varying from 174.0-178.9 kHz (depending on the location), here it was thus set to 175 kHz.

The asymmetry parameter η_Q is approximated to 0 as it is considered to be very small or 0 for $C-{}^2H$-fragments [46].
Therefore:

$$\omega_Q = \sqrt{\frac{3}{2}\pi^2(175\cdot 10^3 Hz)^2} = 6.7333\cdot 10^5 rad/s \tag{4.21}$$

In trying to solve the equation for R_1 as a function of τ_c you get a 4th degree polynomial, which makes it tricky to solve analytically, thus it could be solved numerically instead. But the problem is, that we need to know the exact value for the order parameter in order to do this. This can be done by fitting the data to the equation for R_1 and setting the correlation time equal to a function of temperature. We used the empirical equation below, originally found to describe water dynamics very well [48], but it also describes our data very well:

$$\tau_c = \tau_0\left(\frac{T}{T_0}-1\right)^{-\gamma} \tag{4.22}$$

τ_0, γ and T_0 are free fitting parameters.
So eq. 4.22 was inserted into the equation for R_1 (eq. 4.17) so it became a function of temperature and the resulting function was fitted to the data $R_1(T)$.
The temperature at which R_1 is at its maximum, was found by inserting the following into the equation (4.22) for τ_c (can be shown by differentiating the equation for R_1 with respect to τ_c):

$$\tau_{max} \equiv \tau_c(R_{1,max}) = 0.615795/\omega_0 \tag{4.23}$$

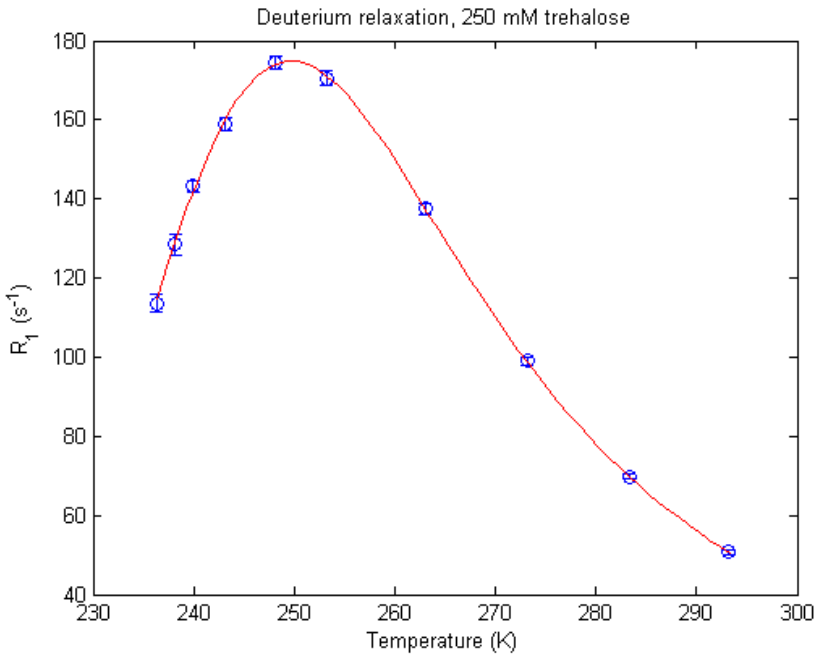

Figure 4.8: *Fitting R_1 to equation 4.17 and 4.22.*

Then:

$$T_{max} = \left(\left(\frac{\tau_0}{\tau_{max}} \right)^{\frac{1}{\gamma}} + 1 \right) T_0 \tag{4.24}$$

The fits are shown in figures 4.8-4.12.

The parameters found in the R_1 fits as well as the calculated T_{max} can be seen in table 4.4. The order parameter can be set to a constant within the error bars (fig. 4.13). The weighted average was found by fitting a horizontal line to the data points incl. error bars, this gave an average of 0.7871 ± 0.0024. But the individual values were used in the calculations.
Baraguey et al. (2002) [97] determined the average order parameter for sucrose to be 0.87 by ^{13}C NMR. Batta et al. (1997) [60] determined the order parameter for each carbon atom in trehalose in D_2O with ^{13}C NMR at different temperatures. The average order parameter for all carbons and temperatures from 263.7 to 299 K is 0.8467. Interestingly Baraguey et al. also observed a similar concentration dependence in R_1 for sucrose.

The fitted parameters were used to directly calculate the correlation time corresponding to each measured R_1 value, by inserting the experimental temperature into the fitted equation for the correlation time, eq. 4.22, see fig. 4.14 and 4.15. The used errors in τ_c are the same as those calculated in the next section that describes numerical calculation of τ_c.

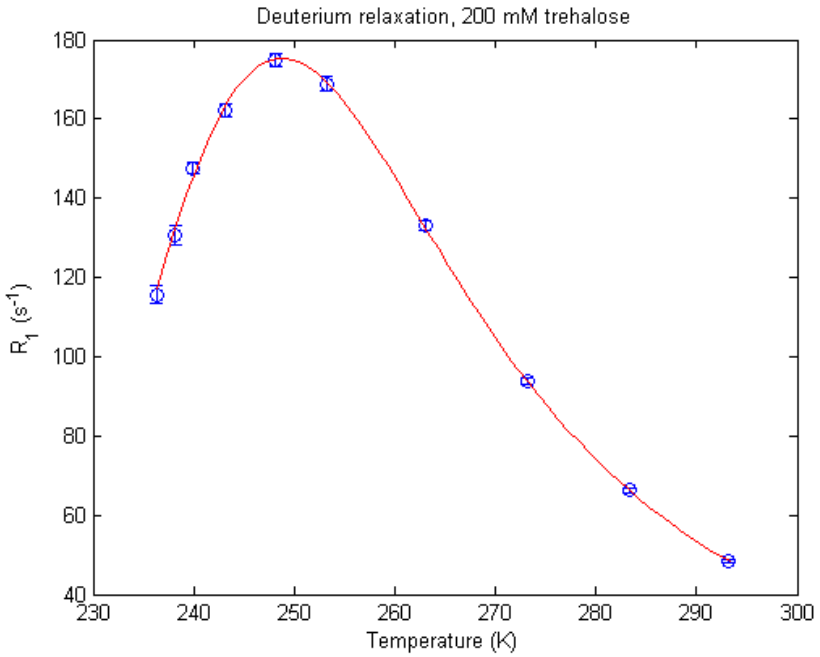

Figure 4.9: *Fitting R_1 to equation 4.17 and 4.22.*

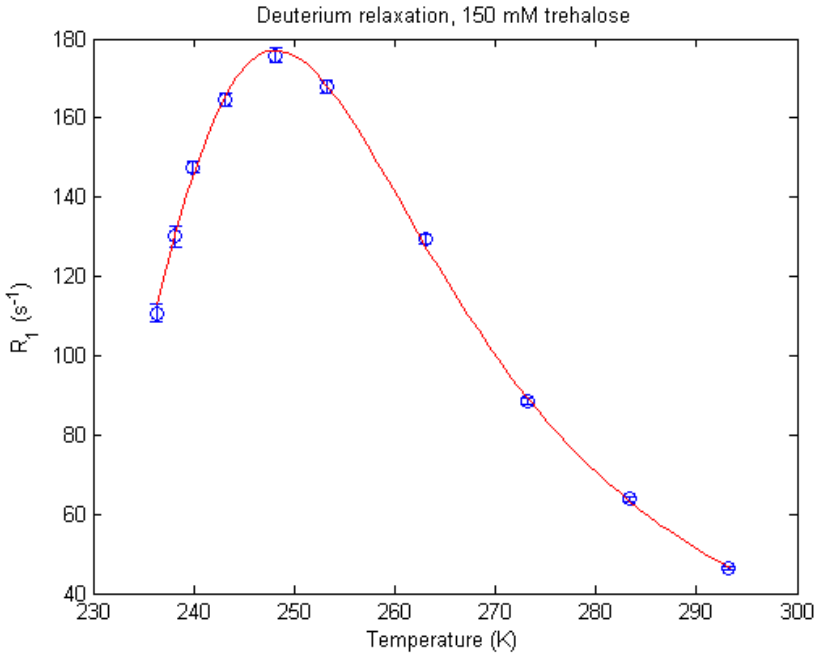

Figure 4.10: *Fitting R_1 to equation 4.17 and 4.22.*

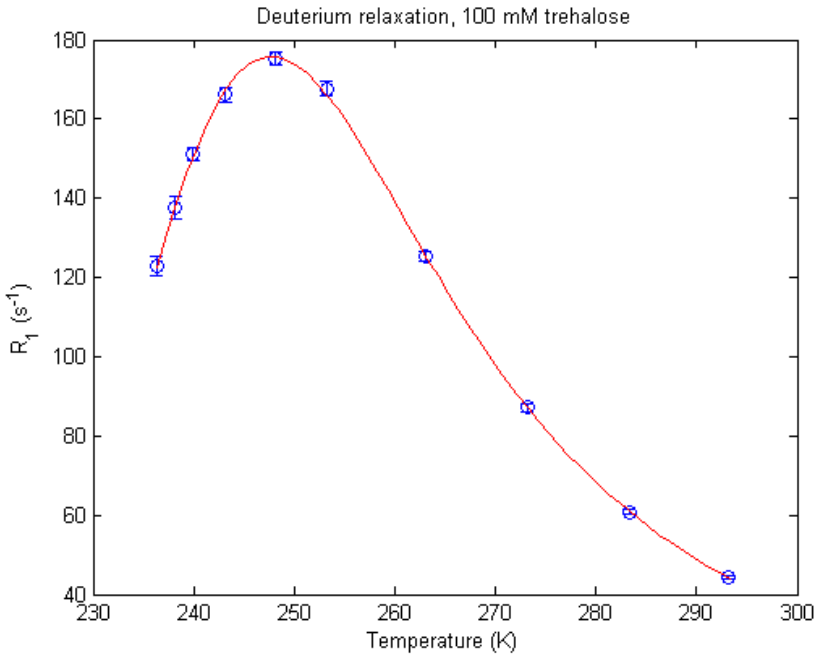

Figure 4.11: *Fitting R_1 to equation 4.17 and 4.22.*

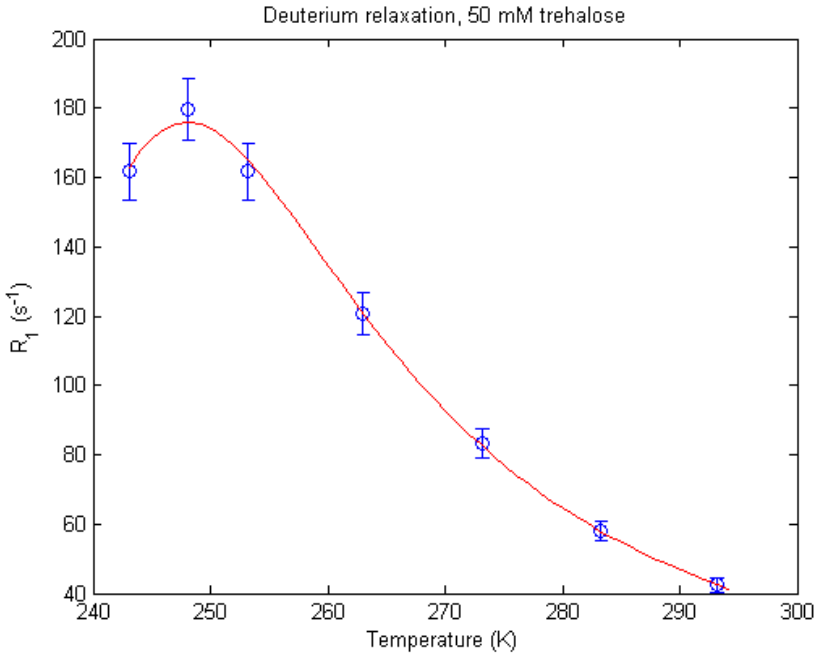

Figure 4.12: *Fitting R_1 to equation 4.17 and 4.22.*

Table 4.4: *Fitting parameters from R_1 fits.*

Concentration	250mM	200mM	150mM	100mM	50mM
S^2	0.7828	0.7854	0.7929	0.7872	0.7877
$\sigma(S^2)$	0.0048	0.0048	0.0048	0.0049	0.0302
τ_0 (ps)	12.3268	11.7711	11.4525	10.3996	10.4137
$\sigma(\tau_0)$(ps)	0.3667	0.3769	0.4323	0.3226	2.4717
T_0(K)	208.5423	211.3721	217.0089	211.4345	221.9647
$\sigma(T_0)$	2.3348	2.0348	1.4115	2.0396	11.5384
γ	2.7459	2.6004	2.3354	2.6257	2.1580
$\sigma(\gamma)$	0.1254	0.1104	0.0814	0.1103	0.5758
T_{max}(K)	249.6662	248.7645	248.1807	247.7149	247.9750

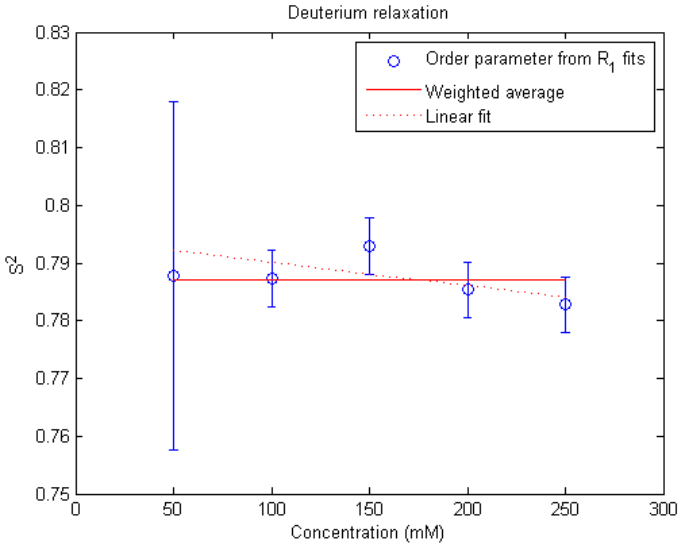

Figure 4.13: *Order parameter (S^2) from R_1-fit.*

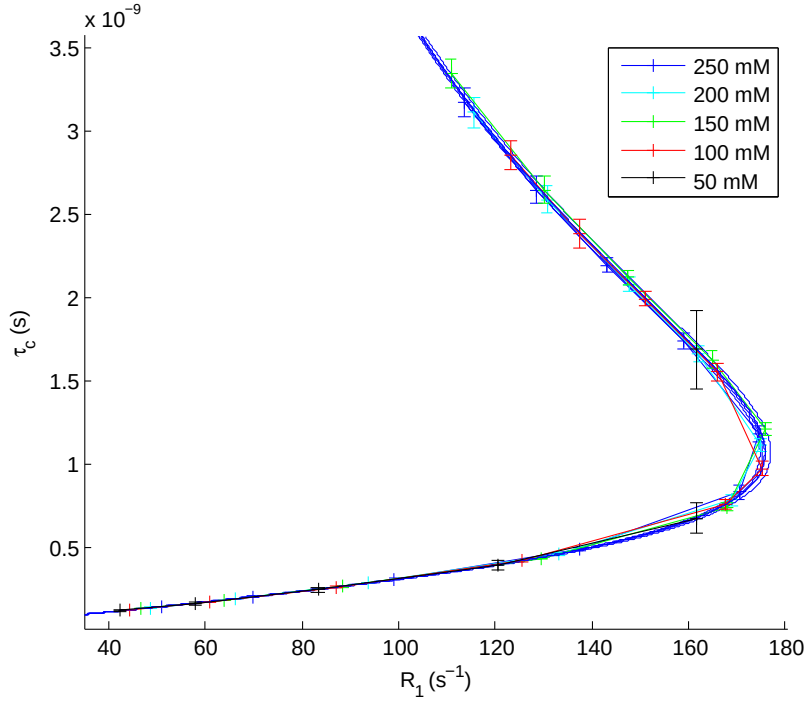

Figure 4.14: *Calculation of τ_c from R_1 fit. The crosses are the calculated data points, the curves are the theoretical R_1 curves calculated from the R_1 fits.*

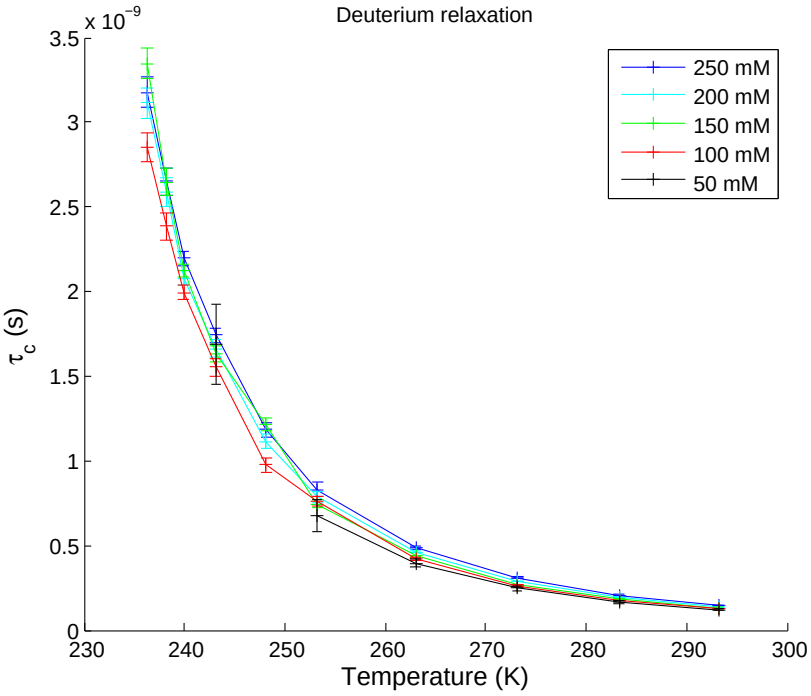

Figure 4.15: *Temperature dependence of calculated trehalose correlation times.*

Numerical calculation of τ_c

When the direct calculation of the correlation times from the fit of R_1 was done, a particular temperature dependence of τ_c was assumed, which had 3 free parameters. In order to test whether this is fair to assume, a more numerical calculation was also done. The matlab function interp1 was used to interpolate the τ_c values corresponding to the measured R_1 values from an interpolation curve given by a vector of chosen correlation times and a vector of the corresponding R_1 values calculated by the previously mentioned equation for R_1:

$$R_1 = \omega_Q^2 S^2 \left(\frac{0.2\tau_c}{1+\omega_0^2\tau_c^2} + \frac{0.8\tau_c}{1+4\omega_0^2\tau_c^2} \right) \tag{4.25}$$

- The only parameter used from the previous fit of R_1 was the fitted order parameter.
Estimation of the error in correlation time was done by numerical calculation of the differential of the curve and multiplying this by the set standard deviation in R_1:

$$\sigma_{\tau_c} = \frac{\partial \tau_c}{\partial R_1} \cdot \sigma_{R_1} \tag{4.26}$$

Where

$$\frac{\partial \tau_c}{\partial R_1} = \frac{2\Delta\tau_c}{R_1(\tau_c+\Delta\tau_c) - R_1(\tau_c-\Delta\tau_c)} \tag{4.27}$$

And $\Delta\tau_c = 10^{-13}s$.

In principle the error in the order parameter should be included in this calculation, but I have no analytic equation for the correlation time as a function of order parameter, and the error in order parameter at each concentration was calculated to be 0.6% (except for 50mM) and the average order parameter had a standard deviation of only 0.3% which is not very significant compared to the error from R_1 which lies in the range of 1-2%.

Furthermore it could be argued that the error in the calculated correlation time should instead be calculated from the errors in the fitted parameters τ_0, T_0 and γ. But since these parameters are not independent, the error would be overestimated with normal error propagation (that has not been complicated with covariances).

The interpolated correlation times are shown in figure 4.16.

The directly calculated correlation times are compared to the interpolated correlation times in figures 4.17-4.21. The plots show that only 1-2 of the data point pairs are not located within each others errorbar, which makes the difference between the two calculation methods, most likely negligible.

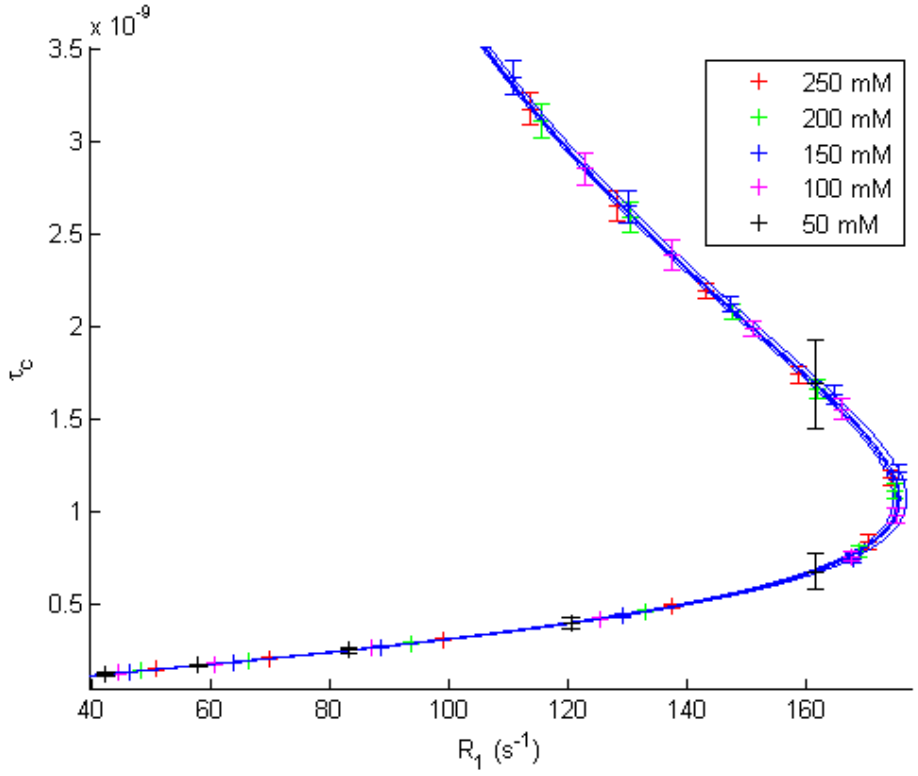

Figure 4.16: *Interpolated ^{2}H correlation times.*

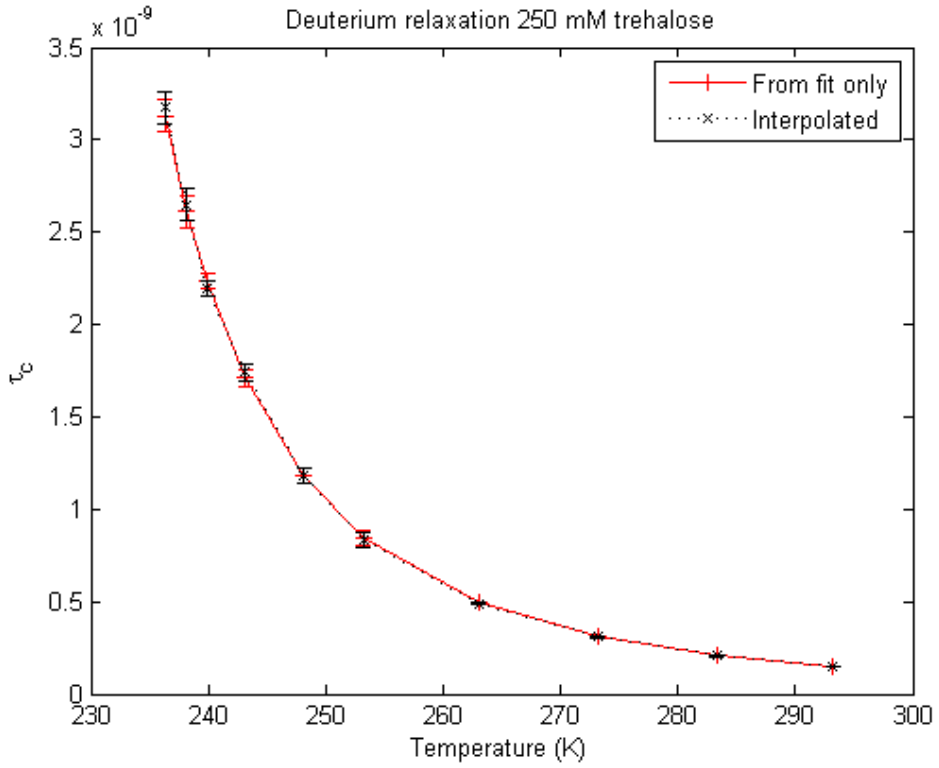

Figure 4.17: *Comparison of interpolated and fitted correlation times.*

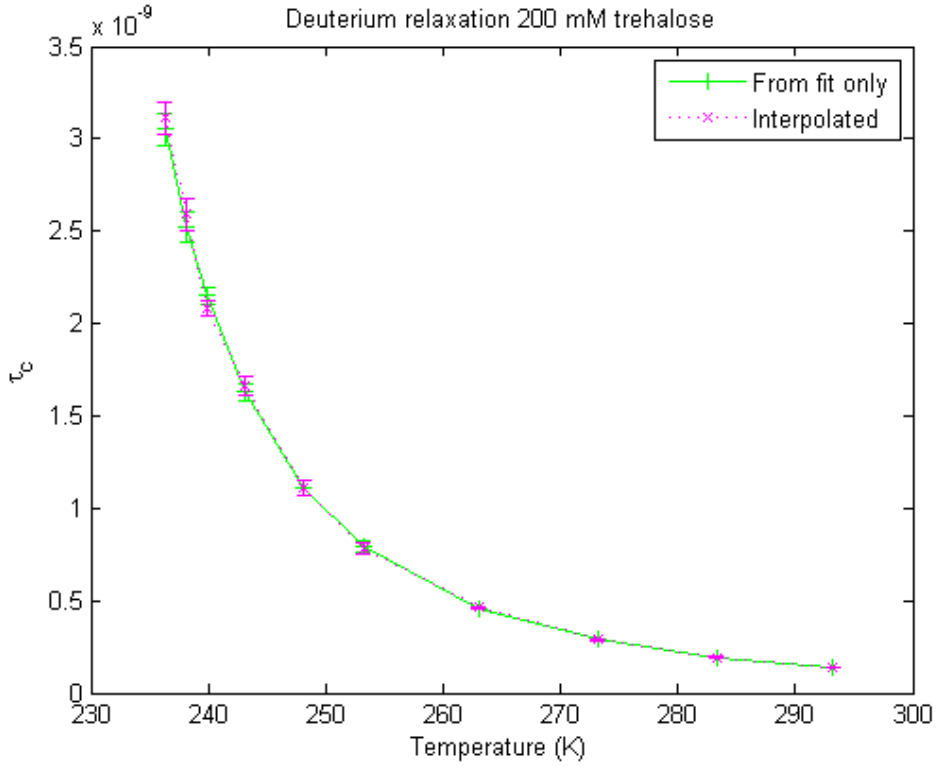

Figure 4.18: *Comparison of interpolated and fitted correlation times.*

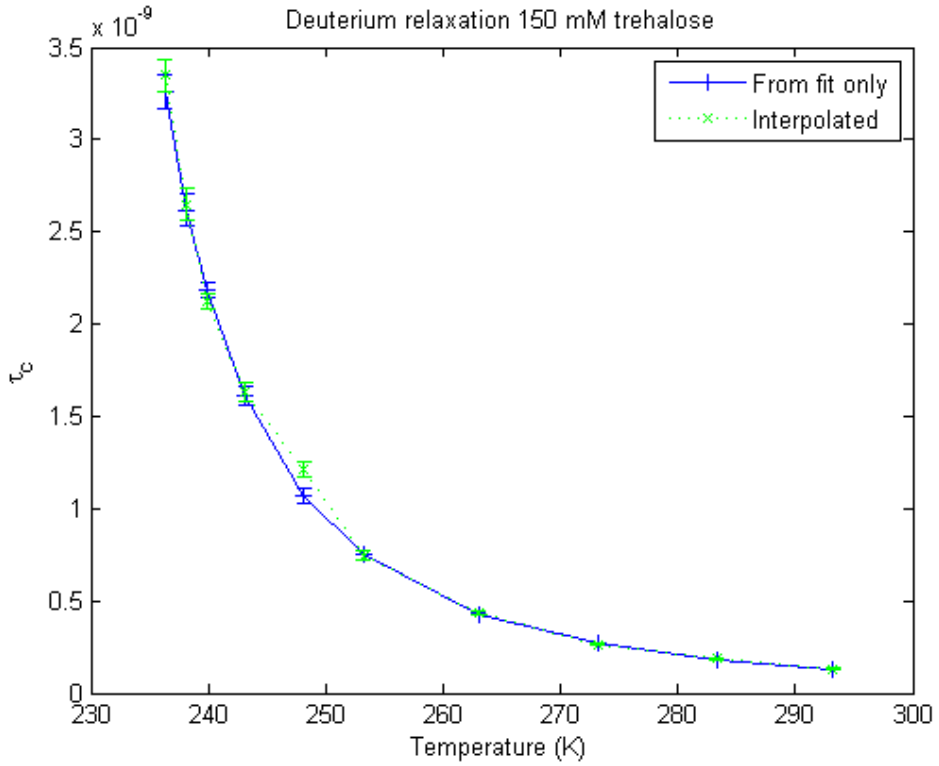

Figure 4.19: *Comparison of interpolated and fitted correlation times.*

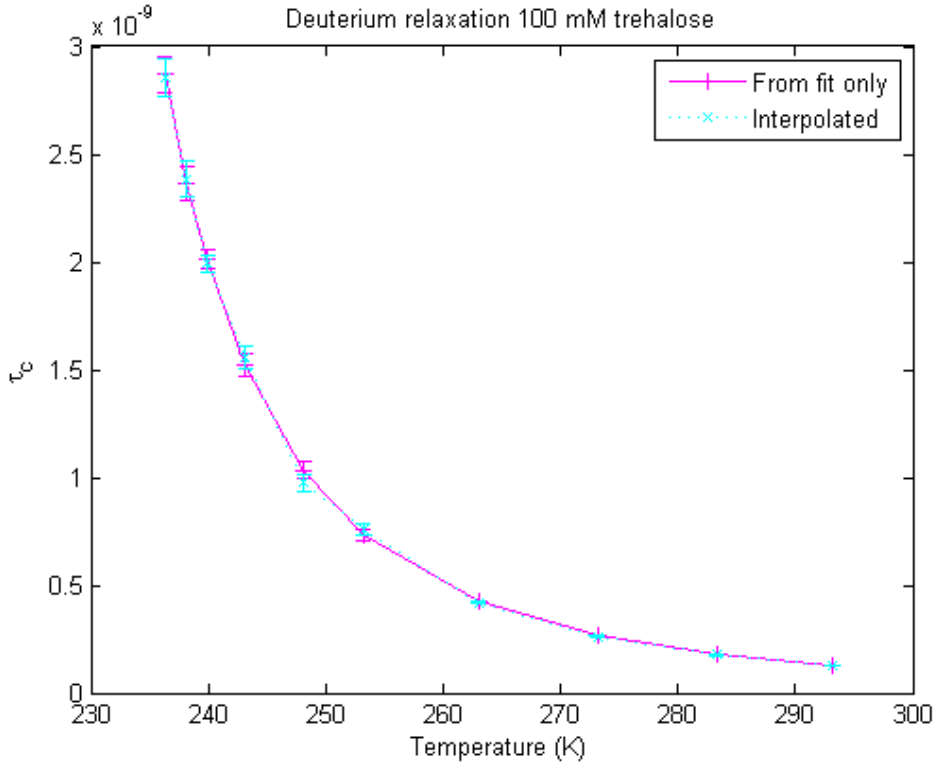

Figure 4.20: *Comparison of interpolated and fitted correlation times.*

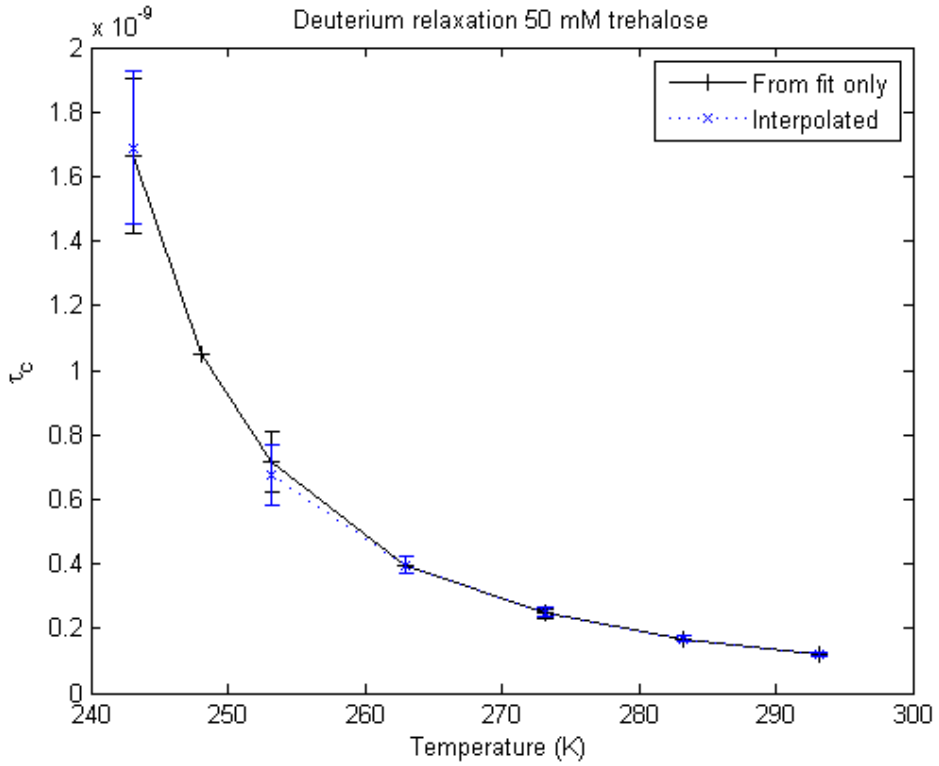

Figure 4.21: *Comparison of interpolated and fitted correlation times.*

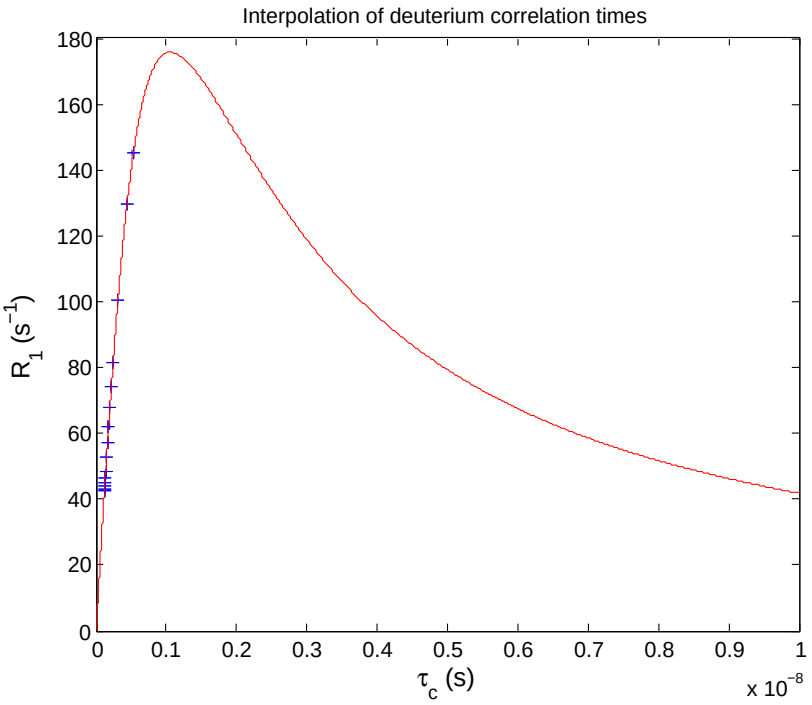

Figure 4.22: *Numerically calculated ^2H correlation times from pure trehalose-water samples.*

4.4.2 ^{2}H correlation times for trehalose-water samples at $20°C$

To test the concentration dependence of correlation time, the correlation time for the trehalose-water samples at 20°C were calculated numerically using the mean order parameter found. See figures 4.22 and 4.23. The reason for choosing interpolation to calculate the correlation time here instead of fitting to the previously used equation for correlation time as function of temperature, is that this equation contains the variable T_0 and τ_0, which the emulsion data had shown were slightly dependent on concentration.

Figure 4.24 shows that there is a clear increase in τ_c with concentration indicating trehalose-trehalose interactions at least down to 75mM trehalose, perhaps even 50mM.

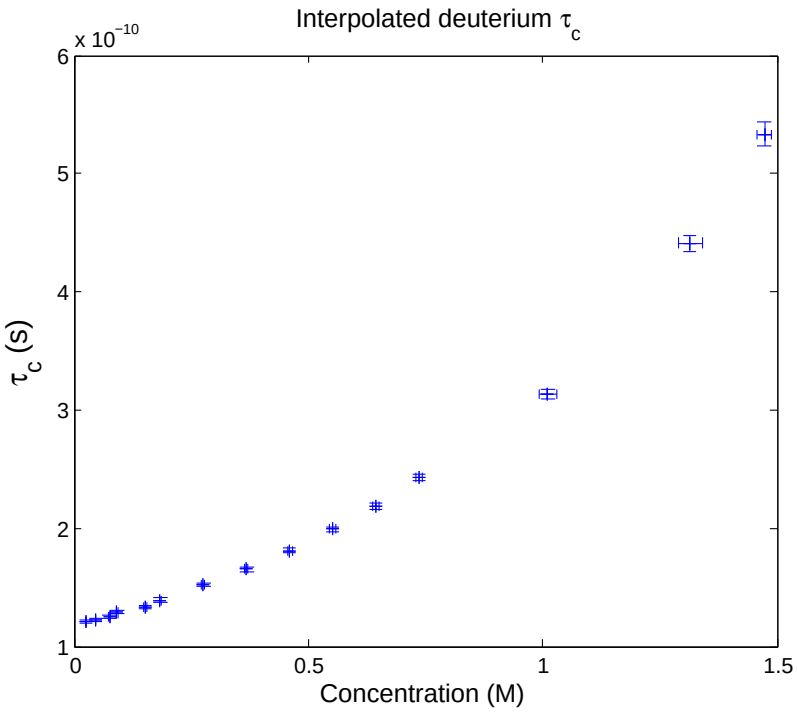

Figure 4.23: *Numerically calculated ^{2}H correlation times from pure trehalose-water samples.*

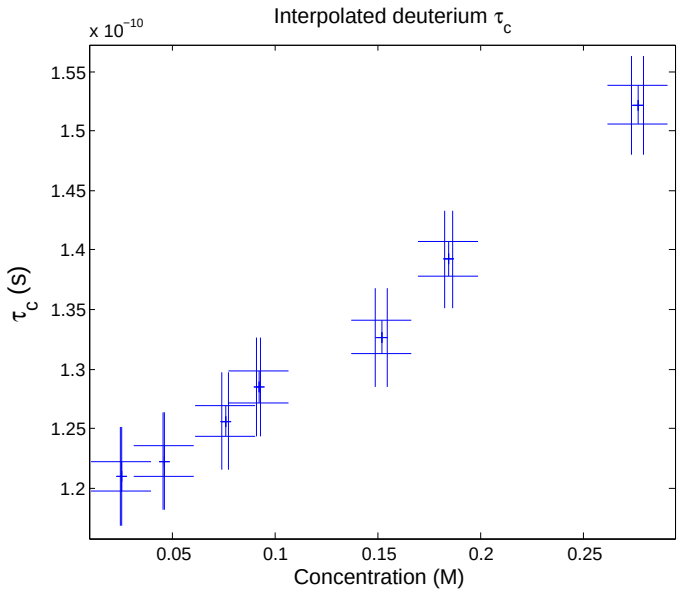

Figure 4.24: *Zoom in of previous figure.*

4.4.3 Estimation of the effect of hydrodynamic interactions on the rotational correlation time

The small increase in rotational correlation time with concentration in the low concentration range may well be due to hydrodynamic interactions between the trehalose molecules. In order to test if this is the case, it must be determined if this effect is large enough to account for the increase measured.
Particles diffusing in a liquid interact not only when they collide with each other, but also (when they get close) via the surrounding water. The translation and rotation of the particle creates a flow in the adjacent water, and this flow in turn affects the translation and rotation of nearby particles. If we consider a rotating sphere that does not translate, the water perturbed by the rotating motion is distributed in a spherical shell around the particle. The influence this has on neighbouring particles can be estimated by associating each particle (radius a) with their own free volume described as a water sphere of radius R around it. The larger the concentration, the smaller the free volume will be. Since the effect of particle rotation on the adjacent water decreases with R, also the perturbation of the rotation of neighbouring particles decreases with R. The effect on the rotational diffusion coefficient can roughly be described with the following equation:

$$D_r = D_r^0(1 - k_1\left(\frac{a}{R}\right)^3) \tag{4.28}$$

Where k_1 is a constant and D_r^0 the rotational diffusion coefficient at infinite dilution. By changing the constant, $\left(\frac{a}{R}\right)^3$ can be rewritten into the volume fraction ϕ of the solute/particle:

$$D_r = D_r^0(1 - k_2\phi) \tag{4.29}$$

In the presence of hydrodynamic interactions the time correlation function probed by NMR relaxation does not decay perfectly exponentially at the short time scales, but at longer time scales the decay becomes exponential. The long time decay is most important for R_1 since we are close to the extreme narrowing limit at 20°C.

Jones (1989) [83] calculated the long time rotational diffusion for colloid particles in NMR, modeling the particles as hard spheres (impenetrable and no overlaps in space) and using stick boundary conditions. The latter means that when the boundary conditions of the fluid flow at the particle surface was given, it was assumed that the particle interacts so strongly with the layer of fluid right next to the particle surface, that this fluid moves with the same velocity as the particle. The result was that the long time diffusion coefficient D_r^l as a function of the volume fraction of the solute ϕ can be expressed as:

$$\frac{D_r^l}{D_r^l(0)} = 1 - 0.67\phi + O(\phi^2) \tag{4.30}$$

Where $D_r^l(0)$ is the long time rotational diffusion coefficient at infinite dilution.
In this model the particles are randomly placed in the liquid, so some of them are touching. The model is very rough since it assumes that the particles are spherical, and that the medium in which the particles are diffusing (water) can be modelled as a continuous medium. Whether the water can be seen as a continuous solvent or not depends on the

size of the diffusing particles relative to the size of water molecules. If the diffusing particles are much larger than water molecules, as is the case for colloids, it is fair to assume a continuous medium. But trehalose is not much larger than water molecules, which means that increasing concentration will have a smaller effect on D_r than in the model by Jones (1989). The reason is that the effect is strongest when the distance between two particles is smaller than 1 Å for small molecules (the limit lies higher for larger molecules), but in reality they do not get that close since it is not favourable for the hydration water molecules to be removed.

Thus if the slope of $D_r/D_r(0)$ as a function of ϕ is numerically larger than 0.67 at low concentrations, then the increase in τ_r cannot be explained by hydrodynamic interactions and there are attractions/aggregation tendencies even at low concentrations.
The rotational diffusion coefficient can be calculated as (see theory section):

$$D_r = \frac{1}{6\tau_r} \tag{4.31}$$

The volume fraction of trehalose was calculated from the molar concentration c:

$$\phi = c \cdot V_{tre}^p \tag{4.32}$$

- The molar volume was calculated in 2 different ways: From the partial molar volume of trehalose and from a sphere with a diameter that equals the longest dimension of the trehalose molecule, measured on the chemical structure of trehalose in Chimera, see fig. 4.25.

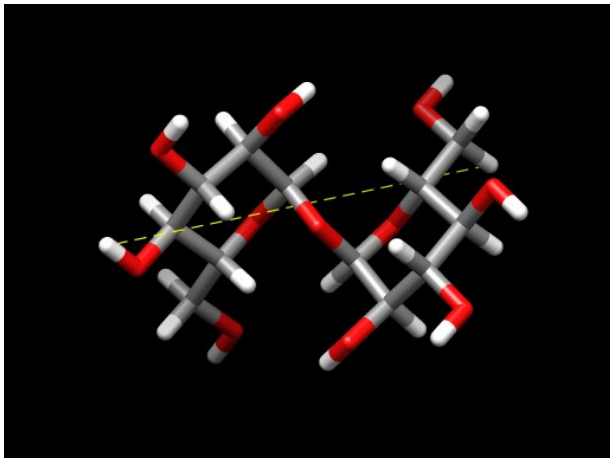

Figure 4.25: *The longest atom-atom distance in trehalose measured with Chimera: 9.42 Å.*

$D_r(0)$ was calculated by extrapolating D_r to $\phi = 0$, and $D_r/D_r(0)$ is plotted in figure 4.26. The slope of this plot was calculated from 3 neighbouring points see figure 4.27. It shows that the slope is indeed larger than 0.67 for all concentrations, and the trehalose-trehalose interactions are thus not (only) hydrodynamic interactions.

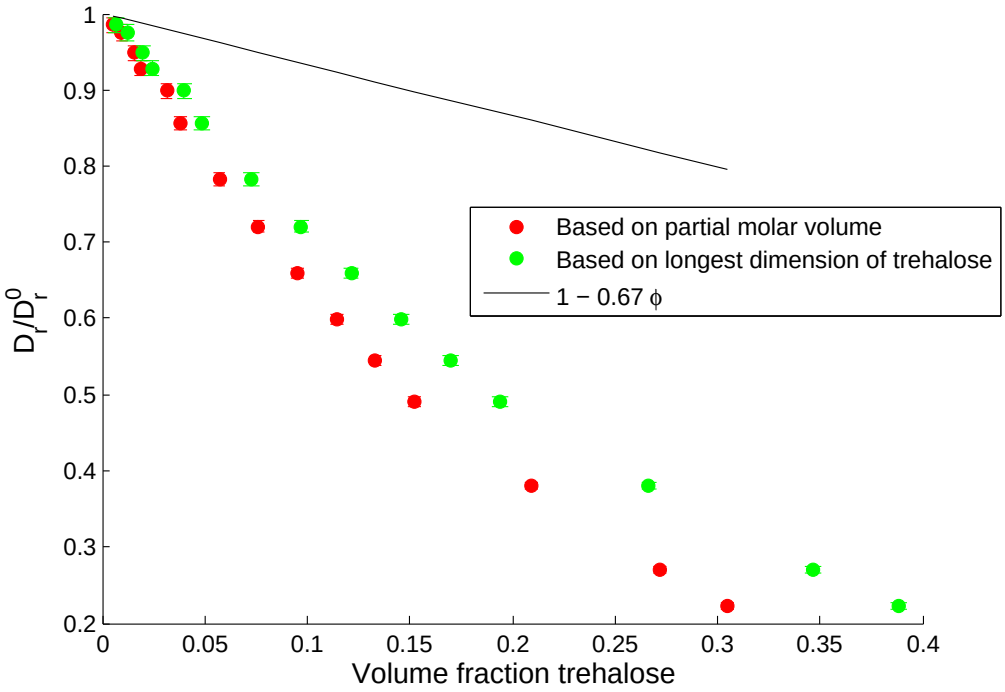

Figure 4.26: *$D_r/D_r(0)$ as function of the volume fraction of trehalose calculated in 2 different ways all assuming a spherical shape of trehalose but different radii: 1) radius calculated from the partial molar volume, 2) radius set equal to half the longest atom-atom distance in trehalose.*

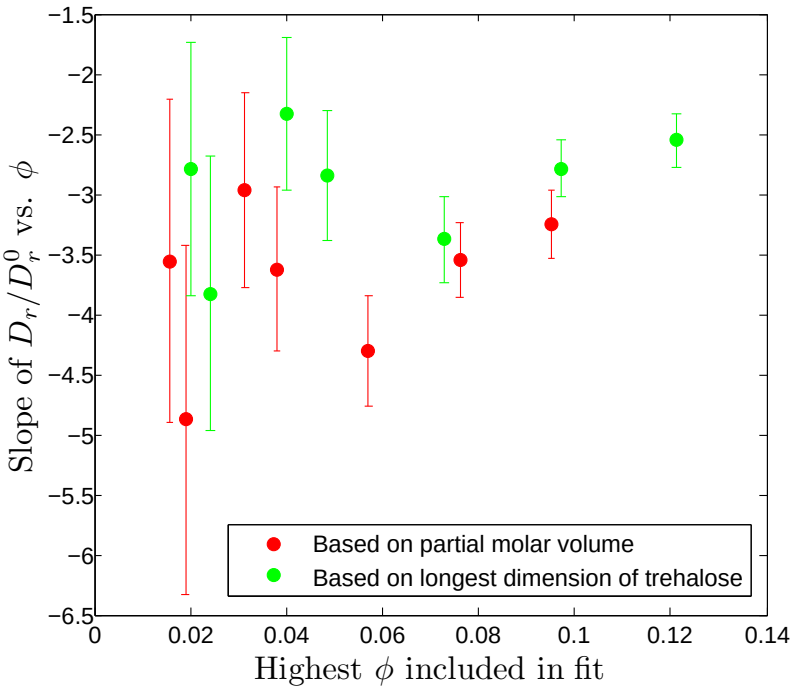

Figure 4.27: *The slope of linear fit of $D_r/D_r(0)$ vs. volume fraction of 3 neighbouring points as a function of the highest concentration included in the linear slope fit.*

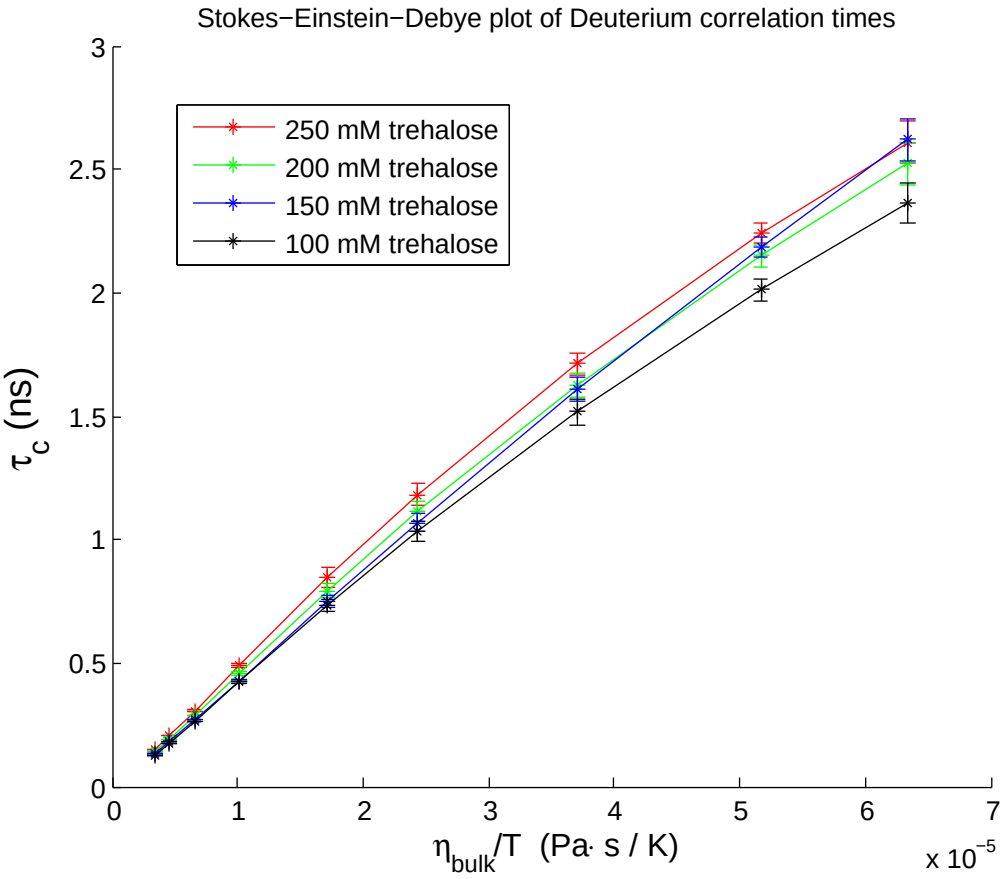

Figure 4.28: *Testing the Stokes-Einstein-Debye equation.*

4.4.4 Analysis using Stokes-Einstein-Debye equation

If there are trehalose-trehalose interactions/attractions even at low concentrations as indicated by the calculations in the previous section, then the Stokes-Einstein-Debye (SED) equation should also not be fulfilled, due to the fact that the SED equation was derived on the assumption that there are no solute-solute interactions (see Theory section).
The Stokes-Einstein-Debye equation reads (eq. 2.9):

$$\tau_c = \frac{V_h \eta}{k_B T} \tag{4.33}$$

Recall that V_h is the hydrodynamic volume of the solute and η is the medium viscosity, in this case bulk water viscosity.
Since there is a small increase in τ_c even at the lowest concentrations, the concentration dependence of τ_c clearly does not follow the Stokes-Einstein-Debye equation, the right side of the equation should be independent of concentration and thus τ_c should also be constant.
To investigate whether the rotational correlation time follows the temperature dependence given by the Stokes-Einstein-Debye relation, the rotational correlation time was plotted as a function of η/T which according to the relation should give a straight line, see figure 4.28.

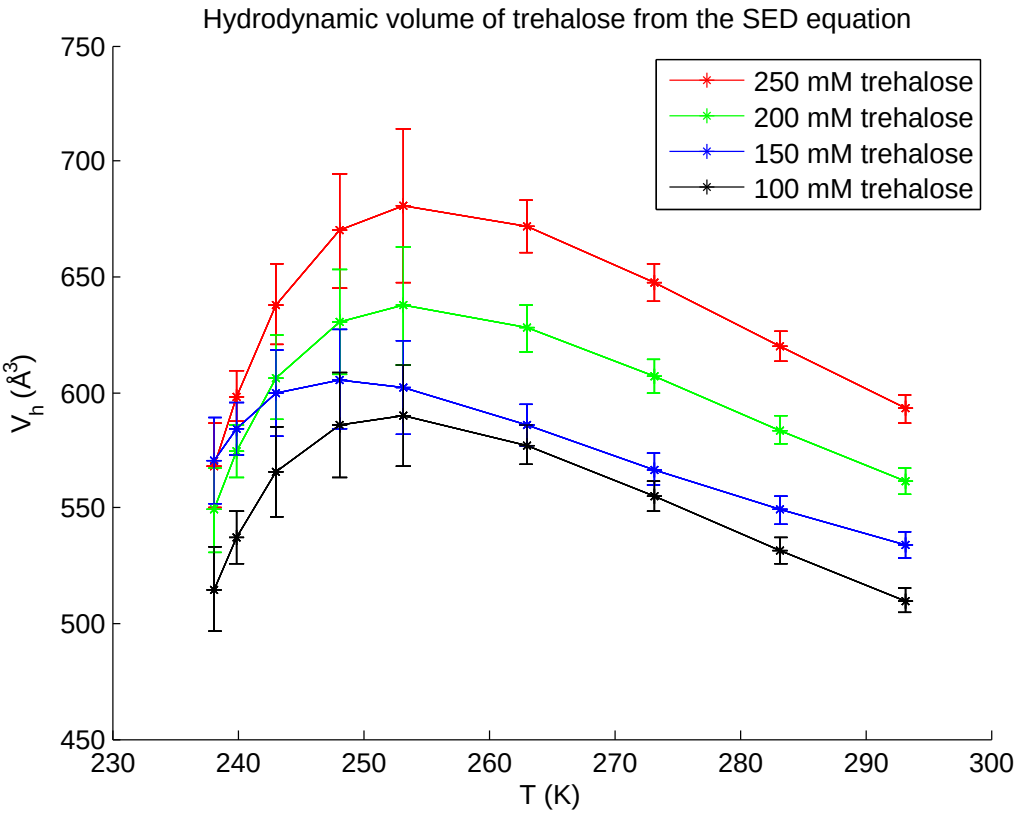

Figure 4.29: *The hydrodynamic volume of trehalose calculated with the Stokes-Einstein-Debye equation.*

It is clear that at least at the three lowest temperatures, the plot deviates from linearity. The Stokes-Einstein-Debye equation can also be used to calculate the hydrodynamic volume:

$$V_h = \frac{\tau_c k_B T}{\eta} \tag{4.34}$$

The error in V_h was calculated from the error in τ_c:

$$\sigma_{Vh} = \frac{\partial V_h}{\partial \tau_c}\sigma_\tau = \frac{k_B T}{\eta}\sigma_\tau \tag{4.35}$$

- Although the SED relation may not be fulfilled, in which case it is not possible to calculate V_h this way, the variations in the apparent V_h may tell us something about the system. The temperature dependence of the calculated hydrodynamic volume is plotted in figure 4.29.

If the Stokes-Einstein-Debye equation was fulfilled at least in some temperature range, the calculated hydrodynamic volume should be constant in that range. But V_h is not constant at all, so the SED relation is either not true for this system because of transient trehalose-trehalose interactions or the observed variations are caused by actual changes in the hydrodynamic volume. And even though at first sight the plot in figure 4.28 could be linear in some range, the variations in V_h show that it is not linear in any part of the measured temperature range.
Interestingly V_h shows a maximum, and on average it is smaller and much more temperature dependent in the slow motion/cold regime. For comparison the molecular volume

of a trehalose molecule at 20°C is 343.5 Å^3. Under the assumption that the trehalose molecule is a sphere its radius is then 4.34 Å. The largest calculated hydrodynamic volume gives a radius of 5.46 Å, which is 1.12 Å larger. This is less than half a water layer.

The temperature dependence of V_h may be due to three different reasons:

- Temperature-dependent trehalose-trehalose interactions or perhaps even aggregation, in which case real changes in V_h should occur. If the interactions are short-lived it would be more reasonable to represent them as a temperature and concentration dependent effective viscosity than a varying hydrodynamic volume.
- A real change in the hydrodynamic volume due to a temperature-dependence of the number of strongly hydrated water molecules/the size of the hydration layer.
- A temperature dependent conformational equilibrium.

The reality could be a combination of the possibilities listed. The concentration dependence of the rotational correlation time shows that there are indeed trehalose-trehalose interactions, the question is then if they can also account for the temperature dependence of V_h, that is if the interactions are temperature dependent enough.
Whether the temperature dependence of V_h is (at least partially) caused by changes in the hydration layer, can be tested by comparing with the ^{17}O relaxation data, which gives the water dynamics. This will be investigated in a later section (sec. 4.6.2).

The concentration dependence of the hydrodynamic volume at different temperatures is shown in figure 4.30. The concentration dependence is not the same at all temperatures.

The hydrodynamic volume of trehalose in the trehalose-water samples at a constant temperature of 20^oC was also calculated and plotted in figure 4.31, to see the behavior over a larger concentration range. The plot shows that the concentration dependence can only be approximated with a straight line at low concentrations.

The extreme increase in V_h with concentration seen in figure 4.31, is however *not* a realistic change in the hydrodynamic volume. At relatively high trehalose concentrations, there will be solute-solute interactions, just because of the short distance between them, also if the solute does not self-aggregate. This interaction will slow (=increase) the rotational correlation time and show up as an increase in V_h in figure 4.31, even if the solute is still in its monomer form and has not changed size.
But the calculations on the rotational diffusion coefficient as a function of volume fraction in the previous section, showed that the change in rotational correlation time cannot only be accounted for by these hydrodynamic interactions, but must be due to trehalose-self-association even at the lowest concentrations.

To sum up the concentration dependent increase in V_h seen already at low concentrations may be caused by either:

- Short-lived trehalose-trehalose interactions, in which case the SED relation does not hold at any concentrations.
- Long-lived trehalose-trehalose interactions resulting in aggregates. In this case the SED relation holds at low trehalose concentrations.

- Or of course something in between.

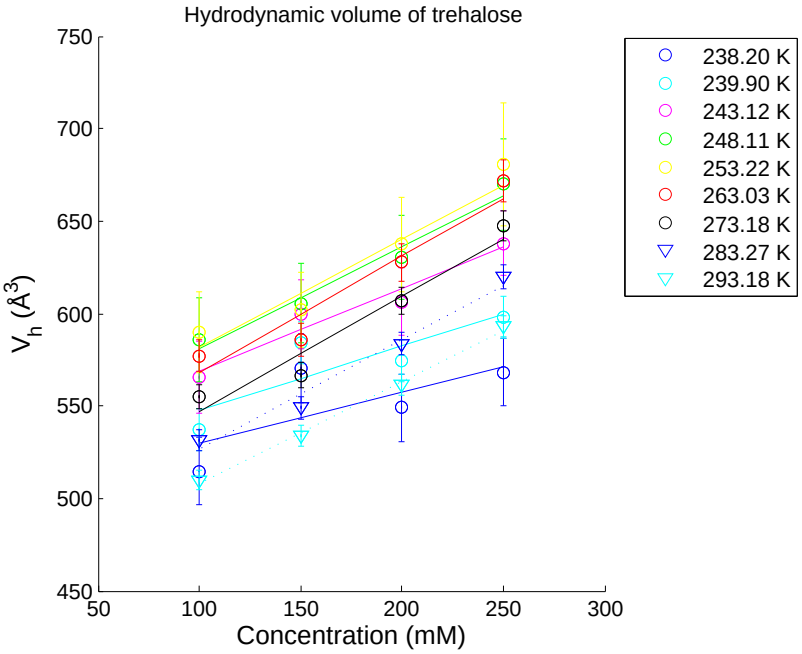

Figure 4.30: *The concentration dependence of the hydrodynamic volume calculated with the Stokes-Einstein-Debye equation. Each series of points was fitted to a straight line.*

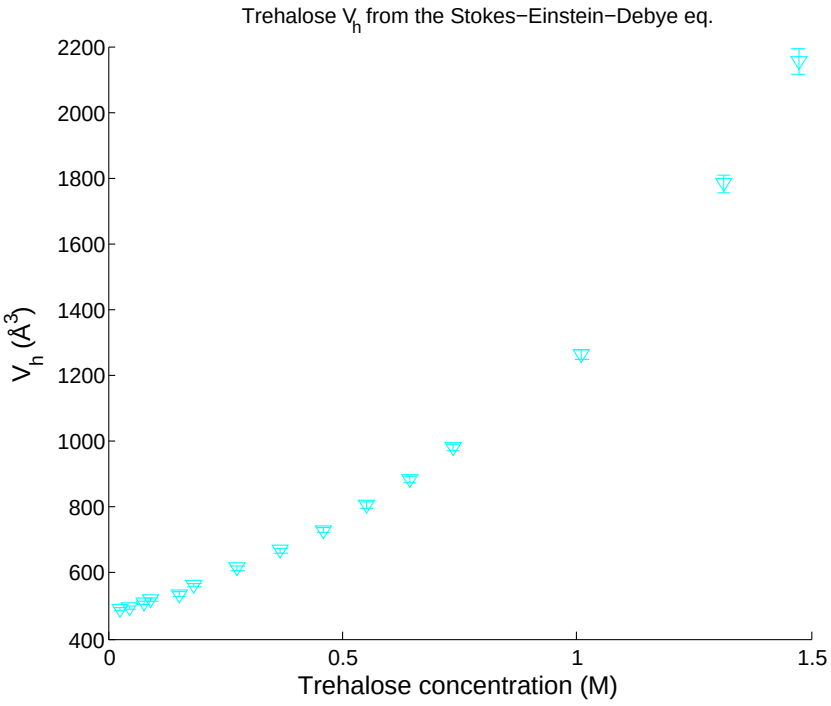

Figure 4.31: *The hydrodynamic volume calculated with the Stokes-Einstein-Debye equation and bulk water viscosity.*

It is difficult from our data to determine which of the three possibilities listed above is the most realistic. Instead we turn to the results of a Molecular Dynamics study of trehalose-self-association by Sapir et al. (2011) [77] Their study shows that trehalose aggregates in their entire concentration range: 0.2-1.8 M and the cluster decay time in this concentration range ranges from 11-360 ps (at 298K). The range of our measured rotational correlation times is 121-534 ps at 293K and concentrations ranging from 0.025-1.5M. So the life time of trehalose aggregates is short compared to the rotational correlation time. Thus the aggregation effect should not be taken into account by a concentration dependent hydrodynamic volume, but instead an increased concentration dependent effective viscosity. If you look from the perspective of one trehalose molecule that shortly aggregates with other trehalose molecules, they will slow the molecule down. These heterogeneities should give an effective viscosity that is larger than bulk water viscosity. Only if the solution is homogeneous and the concentration fairly low would the viscosity felt by the solute equal bulk water viscosity.
The viscosity that is usually measured with different kinds of viscometers is called the macroscopic viscosity and is measured with an object (fx. a rotating pendulum) that is a lot larger than the molecules present in the solution. Therefore it is not the viscosity that each molecule in solution feels when it moves around - called the microscopic viscosity. This viscosity can be difficult to predict because it is affected by small heterogeneities and hydration layer size which are perhaps not well described.
It is however possible to estimate the microscopic viscosity from the rotational correlation time, using again the Stokes-Einstein-Debye equation:

$$\eta_{eff} = \frac{\tau_c T k_B}{V_h^0} \tag{4.36}$$

Where V_h^0, the hydrodynamic volume of trehalose at infinite dilution was found by extrapolating the hydrodynamic volume calculated from water viscosity (fig. 4.31) to c = 0. This gave a volume of $V_h^0 = 480.45$ Å^3. The result can be seen in figure 4.33.
It was earlier shown that the Stokes-Einstein-Debye equation does not hold for the trehalose-water system, so in principle we cannot use this equation. But the effective viscosity is here *defined* from the Stokes-Einstein-Debye equation as shown above.
To compare the effective viscosity to the macroscopic trehalose-solution viscosity I looked for studies that measure the concentration and temperature dependence of this variable. But I have been unable to find any trustworthy, tabulated experimental studies that measure trehalose viscosity at both low concentrations (<10 wt% or 0.3 M) and temperatures below $0°C$.
Thus I chose to only calculate the effective viscosity at $20°C$, since Magazu et al. (1999) [70] has nice tabulated data in our concentration range at this temperature. This study measured the viscosity of trehalose solutions with standard Ubbhelode viscometers (capillary based method) of different capillary sizes.

Figures 4.32-4.33 show that the effective viscosity is lower than the macroscopic viscosity at all concentrations and higher than pure water viscosity. At low trehalose concentrations the effective viscosity is very close to the macroscopic viscosity, which means that in this range surprisingly $\tau_c \propto \eta_{mac}$. Furthermore the effective viscosity increases less steeply with concentration than the macroscopic viscosity, so the gap between them increases with concentration especially above about 1 M. This is exactly what would be expected for short-lived concentration dependent trehalose aggregation. The macroscopic viscosity

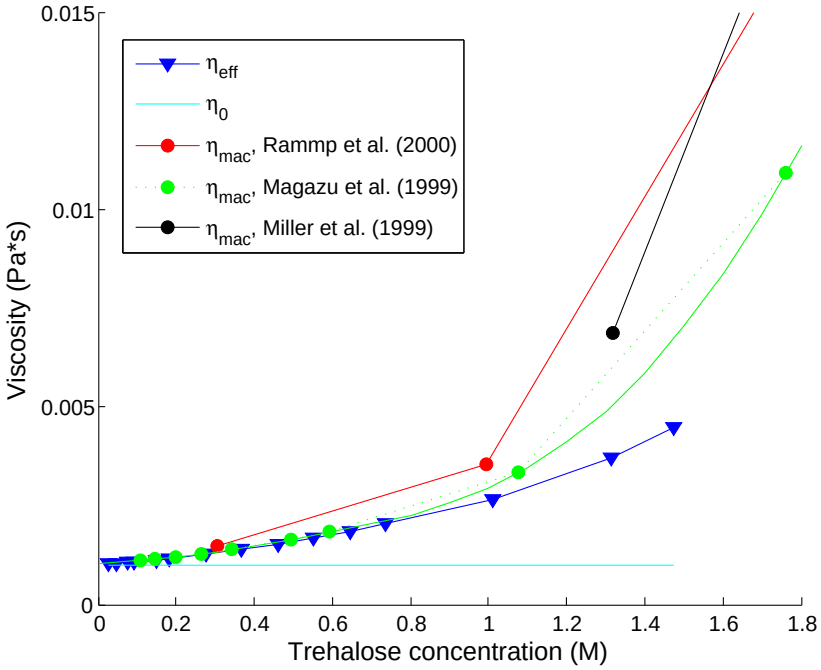

Figure 4.32: *Comparison of the effective viscosity of trehalose with the macroscopic trehalose viscosity measured by different groups, all at* $20^{\circ}C$*. The full green line is a spline interpolation.*

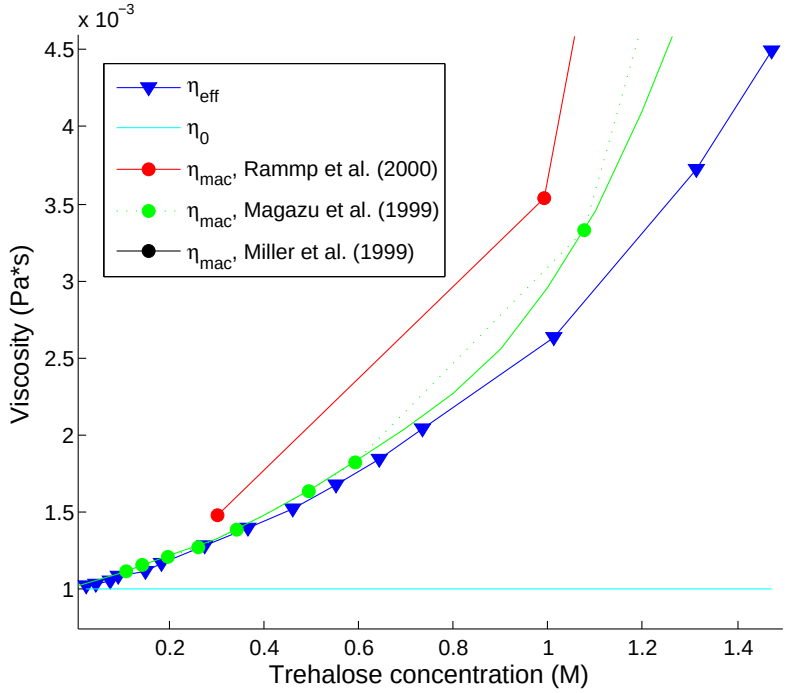

Figure 4.33: *Zoom in of previous figure.*

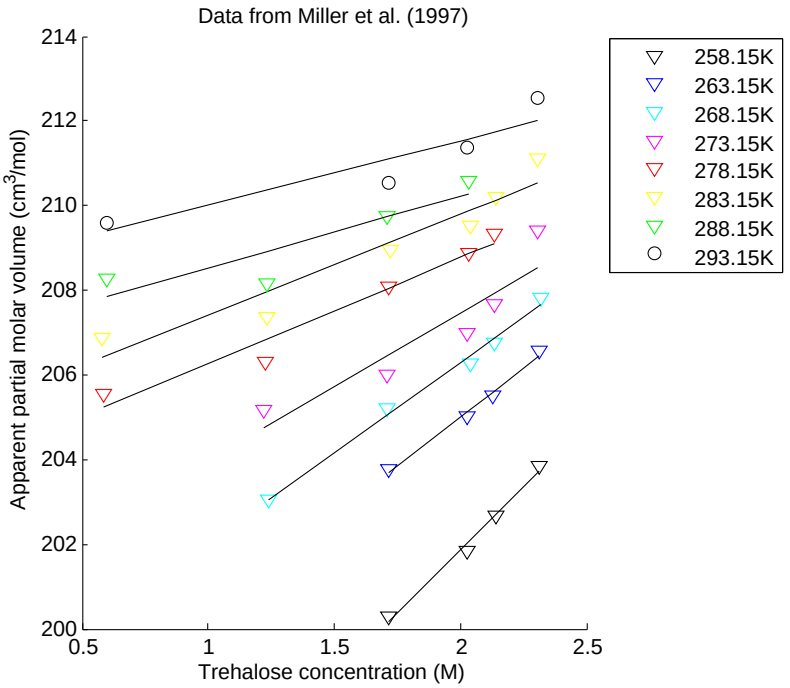

Figure 4.34: *The concentration and temperature dependence of the apparent partial molar volume of trehalose measured by Miller et al. (1997).*

shown probes longer time scales and volumes, so it will be more affected by the formation of large aggregates than the microviscosity felt be individual trehalose molecules if their interactions with the aggregates are short.

4.4.5 Temperature and concentration dependence of the partial molar volume

To check if the temperature and/or concentration dependence of the hydrodynamic volume is primarily due to intramolecular changes in trehalose, I checked the literature for studies on the concentration and temperature dependence of the partial molar volume. The only study I could find that measured the apparent partial molar volume at subzero temperatures was one done by Miller et al. (1997) [66], who calculated the apparent partial molar volume of trehalose from density measurements of samples with varying trehalose concentration. Their data can be seen in figure 4.34. The data was fitted to straight lines (fig. 4.34) to get the concentration dependence of the partial molar volume. The slopes are plotted in figure 4.35.

The linear slope from measurements at 20^oC shows that the apparent partial molar volume should increase by 1.09% when the trehalose concentration is increased from 0 M to 1.5 M.
According to data from Banipal et al. [50], the partial molar volume should increase by 1.2% when the concentration is increased from 0 to 1.5 M.
For comparison the hydrodynamic volume of trehalose calculated here increases by 342% from 0.025M to 1.5M trehalose. From the two lowest measured concentrations 0.025M to 0.05M it increases by 1.08%, which is comparable to the increase observed in partial

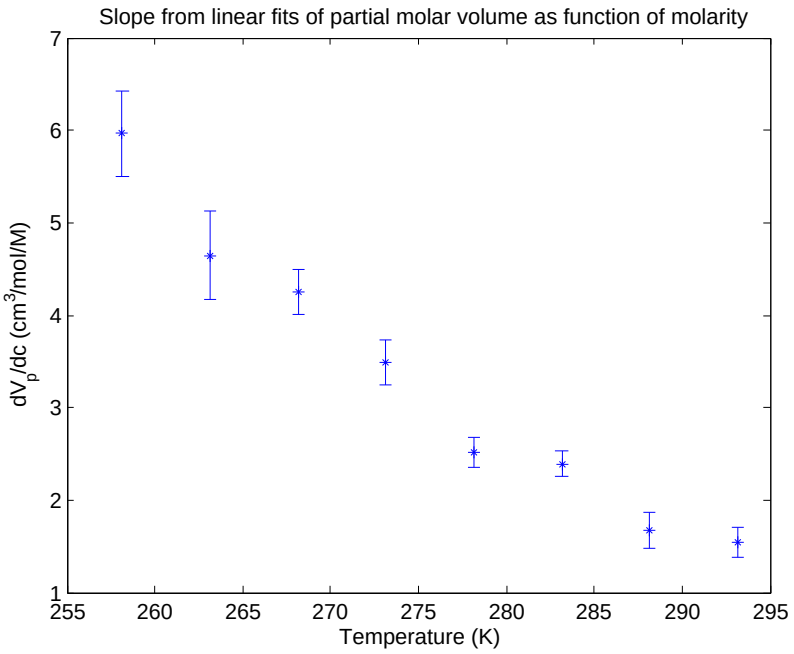

Figure 4.35: *The slopes from linear fits of trehalose partial molar volume as function of molarity.*

molar volume over the entire concentration range. Thus the increase in the hydrodynamic volume with concentration cannot be explained by increase in apparent partial molar volume at any concentration.

Miller et al. also extrapolated the partial molar volumes shown in figure 4.34 to c = 0, to get the temperature dependence of the partial molar volume at infinite dilution, shown in figure 4.36. They write that the volumes should though be taken with caution, since they are found by extrapolation to zero concentration from only 4-5 data points per temperature.

But their data shows an increase in partial molar volume with temperature in the temperature regime where we found a decrease in hydrodynamic volume!
Miller et al. [66] suggested that the increase in partial molar volume with temperature could be caused by increased trehalose folding with decreasing temperature. It has also been suggested by several other authors (eg. [69], [68]) that trehalose has a folded conformation at low temperatures or high trehalose concentration. But folding at higher concentrations should decrease the hydrodynamic volume, because the folded conformation has a smaller hydrodynamic volume, thus conflicting with the increase seen in our data. If trehalose folding is true at high concentrations, it is either not significant or it is overshadowed by trehalose-trehalose interactions that increase the hydrodynamic volume. The studies mentioned did not do measurements below the measured maximum in V_h at 250-260K, thus the temperature region in which they claim there could be increased trehalose folding with decreasing temperature, our measurements show that V_h is increasing, so it seems that trehalose folding is not relevant.

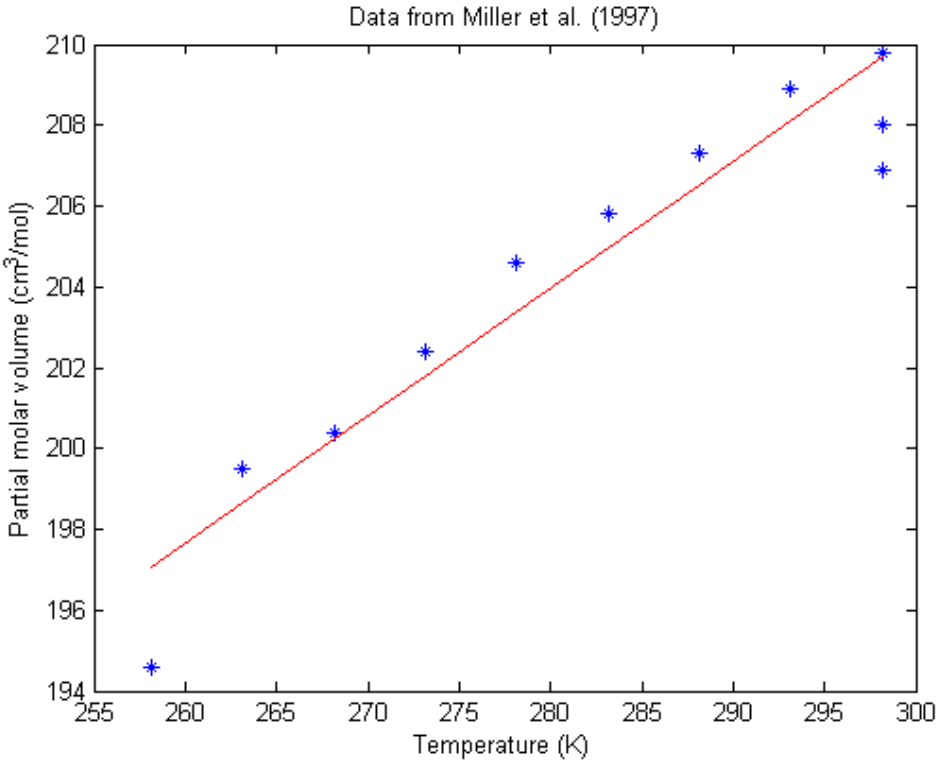

Figure 4.36: *The temperature dependence of the partial molar volume of trehalose at infinite dilution, determined by Miller et al. 1997. The two lower data points at 298K are from two other sources.*

4.5 ^{17}O relaxation

4.5.1 Concentration dependence of the ^{17}O relaxation rate

The relaxation time measured is really an average of the relaxation times of all atoms (of species i) measured on:

$$R_1 = \sum_i \frac{n_i R_i}{n_{tot}} \tag{4.37}$$

n_{tot} it the total no. of different atoms measured on and n_i is the no. of atoms of species i. In the case of ^{17}O relaxation we are only measuring on the water molecules, which can be divided into two groups: bulk water and hydration water. But the hydration water is not a static water layer, it is constantly exchanged with bulk water, so a strict division of water into two groups, bulk and hydration water is not perfectly valid. In the special case where the exchange between the two "states" is fast, also called the fast-exchange limit, it is however fair to make this assumption and 4.37 remains valid. The fast exchange limit applies if [55]:

$$\frac{1}{\tau_H} + \frac{1}{\tau_0} >> \frac{1}{T_{1,H}} - \frac{1}{T_{1,0}} \tag{4.38}$$

$T_{1,H}$ is the longitudinal relaxation time of hydration water, and $T_{1,0}$ is the longitudinal relaxation time of bulk water. τ_H and τ_0 are the rotational correlation times of hydration and bulk water respectively.
As will be shown later in this chapter, τ_0 and τ_H are on the order of 10^{-11}s, whereas $T_{1,0}$ and $T_{1,H}$ are on the order of 10^{-3}s. Therefore the inequality is satisfied by several orders of magnitude and eq. 4.37 is valid and can be rewritten to:

$$R_1 = \frac{n_{bulk} R_{bulk} + n_{hyd} R_{hyd}}{n_{not}} \tag{4.39}$$

Where n_{bulk} is the total no. of bulk water molecules in the sample and R_{bulk} is the relaxation time characteristic for the ^{17}O atoms in these molecules. n_{hyd} is the total no. of hydration water molecules in the sample and R_{hyd} is the relaxation time characteristic for the ^{17}O atoms in the hydrated water molecules. The larger the relaxation rate, the smaller the mobility of the molecule, since $R_1 = \omega_Q^2 \tau_c$. Hydration water is less mobile than bulk water, so $R_{hyd} > R_{bulk}$.
Using the relation: $n_{bulk} = n_{tot} - n_{hyd}$, this can be rearranged to get:

$$R_1 = R_{bulk} + \frac{n_{hyd}}{n_{tot}} \left(R_{hyd} - R_{bulk} \right) \tag{4.40}$$

By defining the hydration number ν_H as the number of hydration water molecules per solute molecule, the total number of hydration water molecules can be calculated as:

$$n_{hyd} = n_s \nu_H \tag{4.41}$$

Where n_s is the number of solute molecules in the sample. In this study the hydration number is furthermore defined to be the number of water molecules present in the first coordination shell or the first water layer around the solute. It is a first approximation,

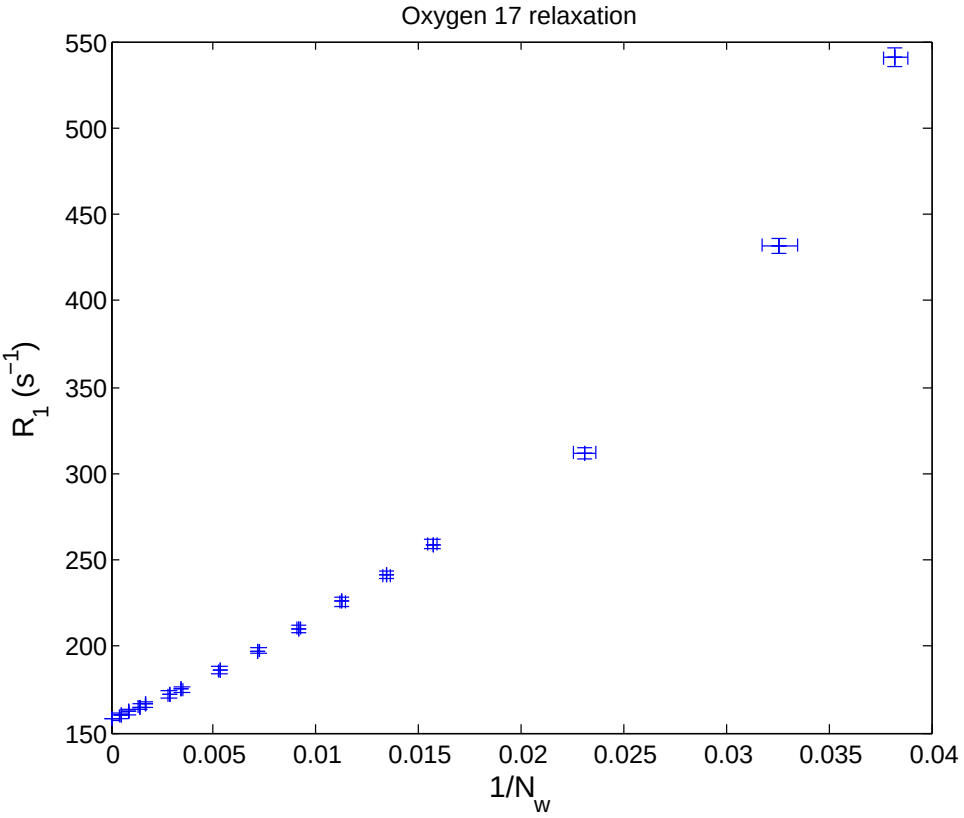

Figure 4.37: *Concentration dependence of water ^{17}O relaxation rate in trehalose solution at 19.98 ± 0.0484 °C.*

but it is based on the findings by numerous simulation studies eg. [56],[57],[58], that it is primarily the water in the first hydration shell that is perturbed, and out of the water molecules in this layer it is not the water molecules that experience H bonds to the solute, which are the least mobile, it may in fact be opposite. If the hydration number is calculated this way for all the hydration studies of different molecules which are compared, the comparisons will be justified regardless of whether this assumption is true.

The fraction of hydrated water molecules out of the total amount of water molecules, can then be calculated as:

$$\frac{n_{hyd}}{n_{tot}} = \frac{n_s \nu_H}{n_{tot}} = \frac{\nu_H}{N_w} \tag{4.42}$$

Where $N_w \equiv n_w/n_s$, $n_w = n_{tot}$ total no of water molecules. Thus we get that:

$$R_1 = R_{bulk} + \frac{\nu_H}{N_w}\left(R_{hyd} - R_{bulk}\right) \tag{4.43}$$

Plotting R_1 as a function of $1/N_w$ should therefore give a straight line with slope $\nu_H(R_{hyd} - R_{bulk})$. See figure 4.37. Since R_{hyd} is not known, it is not possible to determine the effective hydration number from the slope of the curve.

As can be seen from figure 4.37 the graph is approximately linear only up until a certain concentration, hereafter it increases more steeply.

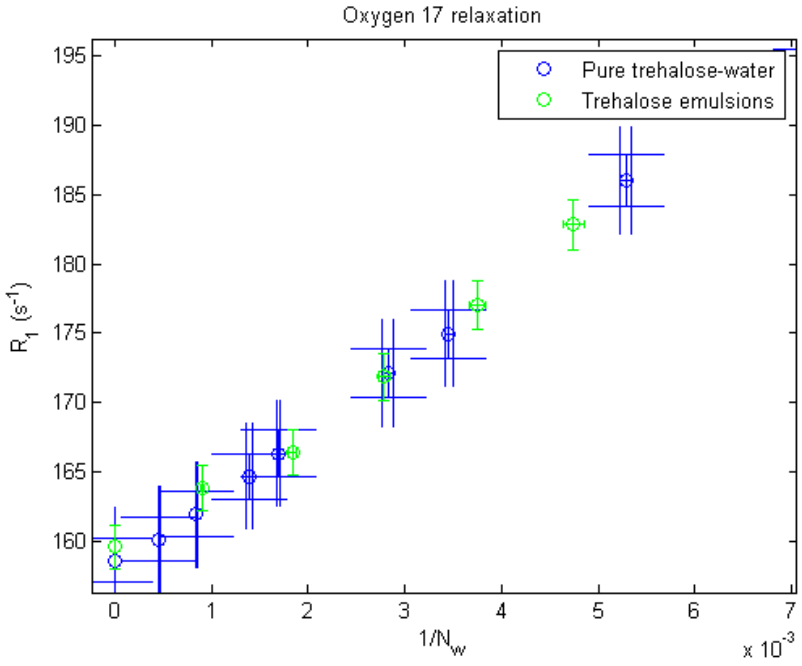

Figure 4.38: *The relaxation rate for ^{17}O atoms at 20^oC (pure trehalose-water samples: 19.98 $\pm$ 0.0484 $^\circ C$, trehalose emulsions: 20.03 $\pm$ 0.0351 $^\circ C$).*

The relaxation rate from trehalose-water samples and trehalose-water emulsions are compared in figure 4.38. It seems that there is no significant difference between the two data series, which justifies using trehalose emulsions.

By defining the reduced relaxation rate:

$$R_{red} = \frac{R_1 - R_{bulk}}{R_{bulk}} \tag{4.44}$$

Equation 4.43 can be rewritten into the form:

$$R_{red} = \frac{\nu_H}{N_w}\left(\frac{R_{hyd}}{R_{bulk}} - 1\right) \tag{4.45}$$

Now multiplying by N_w on both sides gives:

$$R_{red} \cdot N_w = \nu_H \left(\frac{R_{hyd}}{R_{bulk}} - 1\right) \tag{4.46}$$

Since the right side of the equation only has constants, the product on the left hand side must also be constant. But in reality the relaxation rates and the hydration number may not be constant at all, but instead a function of concentration / N_w, which could for example be due to hydration shell overlap because of interactions between trehalose molecules. To test whether the equation gives constant values for some concentrations, $R_{red} \cdot N_w$ was plotted in figure 4.39 and 4.40. The error bars were calculated as:

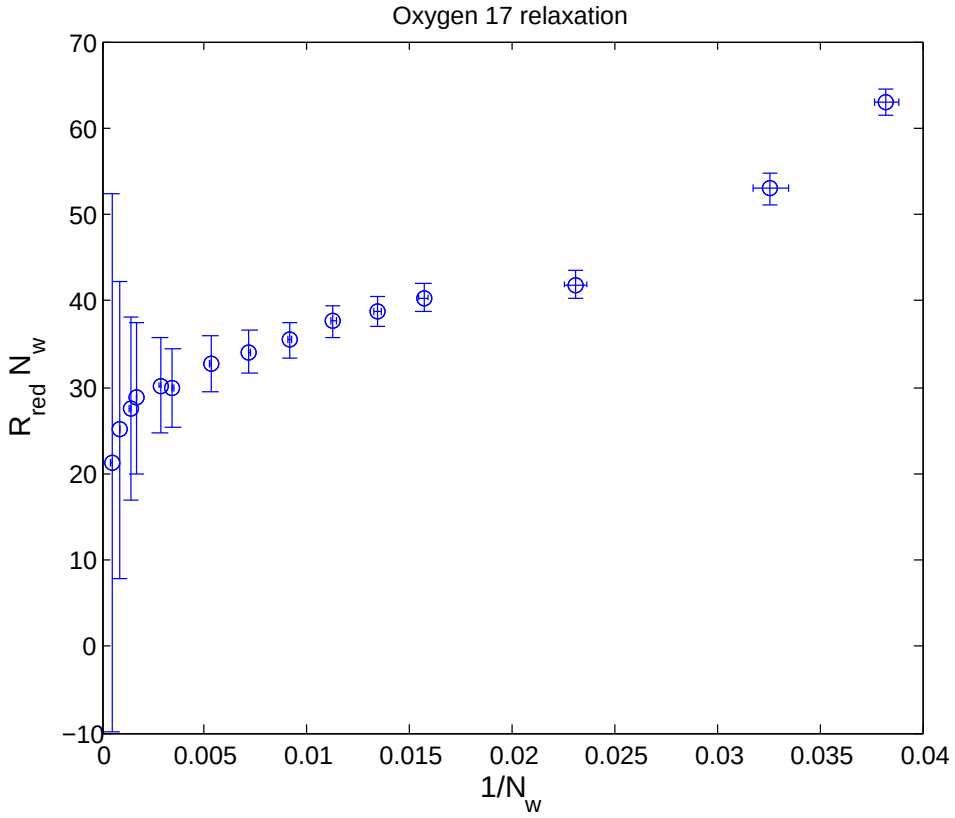

Figure 4.39: *The product of reduced relaxation rate for ^{17}O atoms and N_w at 20^{o}C.*

$$\sigma^2_{R_{red}} = \sigma^2_{R_1}\left(\frac{\partial R_{red}}{\partial R_1}\right)^2 + \sigma^2_{R_{bulk}}\left(\frac{\partial R_{red}}{\partial R_{bulk}}\right)^2 \Leftrightarrow \tag{4.47}$$

$$\sigma^2_{R_{red}} = \sigma^2_{R_1}\frac{1}{R^2_{bulk}} + \sigma^2_{R_{bulk}}\frac{R^2_1}{R^4_{bulk}} \tag{4.48}$$

And the error in the $R_{red}N_w$ product:

$$\sigma^2_{prod} = \left(\frac{\sigma_{R_{red}}}{R_{red}}\right)^2 + \left(\frac{\sigma_{N_w}}{N_w}\right)^2 \tag{4.49}$$

The figures show that $R_{red}N_w$ is not constant in any concentration regime, which means that R_1 as function of $1/N_w$ was not perfectly linear at any concentration either. But at concentrations below about 0.25 M the product can be taken to be constant within the error bars. With the uncertainties given by the experiments, we cannot determine whether the slope in the curve at this low concentrations is real or not.
Nonetheless above about 0.25 M the plot in figure 4.40 has a significant positive slope, and ν_H and/or R_{hyd} must thus be increasing (eq. 4.46).
If there is concentration dependent trehalose self-association, as was indicated by the ^{2}H relaxation data, the average apparent hydration number would decrease with increasing

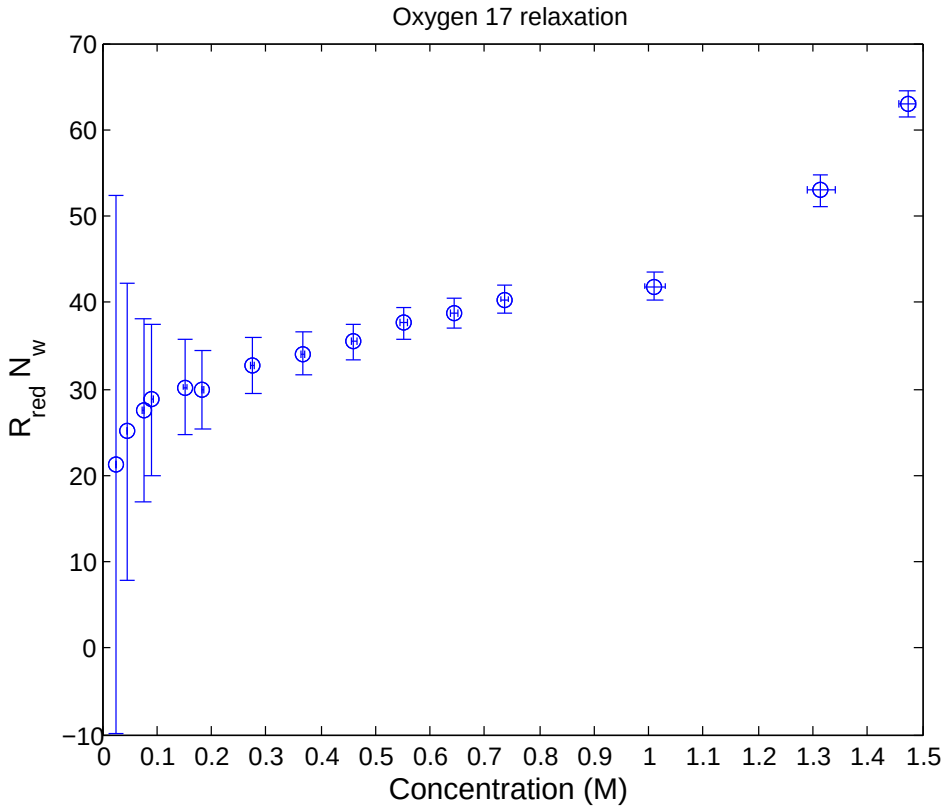

Figure 4.40: *The product of reduced relaxation rate for* ^{17}O *atoms and* N_w *at* 20^oC.

concentration because of an increasing number of hydration shell overlaps. Since we actually see an increase in $R_{red}N_w$, this means that R_{hyd} must be increasing enough to overcompensate for the decrease in ν_H.

But in order to figure out if the ^{17}O data shown really supports the result indicated by ^{2}H relaxation, that trehalose self-associates, we must figure out roughly at what concentration we would expect hydration shell overlap and thereby a non-constant $R_{red}N_w$ product, if the solution was completely homogeneous.
Since we do not know the exact hydration number it is difficult to tell where this boundary is. But as a first assumption the hydration number is again defined as the number of water molecules in direct contact with the molecule, so the number of water molecules in the first water layer surrounding the molecule. This hydration number can be calculated from the surface area.
The surface area of trehalose was calculated from molecule coordinates found on pdb.org with the online program GetArea [62] using 1.7 Å [80] as probe radius:
The solvent accessible surface area for trehalose was calculated to be: $A_s = 498.30$ Å^2. Assuming every water molecule takes up an area of $a_w = 10.75$ Å^2 [80], the hydration number can be estimated as:

$$\nu_H = A_s/a_w = 498.30\text{Å}^2/10.75\text{Å}^2 = 46.35 \tag{4.50}$$

The calculated hydration number can be used to estimate the fraction of water that is present in the first hydration shell:

$$\frac{n_{hyd}}{n_{tot}} = \frac{\nu_H n_s}{n_w} = \frac{\nu_H}{N_w} \tag{4.51}$$

The result is plotted in figure 4.41- 4.42. At 0.9584 M trehalose or $1/N_w = 0.0216$ all water molecules are in this simple model bound to trehalose.

Hydration shell overlap is much more complex than indicated by the fraction of hydration water, and actually should include complex steric considerations. But this would require computer simulations, so instead I did a more simple calculation of the surface-surface distance between adjacent water molecules assuming expanded cubic close packing and that the molecules can be treated as spheres. The result can be seen in figure 4.43. Hydration shell overlap of course happens when the surface-surface separation is smaller than two water layers, figure 4.43 shows that this occurs around 0.8 M. This concentration is a bit smaller than the limit of 0.96 M found with the non-geometric approach. If the sugar molecules were shaped as perfect cubes, there would be no difference, but since they are not, there will be small ”holes” of free bulk water even when many of the hydration shells are overlapping.

Returning to the results from the relaxation experiments, $R_{red}N_w$ showed an approximately linear increase of about 30% from ∼0.25-1 M trehalose. In this concentration range, the hydration calculations showed that the surface-surface distance decreases from roughly 4 to below 2 water layers and the fraction of hydration water increases from 0.2 to 1. So at least in the low end of this concentration range $R_{red}N_w$ presumably should be constant, because the hydration shells don’t overlap and are all identical regardless of the concentration. Whether this assumption is true will be determined later by calculating the same product for some small molecules that are not expected to aggregate.

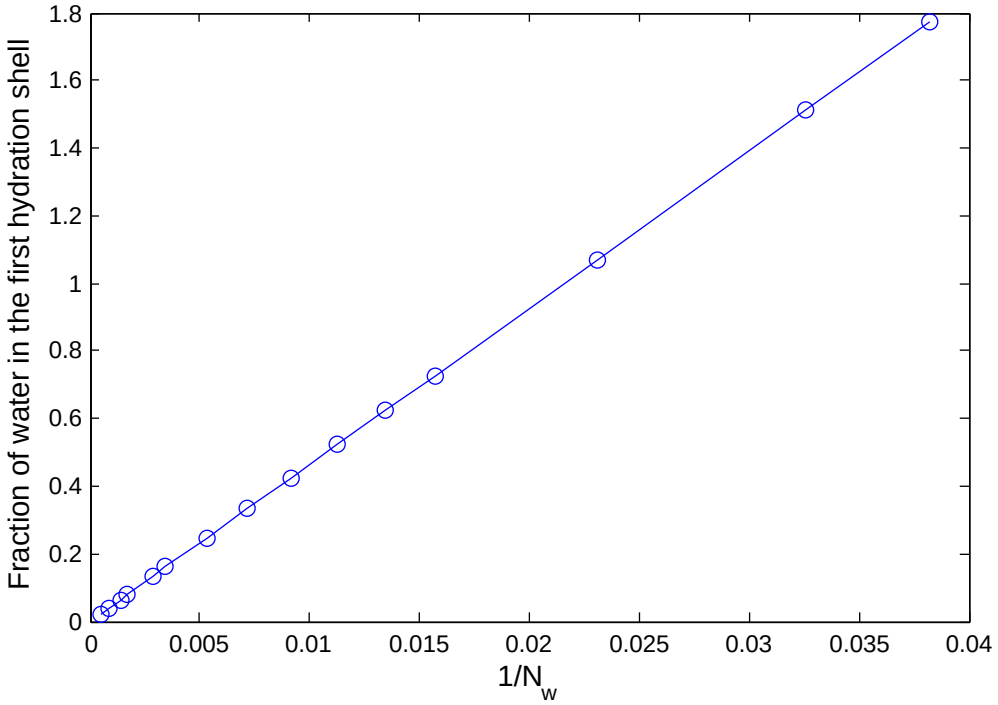

Figure 4.41: *Fraction water in first hydration shell assuming a hydration no of 46.35.*

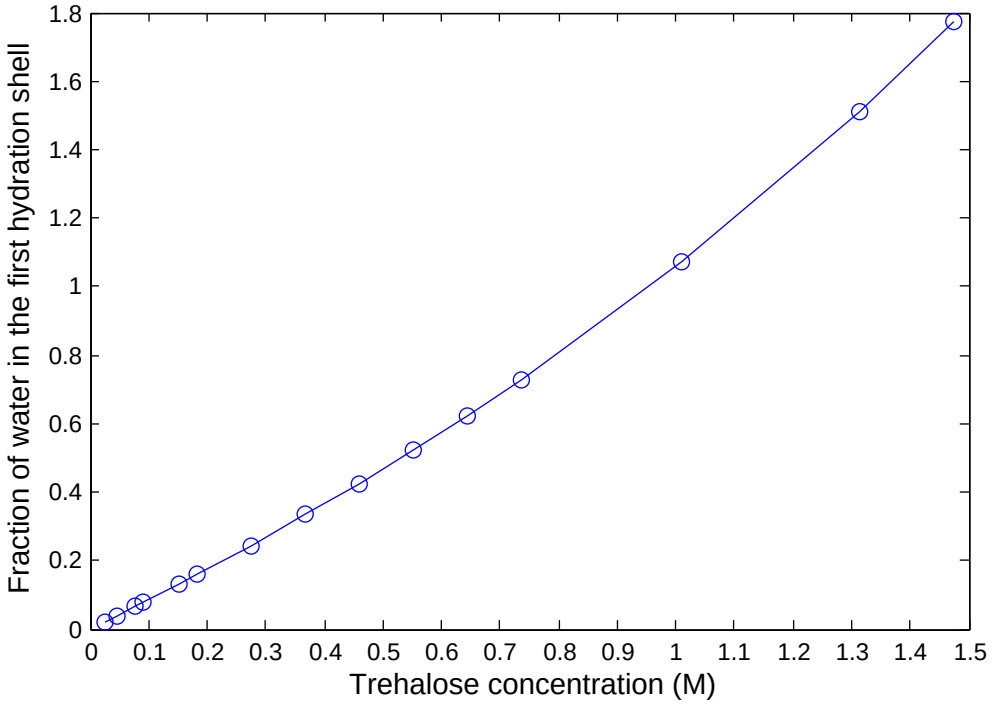

Figure 4.42: *Fraction water in first hydration shell assuming a hydration no of 46.35.*

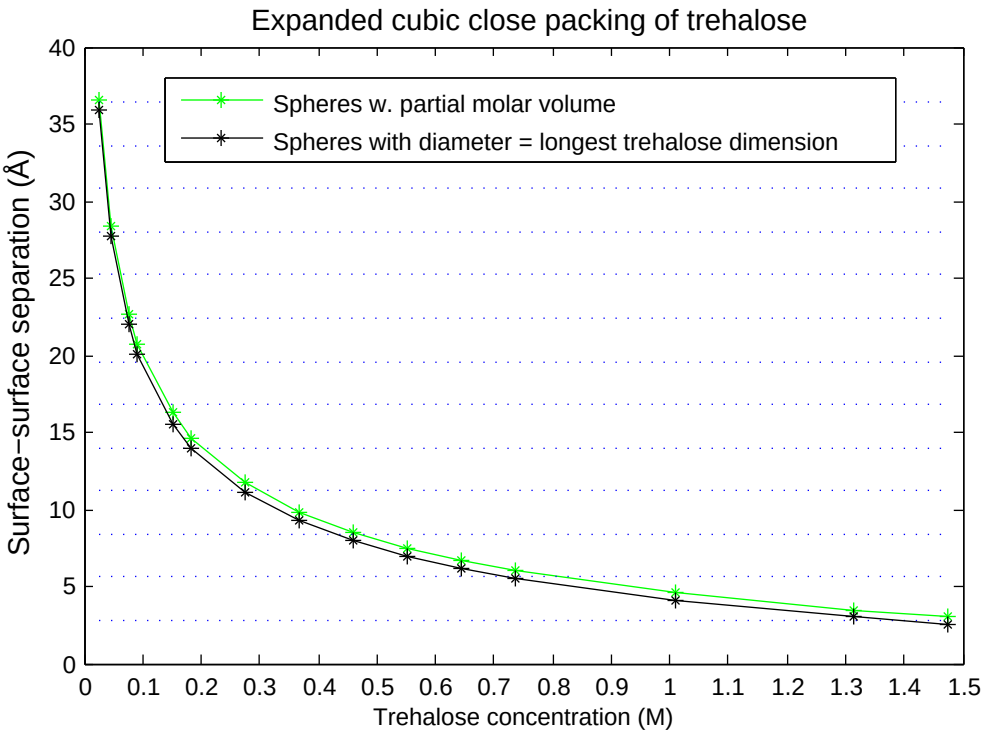

Figure 4.43: *Cubic close packing of trehalose molecules at 20^{o}C. The water layers are indicated with blue stapled lines with a separation of 2.8 Å.*

The reason for the increase in $R_{red}N_w$ could then be explained by trehalose-trehalose association, in which case some of the water molecules might be slightly confined or perhaps even bridge the trehalose-trehalose interactions, making them less mobile and thus increasing R_{hyd}.

The $R_{red}N_w$ product also shows a sharp increase around $1/N_w = 0.02$ and 1 M trehalose in figure 4.39 and 4.40. This was just the concentration where the non-geometric calculation of the fraction of hydration water in figure 4.42 shows that all water molecules are in contact with trehalose. If the assumption made by these calculations that the solution is homogeneous and trehalose does not aggregate were correct, it seems that it is the lack of bulk water that gives a large increase in R_{hyd}. Intuitively this makes sense: When all water molecules are hydrated and even more solute molecules are added to the solution, some of the water molecules will be squeezed in between two solute surfaces and thus have very little freedom to reorient, because it now only has a couple of neighbouring water molecules to hydrogen bond to. This gives the molecule a very high R_1 and it will give a large contribution to the average R_{hyd}.
But since the ^{2}H relaxation data indicates trehalose self-association, it is a bit striking that the steep increase in $R_{red}N_w$ happens at the concentration where all water is hydrated according the homogeneous model. One possible explanation is that according to the MD study by Sapir et al. (2011) [77], the trehalose clusters begin to transcend the borders of the simulation box / become “infinite” at 1.14 M trehalose, which would create many pockets of confined water molecules, if the clusters look like the results of Sapir.

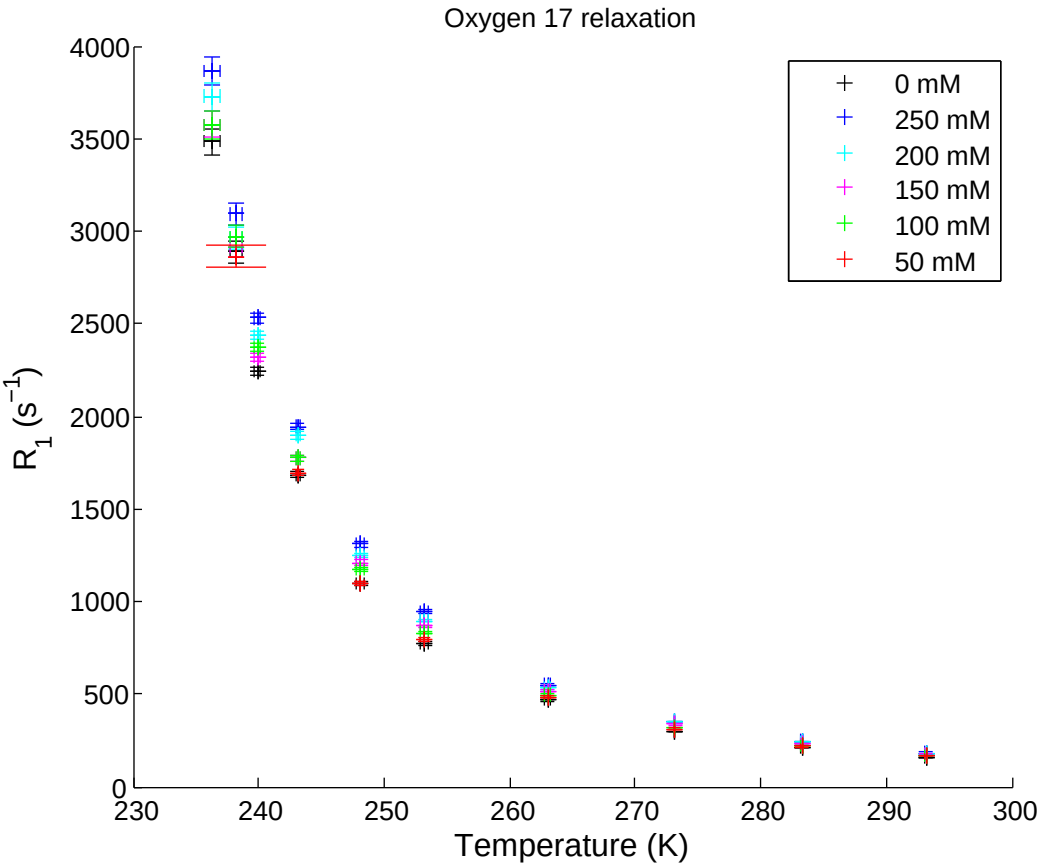

Figure 4.44: *The temperature dependence of ^{17}O relaxation rates of ^{17}O enriched water in trehalose-water solutions.*

4.5.2 Temperature dependence of the ^{17}O relaxation rate

The temperature dependence of the relaxation rate of ^{17}O is shown in figure 4.44. There is no maximum as was seen for the ^{2}H data, since the water molecules are small enough to be in the fast motion regime in the entire temperature interval, so the longitudinal relaxation is just proportional to the rotational correlation time (see Theory section):

$$R_1 = \omega_Q^2 \tau_c \tag{4.52}$$

The concentrations used in the experiments where the temperature was varied were very low: 0 - 250 mM, this means that it is a fair approximation to assume that R_{red} is linearly dependent on $1/N_w$, see figures 4.45-4.54.

The reduced relaxation rate was earlier shown to be equal to (eq. 4.45):

$$R_{red} = \frac{\nu_H}{N_w}\left(\frac{R_{hyd}}{R_{bulk}} - 1\right) \tag{4.53}$$

Where we can define the dynamic perturbation factor ξ as the ratio between the average correlation time of hydration and bulk water (assuming that bulk water and hydration

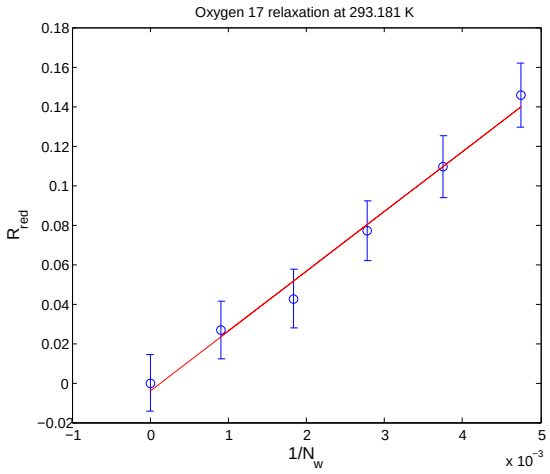

Figure 4.45: *Linear fit of R_{red} as a function of $1/N_w$.*

water has the same ω_Q):

$$\frac{R_{hyd}}{R_{bulk}} = \frac{\omega_Q^2 \tau_H}{\omega_Q^2 \tau_{bulk}} = \frac{\langle \tau_H \rangle}{\tau_{bulk}} \equiv \xi \tag{4.54}$$

Thus equation 4.53 becomes

$$R_{red} = \frac{\nu_H}{N_w} (\xi - 1) \tag{4.55}$$

Plotting R_{red} as a function of $1/N_w$ should therefore give a straight line with slope [80]

$$\nu_{dyn} = \nu_H (\xi - 1) \tag{4.56}$$

- also defined as the dynamical hydration number ν_{dyn}.
R_{red} as a function of $1/N_w$ was fitted to straight lines in figures 4.45-4.54.

So the dynamic perturbation factor can be calculated from the slope ν_{dyn}:

$$\xi = \frac{\nu_{dyn}}{\nu_H} + 1 \tag{4.57}$$

But it requires a known hydration number, which is problematic since it is debated how many water layers are dynamically perturbed and should be regarded as hydration water. Here the hydration number is as earlier set to the number of water molecules in the first hydration layer, as a first assumption. The calculated dynamic perturbation factor is plotted in figure 4.55.

The error in ξ was calculated from the error in the fitted linear slopes:

$$\sigma_\xi = \frac{\partial \xi}{\partial \nu_{dyn}} \sigma_{\nu_{dyn}} = \frac{\sigma_{\nu_{dyn}}}{\nu_H} \tag{4.58}$$

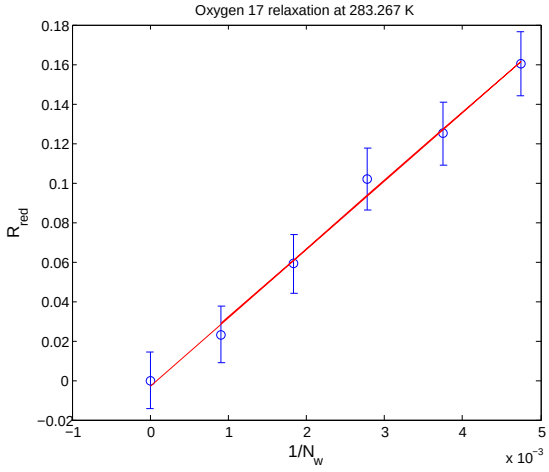

Figure 4.46: *Linear fit of R_{red} as a function of $1/N_w$.*

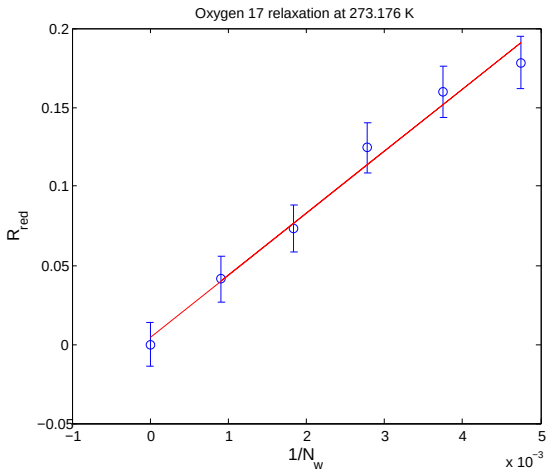

Figure 4.47: *Linear fit of R_{red} as a function of $1/N_w$.*

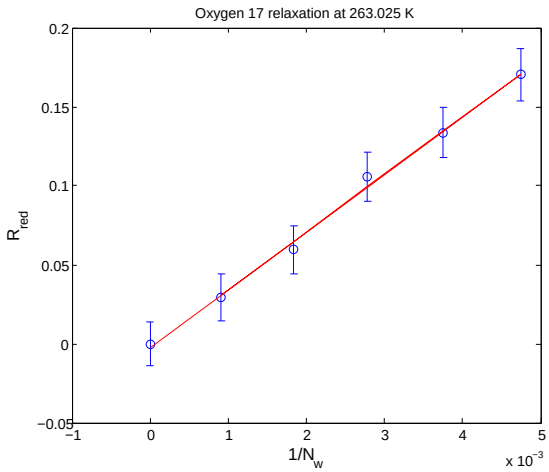

Figure 4.48: *Linear fit of R_{red} as a function of $1/N_w$.*

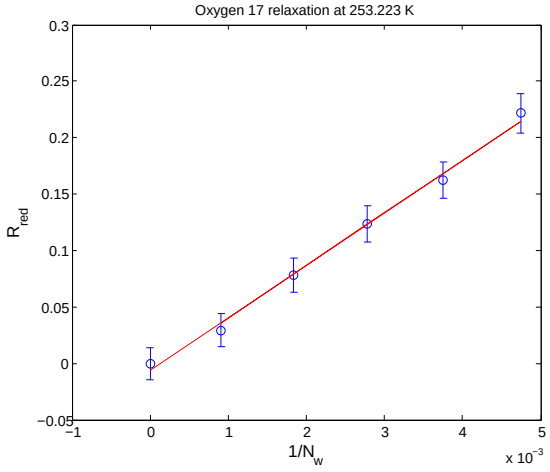

Figure 4.49: *Linear fit of R_{red} as a function of $1/N_w$.*

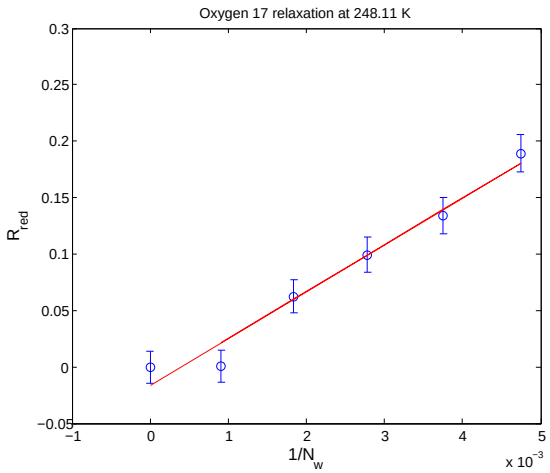

Figure 4.50: *Linear fit of R_{red} as a function of $1/N_w$.*

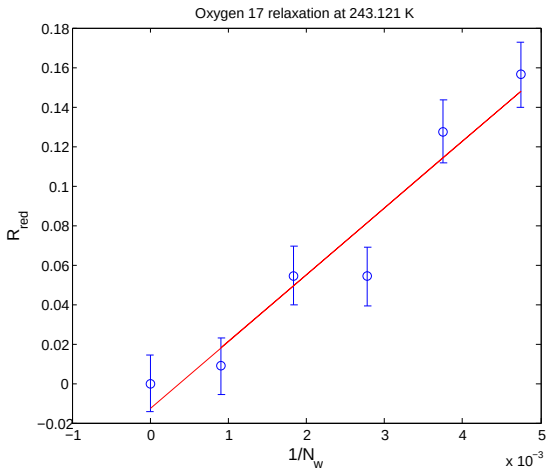

Figure 4.51: *Linear fit of R_{red} as a function of $1/N_w$.*

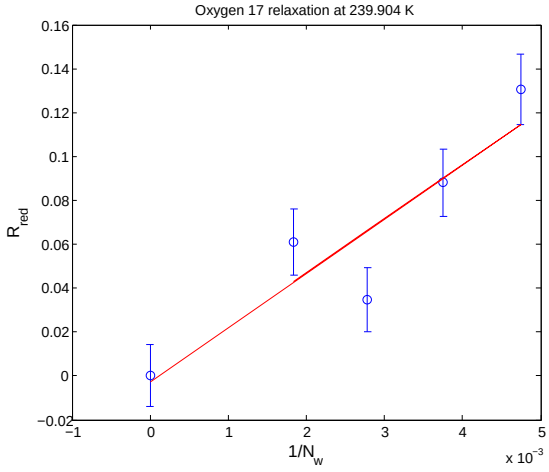

Figure 4.52: *Linear fit of R_{red} as a function of $1/N_w$.*

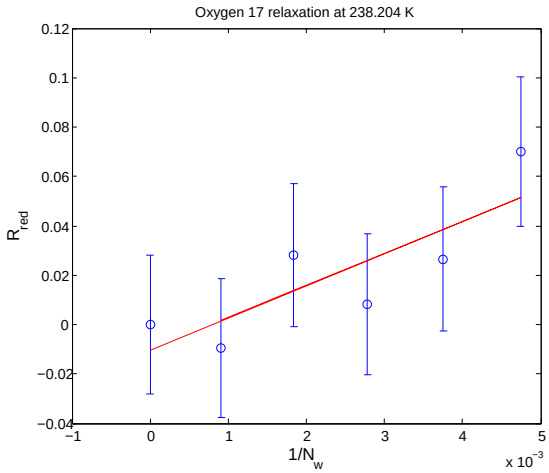

Figure 4.53: *Linear fit of R_{red} as a function of $1/N_w$.*

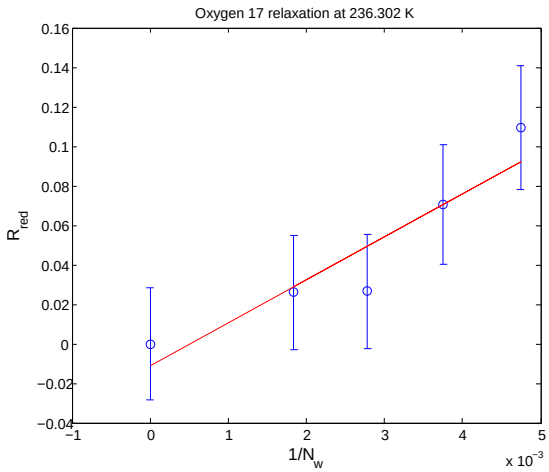

Figure 4.54: *Linear fit of R_{red} as a function of $1/N_w$.*

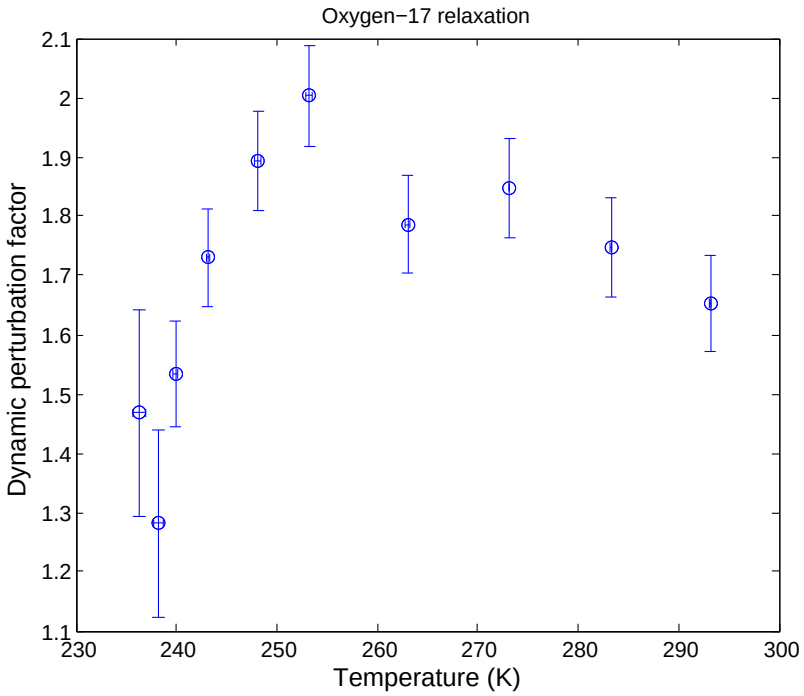

Figure 4.55: *The dynamic perturbation factor assuming a hydration no of 46.35.*

What can be read from figure 4.55, is that the rotational correlation time of hydration water is about 1.3-2 times slower than the rotational correlation time of bulk water, depending on the temperature. So the hydration water is only 1.3-2 times less mobile than bulk water. The shape of figure 4.55 is strikingly similar to the shape of temperature dependence of the hydrodynamic volume of trehalose. Whether this similarity is of relevance will be discussed in the next chapter.

The bulk water correlation time τ_0 can be calculated from the relaxation rate of pure water:

$$\tau_0 = \frac{R_{bulk}}{\omega_Q^2} \tag{4.59}$$

The error in τ_0 is:

$$\sigma_{\tau_0} = \frac{\sigma_{R_{bulk}}}{\omega_Q^2} \tag{4.60}$$

Where the nuclear quadrupole frequency is set to [47]:

$$\omega_Q = \sqrt{\frac{12}{125}\pi^2\chi_o^2\left(1+\frac{\eta_o^2}{3}\right)} \Rightarrow \tag{4.61}$$

$$\omega_Q = \sqrt{\frac{12}{125}\pi^2(8.4\cdot 10^6 Hz)^2\left(1+\frac{0.855^2}{3}\right)} = 9.12\cdot 10^6 rad/s \tag{4.62}$$

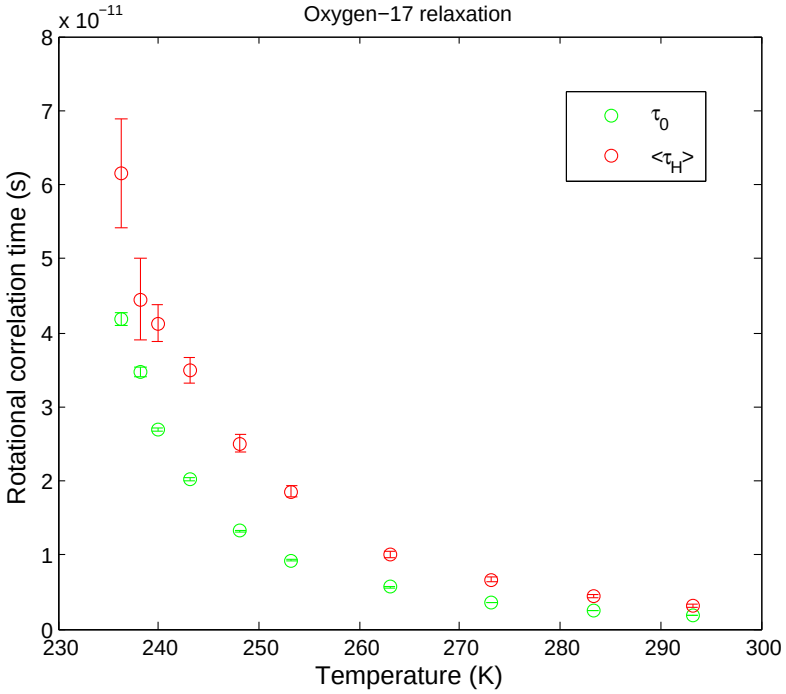

Figure 4.56: *The correlation time of bulk water compared to the mean correlation time of hydration water assuming a hydration no of 46.35.*

It then follows from the definition of the dynamic perturbation factor (eq. 4.54) that the mean hydration shell correlation time can be calculated as:

$$\langle \tau_H \rangle = \xi \cdot \tau_0 \tag{4.63}$$

The error in $\langle \tau_H \rangle$ becomes:

$$\sigma_{\tau_H} = \langle \tau_H \rangle \sqrt{\left(\frac{\sigma_{\tau_0}}{\tau_0}\right)^2 + \left(\frac{\sigma_\xi}{\xi}\right)^2} \tag{4.64}$$

The result can be seen in figure 4.56. The correlation time of the hydration water is slower than the correlation time of bulk water for all the temperatures measured, and this conclusion is independent of the hydration number chosen. But the difference between them shows a maximum which could also be concluded from the size of the dynamic perturbation factor.

Similar results have been found for small hydrophobic compounds by Qvist and Halle (2008) [80] who explains the maximum in ξ by a stronger temperature dependence of R_{hyd} or τ_H compared to R_{bulk} or τ_0 above the temperature at which the maximum occurs, but a weaker one below. This is believed to be due to the fact that at the high temperatures, the hydration water is more ordered than the bulk water because it has sterical constraints, and thus also a longer rotational correlation time, which increases with decreasing temperature. But the hydration water cannot form the tetrahedral/ice-like configurations which become increasingly prevalent in bulk water with decreasing temperature, thus on cooling below 250-260 K the rotational mobility of bulk water decreases faster than the mobility of hydration water [80].

4.6 Investigating possible correlations between the ^{2}H and ^{17}O relaxation data

4.6.1 Explanations for the concentration dependent increase in the rotational correlation times

In order to compare the concentration dependence of the dynamics of trehalose and hydration water, the dynamic perturbation factor of trehalose was calculated, here defined as the ratio of the rotational correlation time of trehalose at a given concentration to the rotational correlation time interpolated to c=0. In other words, this indicates how many times slower a trehalose molecule *on average* rotates at concentration c, relative to the rotational correlation time of a trehalose molecules without any trehalose-trehalose interactions.

$$\xi_{trehalose} = \frac{\tau(c)}{\tau(0)} \tag{4.65}$$

The dynamic perturbation factor for water as a function of concentration was calculated as (from eq. 4.55):

$$\xi = \frac{R_{red} N_w}{\nu_H} + 1 \tag{4.66}$$

The dynamic perturbation factors are compared in figure 4.57.

Figure 4.57 clearly shows that trehalose slows down more rapidly with increasing concentration than hydration water. The perturbation factor at 1 M is 2.6 for trehalose and 1.9 for water, at 1.5 M they are 4.5 and 2.4 respectively. This is what could be expected from concentration dependent trehalose aggregation: As also found by other authors, the water dynamics will decouple from the trehalose dynamics because the latter is of course much more sensitive to the (concentration dependent) size of the aggregates, whereas the water will perhaps move around in pores (at high concentrations). Since the dynamic perturbation factor for water only increases slightly up until 1M, it is not expected that the trehalose-trehalose interactions are bridged by strongly bound water molecules. Furthermore both the dynamic perturbation factors slowly begin to increase more strongly above 1 M, which could indicate the formation of more extended trehalose clusters and perhaps even beginning percolation.

Since it is debated how many water molecules in the hydration layer are dynamically perturbed, that is how large a hydration number should be used, I also calculated the dynamic perturbation factor assuming a hydration number of 10, see fig. 4.58 (other sources give a hydration number on the order of 10-20). This of course gives a higher dynamic perturbation factor for water, but the dynamic perturbation factor just roughly doubles from the lowest to the highest concentration, which is still much less than the factor of 4.5 seen in the trehalose data.

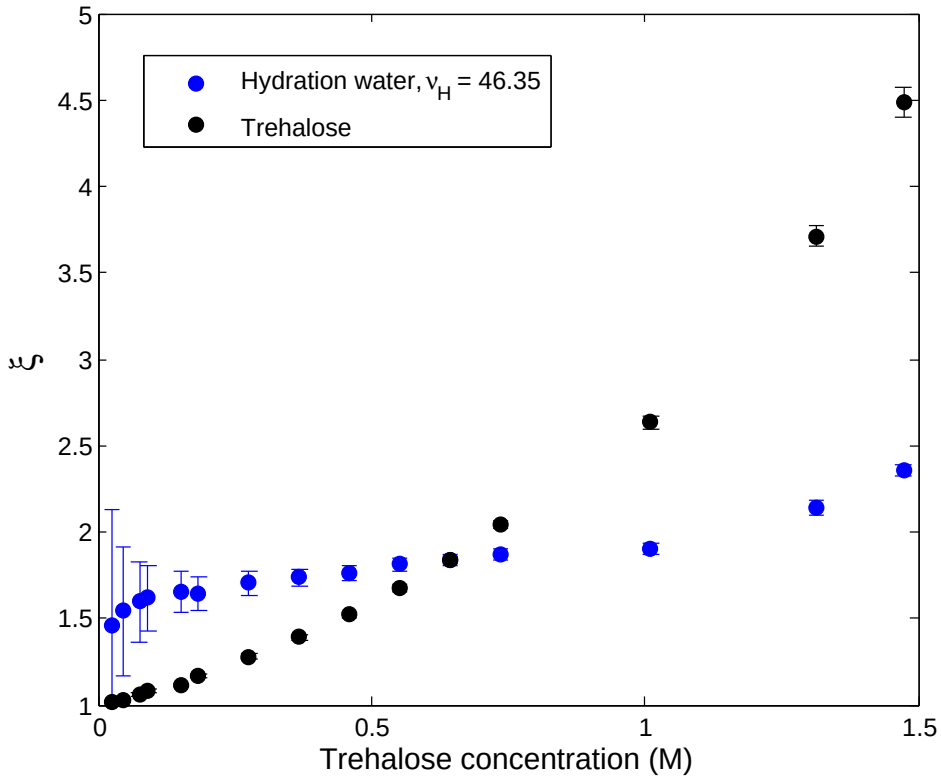

Figure 4.57: *The dynamic perturbation factor for trehalose and hydration water assuming a hydration no of 46.35.*

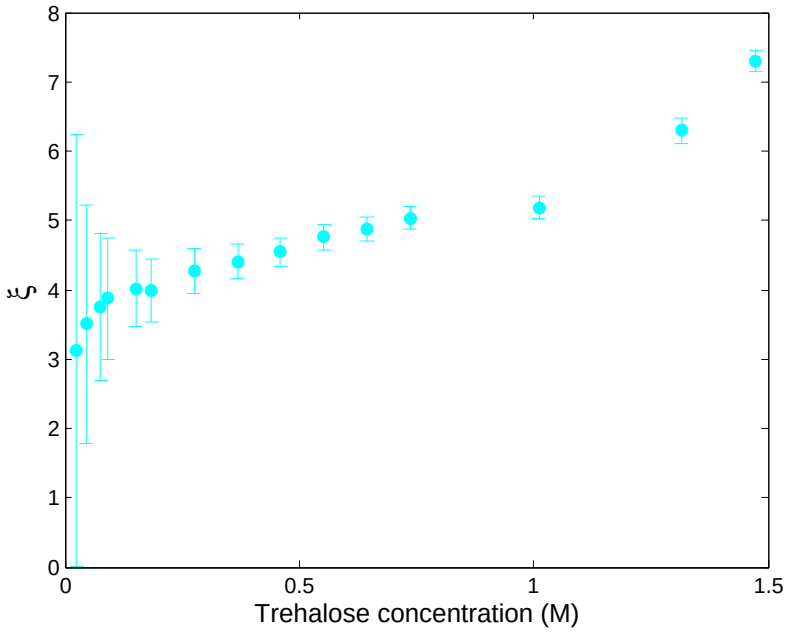

Figure 4.58: *The dynamic perturbation factor of water assuming a hydration no. of 10.*

4.6.2 Explanation of the temperature dependence of the hydrodynamic volume of trehalose

There seems to be a very large similarity between the temperature dependence of the dynamic perturbation factor of water and the hydrodynamic volume of trehalose calculated with bulk water viscosity. They both show a maximum around 250-260 K and the slope of both curves is smaller above than below the maximum. This similarity could be due to the same two reasons that was proposed to explain the temperature dependence of V_h and ξ alone, but combined:
Either

- Trehalose self-association is temperature dependent with a maximum around 250-260 K, and the mobility of the hydration water somehow depends on (decreases with) the formation of trehalose clusters. Fx. because of the creation of hydration pockets or the fact that the water is confined between two trehalose molecules.
- How strongly the hydration water is associated to trehalose or how many water molecules are perturbed by trehalose is a function of temperature with a maximum around 250-260 K. This by itself influences the dynamics of the trehalose molecule in a similar manner.

Whether the last point is reasonable can be investigated with a bit of hydrodynamics.

Halle and Davidovic (2003) [74] determined the effective hydration layer thickness needed to explain the hydrodynamics of proteins using the following correlation derived from the Navier-Stokes equations, between protein diffusion coefficients D_R and bulk and hydration water viscosity, η_0 and η_H respectively:

$$\frac{D_R}{D_R^0} = 1 - (1 - \alpha_R)\left(1 - \frac{\eta_0}{\eta_H}\right) \tag{4.67}$$

Where

$$\alpha_R = \frac{V_p}{V_p + V_s} \tag{4.68}$$

V_p is the partial molar volume of the solute molecule and $V_s = \nu_H V_w$ is the volume of the hydration layer. Here it is assumed that the hydration no is 46.35 as in the calculation of the dynamic perturbation factor.

D_R^0 is the diffusion coefficient in the case of no solvation effects - so no hydration layer. It is calculated as (see Theory section, eq. 2.5):

$$D_R^0 = \frac{k_B T}{8\pi\eta_0 a^3} \tag{4.69}$$

a is the radius of the diffusing particle, assumed to be spherical.
Since viscosity according to the previously mentioned Stokes-Einstein-Debye equation is proportional to rotational correlation time, equation 4.67 can be rewritten into the form:

$$\frac{D_R}{D_R^0} = 1 - (1 - \alpha_R)\left(1 - \frac{\tau_0}{<\tau_H>}\right) \tag{4.70}$$

$\frac{\tau_0}{<\tau_H>}$ is the inverse of the dynamic perturbation factor of water:

$$\frac{D_R}{D_R^0} = 1 - (1 - \alpha_R)\left(1 - \frac{1}{\xi}\right) \tag{4.71}$$

The question now is if the characteristic maximum in the dynamic perturbation factor can explain the maximum in the hydrodynamic volume of trehalose as a function of temperature, through the correlation given above.

To determine if the temperature dependence of the rotational correlation time of trehalose stems from the correlation with the hydration layer thickness described in equation 4.71, first the left hand side of equation 4.71 was calculated from the rotational correlation time of trehalose and the relation:

$$D_R = \frac{1}{6\tau_c} \tag{4.72}$$

Then the right hand side of equation 4.71 was calculated from the dynamic perturbation factor calculated for water. The two sides of the equation are compared in figure 4.59. The plot shows that the left and right hand side of equation 4.71 show a very similar temperature dependence. So it seems that most of the temperature dependence of V_h can be accounted for by the temperature dependence of ξ. Thus the trehalose-trehalose interactions apparently are not very temperature dependent.

Figure 4.59 also shows that the data points calculated from the trehalose relaxation data approaches the points from the water relaxation data as the trehalose concentration approaches 0. This can be explained by the fact that the right hand side of equation 4.71 and the water relaxation data does not take into account trehalose-trehalose interactions. As the concentration increases the actual D_R/D_R^0 deviates more and more from the D_R/D_R^0 that was calculated from bulk water viscosity (the right hand side of the equation).

The hydrodynamic volume of trehalose $V_{h,calc}$ calculated from bulk water viscosity η_0 is proportional to $\frac{D_R}{D_R^0}$ since (eq. 4.72):

$$\frac{D_R}{D_R^0} = \frac{1}{D_R^0}\frac{1}{6\tau_c} \tag{4.73}$$

Inserting

$$\tau_c = \frac{V_{h,calc}\eta_0}{k_B T} \tag{4.74}$$

And eq. 4.69 gives:

$$\frac{D_R}{D_R^0} = \frac{8\pi\eta_0 a^3}{k_B T}\frac{k_B T}{6V_{h,calc}\eta_0} = \frac{V_h^0}{V_{h,calc}} \tag{4.75}$$

Where V_h^0 is defined as the constant :

$$V_h^0 = \frac{4}{3}\pi a^3 \tag{4.76}$$

Thus to confirm more quantitatively that equation 4.71 really does account for the temperature dependence of $V_{h,calc}$ as implied by figure 4.59, it can be tested whether

$$\frac{D_R}{D_R^0} \cdot V_{h,calc} = V_h^0 \tag{4.77}$$

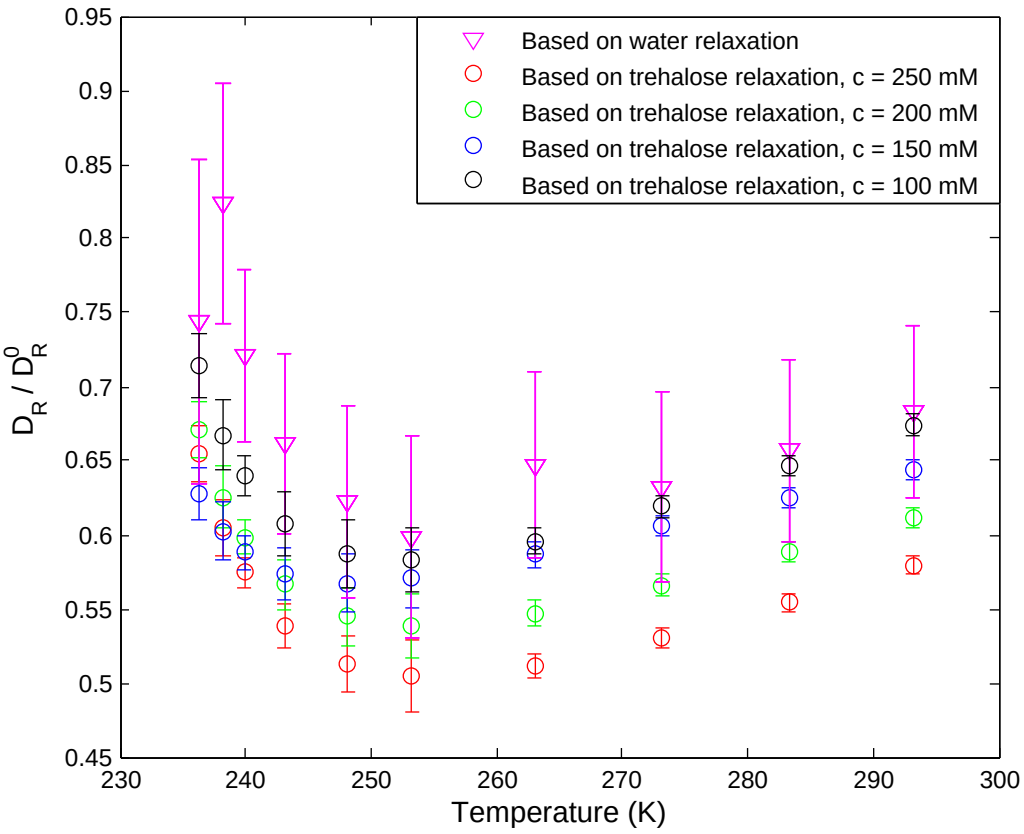

Figure 4.59: *The temperature dependence of the left (circles) and right hand side (triangles) of eq. 4.71*

- gives a constant as a function of temperature.
$\frac{D_R}{D_R^0}$ was calculated from eq. 4.71 and $V_{h,calc}$ from eq. 4.74 (calculated earlier, see fig. 4.29). The result is shown in fig. 4.60.

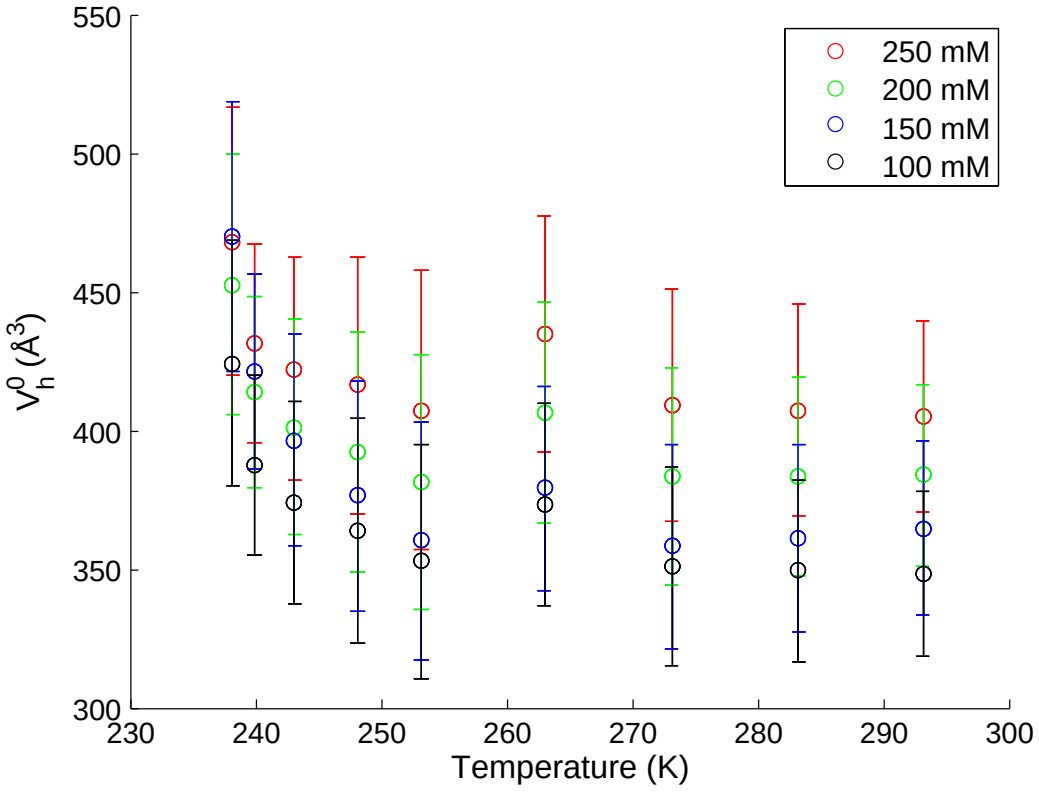

Figure 4.60: *The temperature dependence of* V_h^0.

Comparing V_h^0 in figure 4.60 to V_h in figure 4.29 shows that at least the majority of the temperature dependence is gone, and V_h^0 is almost constant.

Thus it is clear that observed maximum in V_h as function of temperature arises from the fact that the dynamic perturbation factor, or the *ratio* of the hydration water viscosity to the bulk water viscosity has a maximum, the hydration water viscosity itself does not have a maximum as can be seen from figure 4.56. The difference it makes to take into account the hydration layer effect on the diffusion of the molecule, which is indicated by the fraction D_R/D_R^0, will therefore also show a maximum at the same temperature, thus giving rise to the maximum in the calculated V_h.

Chapter 5

Discussion

The ^{2}H relaxation data has shown that there are trehalose-trehalose interactions at least down to 75 mM trehalose. Some scientists believe that many water layers will be dynamically perturbed by carbohydrates. In principle they could argue that the reason why we see trehalose-trehalose interactions at so low concentrations is because they are right: There are long range effects on water dynamics. But at a concentration of 75 mM trehalose, the surface-to-surface distance between adjacent trehalose molecules in a close cubic packing model would be 22.8 Å. So if there is hydration shell overlap at this concentration, the hydration shell should be at least 11.4 Å or about 4 water layers. At 50 mM where there are also (weaker) indications of trehalose-trehalose interactions, the water layer would be even 4.9 water molecules. If the carbohydrates actually perturb water more than other small molecules will be determined later. First I turn to the evidence for trehalose-trehalose association, from the Molecular dynamics studies by Sapir et al. (2011) [77].

5.1 Comparison with Molecular Dynamics studies

Both Lerbret et al. (2005) [76] and Sapir and Harries (2011) [77] found evidence for the existence of trehalose clusters with Molecular Dynamics simulations.
This is not unique to trehalose, MD studies also found that other disaccharides such as sucrose and fructose self-associates [78],[79],[76].

Sapir and Harries (2011) [77] studied trehalose self-association at many different concentrations relevant for our study. They found that trehalose aggregates in a concentration dependent manner by hydrogen bonding. As was indicated by our data, they see finite trehalose clusters even at the lowest concentrations investigated (0.25 molal). The concentration of finite clusters increases with increasing concentration until it reaches a maximum around 1.75 molal (1.28 Molar) where the concentration of infinite clusters (defined as clusters transcending the borders of the simulation box) increases drastically. The clusters seem to be relatively short-lived, over their entire concentration range the decay time of the clusters vary from 11 to 360 ps. The percolation treshold or the concentration where the aggregates become infinite, was found to lie in the range 1.5-2.2 molal (1.14 - 1.51 M). The MD study by Lerbret et al. (2005) [76] found a steep increase in the

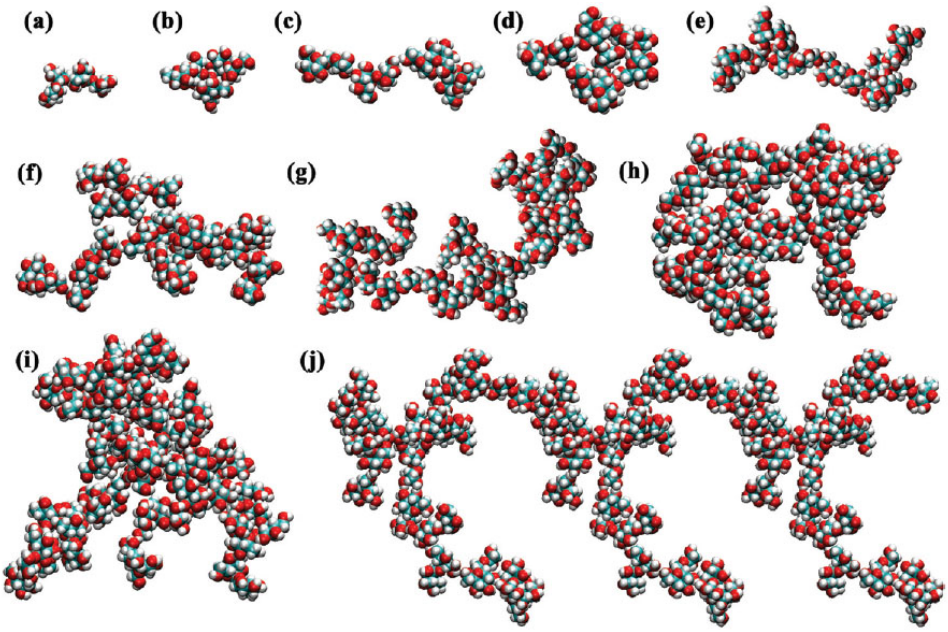

Trehalose molecules bind through H bonds with each other, thereby forming clusters in solution. Shown are typical examples of clusters, as seen in simulations, sorted as aggregates with an increasing number n of molecules (monomers): (a) 2, (b) 3, (c) 4, (d) 5, (e) 8, (f) 15, (g) 22, (h) 30, (i) 37, and (j) an "infinite cluster" that transcends the borders of the periodic simulation cell. All images, shown in VDW representation, are from simulations with CSFF; similar clusters were found using C35.

Figure 5.1: *Examples of clusters in the MD study by Sapir et al. (2011). [77]*

trehalose cluster size around 30 wt% or 1M, confirming that more extensive clusters are formed around 1M.
Sapir et al. also showed that the most probable number of hydrogen bound neighbouring trehalose molecules is smaller than 3 for all concentrations. This means that the trehalose clusters are likely to become quite branched, see figure 5.1.

The observation of infinite clusters from about 1.5 molal or 1.14 M could be related to our observations: $R_{red}N_w$ starts to increase more steeply around 1 M, and around the same concentration, the effective viscosity separates much more from the macroscopic viscosity. The fact that the effective viscosity is smaller than the macroscopic and the gap between them increases with increasing concentration is also what would be expected for increasingly larger branched trehalose clusters where the life time of the trehalose-trehalose bond is short relative to the rotational correlation time. The creation of small trehalose networks would then have a larger impact on the macroscopic viscosity, because it probes longer time scales and distances.

The increasing concentration of finite trehalose clusters up to 1.14 M trehalose reported by Sapir et al. may be the reason for the slow increase in $R_{red}N_w$ and ξ indicated by our data in the concentration range 0.25-1 M. Figure 5.1 shows that there might be a few slightly confined water molecules contributing to this increase, and the branched conformation can perhaps also slow down water more than if the cluster was spherical.

The MD study by Sapir and Harries [77] gives the trehalose momomer concentration as function of total trehalose concentration. This can be used to calculate the fraction of trehalose molecules bound in aggregates X_{bound} as function of trehalose concentration

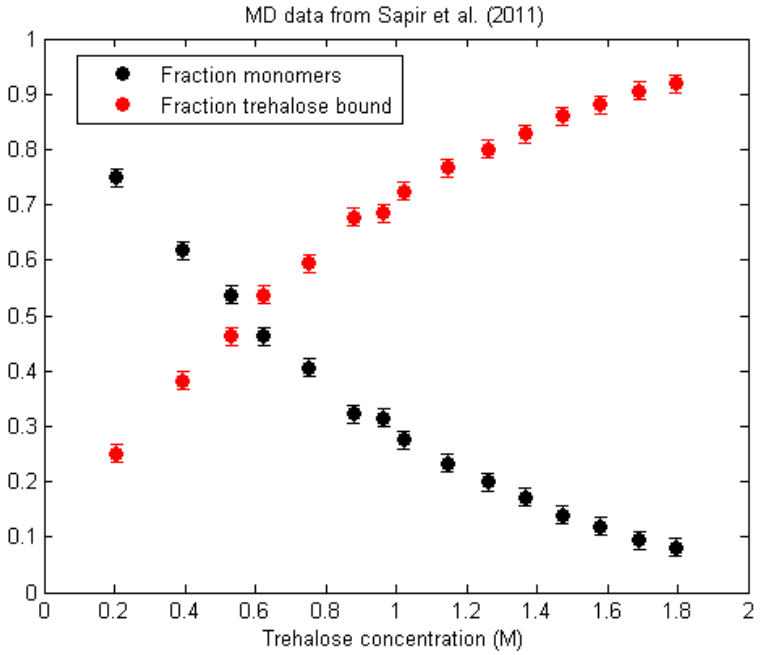

Figure 5.2: *Data from Sapir et al. (2011).*

(see figure 5.2):

$$n_{bound} = n_{tot} - n_{mon} \Rightarrow \frac{n_{bound}}{n_{tot}} = 1 - \frac{n_{mon}}{n_{tot}} \tag{5.1}$$

The R_1 measured for trehalose can be regarded as a weighted average of the relaxation rate of monomers and the average relaxation rate of trehalose molecules bound in aggregates:

$$R_1 = X_{mon}R_{mon} + X_{bound} < R_{bound} > \tag{5.2}$$

Here the fraction of free trehalose monomers and trehalose bound in aggregates was defined as X_{mon} and X_{bound} respectively.
The relaxation rate for monomers was found by extrapolating R_1 vs concentration to c=0: $R_{mon} = 41.7694s^{-1}$. Thus $< R_{bound} >$ can be calculated from the measured R_1 using the equation above:

$$< R_{bound} >= \frac{R_1 - X_{mon}R_{mon}}{X_{bound}} \tag{5.3}$$

(The values of X_{bound} used was interpolated from the data from Sapir et al. [77] to the concentrations used in our experiment, R_1 measurements at concentrations lower than 0.18 M were excluded since the MD study only goes down to 0.2 M trehalose).

The plots show (5.3-5.4) that the trehalose molecules bound in aggregates on average rotate about 2 to 6 times slower than free trehalose molecules in the concentration range approximately 0.2 - 1.5 M trehalose, according to the MD study by Sapir et al. [77] combined with our relaxation measurements. If the aggregates were stable this would give a rough idea of the average aggregate size: Remember Stokes-Einstein-Debyes equation, rotational correlation time is proportional to hydrodynamic volume, thus at about 1.5 M trehalose the hydrodynamic volume of the aggregates would be about 6 times that of

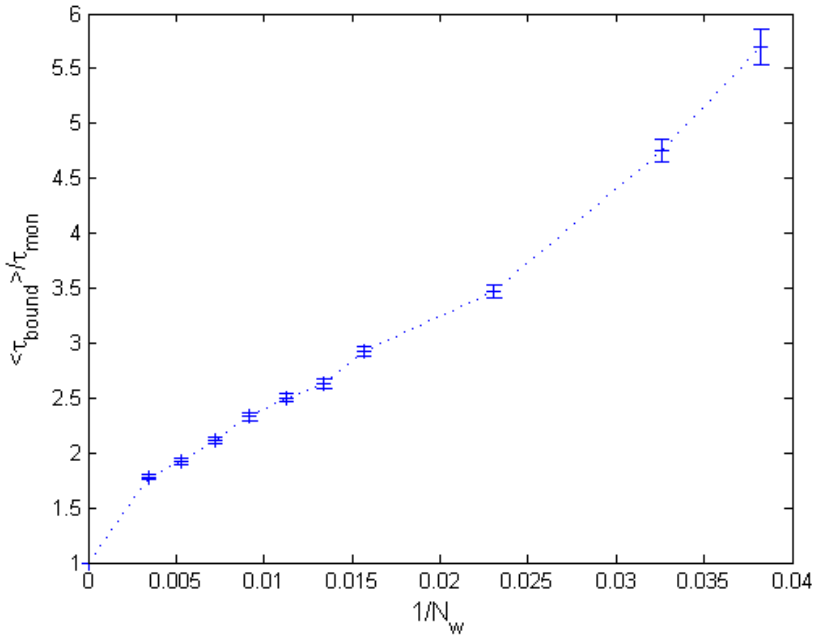

Figure 5.3: *Data from Sapir et al. (2011).*

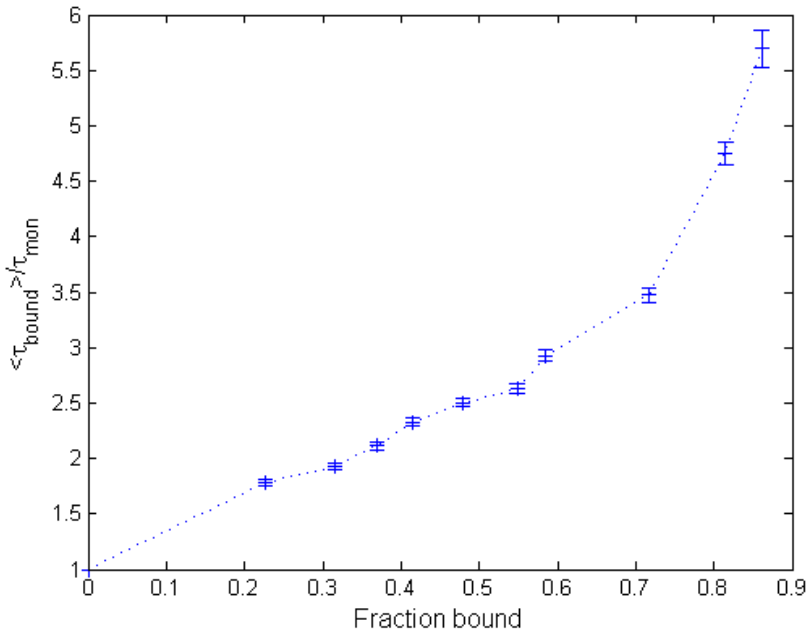

Figure 5.4: *Data from Sapir et al. (2011).*

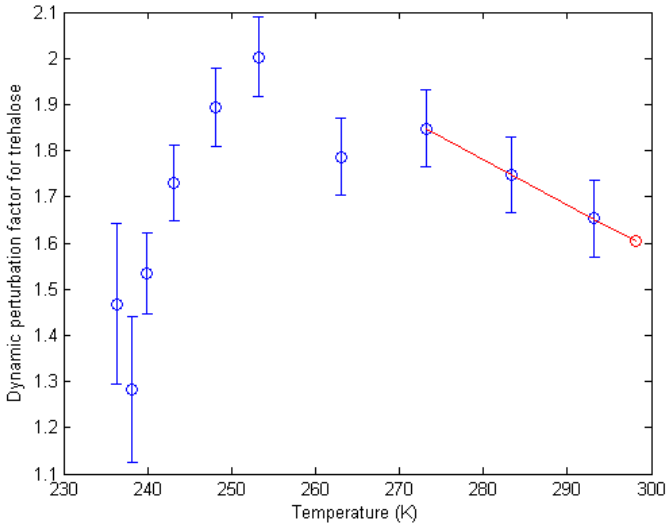

Figure 5.5: *Extrapolation (linear) of our measured trehalose dynamic perturbation factor to* 25°*C.*

a monomer. But the MD study indicates that the aggregates are short-lived, therefore the picture is more complicated and the aggregates may be even bigger. Furthermore if the aggregates consist of extended chains of monomers, they would have quite high hydrodynamic volumes compared to the number of trehalose units, and the interpretation of an increase in hydrodynamic volume becomes complex.

5.2 Comparison with other small molecules

In order to determine whether trehalose has extraordinary hydration characteristics, the hydration data represented by the dynamic perturbation factor of water in trehalose solutions, was compared to the hydration data of a variety of other small molecules, see figures 5.6-5.7. The data for the different kinds of sugars was based on the dynamic hydration numbers (ν_{dyn}) from Uedaira et al. (1989 and 1990) ([81] and [82]). The corresponding dynamic perturbation factors were calculated from the previously mentioned equation (eq. 4.57):

$$\xi = \frac{\nu_{dyn}}{\nu_H} + 1 \tag{5.4}$$

- where the hydration number was calculated from equation 4.50, and the solvent accessible surface area (SASA) used for this calculation was calculated from the compound structure (from pdb.org) with the program GetArea [62] using a probe radius of 1.7 Å. The data for non-sugars stems from Qvist and Halle (2008) [80] (supplemental data), who collected data from different sources and combined them with similar SASA calculations.

As we only measured the dynamic perturbation factor for trehalose up to 20°C, the data point at 25°C in figures 5.6-5.7 was calculated by linear extrapolation from the measured temperature dependence, see figure 5.5.

First of all figure 5.6 shows that:

- the dynamic perturbation factor for trehalose measured by Uedaira et al. [82] is not equal to the value we have determined, but is within the error bars of our data point.

- trehalose does not seem to have extraordinary hydration characteristics compared to both other sugars, but also all other chemical groups shown in the plot, instead a dynamic perturbation factor of 1.60 at 25°C is comparable to many of the other compounds plotted. In fact trehalose has similar hydration dynamics to tetramethylurea (TMU) which is a potent protein *destabilizer* ($\xi = 1.59$ at 25°C), and to the protein stabilizer trimethylamine N-oxide (TMAO) ($\xi = 1.62$ at 25°C) [80]. Thus indicating that slower hydration water dynamics is not the reason for the stabilizing effect of trehalose.

- In general figure 5.6 shows that sugars do not perturb water dynamics more than many other and chemically very different molecules.

The branched clusters proposed by Sapir et al. (2011) [77] could explain why the dynamic perturbation factor for water in trehalose solutions is not significantly larger at low concentrations (at least at concentrations up to 0.25 M) than molecules that do not aggregate, since this model does not have many strictly confined water molecules (i.e. in small pockets as is the case with large proteins).

Qvist and Halle (2008) [80] suggested that the most important factor in hydration dynamics is the amount of apolar surface area: It is the presence of apolar surface area that slows down the hydration water since the lack of hydrogen bond partners to one side decreases its degrees of freedom. They plotted the dynamic hydration number as function of number of carbons to prove this correlation, but as can be seen in eq. 4.56 the dynamic hydration number (ν_{dyn}) should naturally have a trivial linear dependence on size (ν_H). Thus to prove the point it makes more sense to look at the dynamic perturbation factor which should have divided out the dependence on size, as a function of apolar SASA divided by the total SASA.
For most of the chemical groups (except sugars and aminoacids/dipeptides) figure 5.6 indicates that ξ increases with increasing hydration number if you look at each chemical group individually. This may be due to either higher order effects, so a dependence on the size of ν_H that is not accounted for by eq. 4.57, or the fact that the fraction of apolar surface area to total surface area increases with ν_H within the chemical groups, since all the groups except the amino acids and dipeptides and the sugars, consist of series of compounds made by adding extra alkyl groups to the starting-point (or in a few cases changing the location of the alkyl groups). Plotting ξ versus the fraction of apolar surface area (fig. 5.7) indicates that the latter consists a significant part of the explanation: Within each chemical group except sugars and aminoacids/peptides, there is a substantial positive correlation between the dynamic perturbation factor and the fraction of apolar surface area, supporting the idea by Qvist and Halle that increasing the apolar surface area slows the dynamics of hydration water. But the dependence on apolar surface area is clearly not the same for the different chemical groups, and they do not extrapolate to $\xi = 1$ going toward 0 on the x axis, therefore the fraction of apolar surface area is *not* the *only* variable that determines the dynamic perturbation factor. In reality it is strictly speaking not possible to distinguish higher order size effects from increase in the fraction of apolar surface area, from the plots shown. But it is very complex to categorize exactly what other variables come into play, and it is also not the scope of this project.

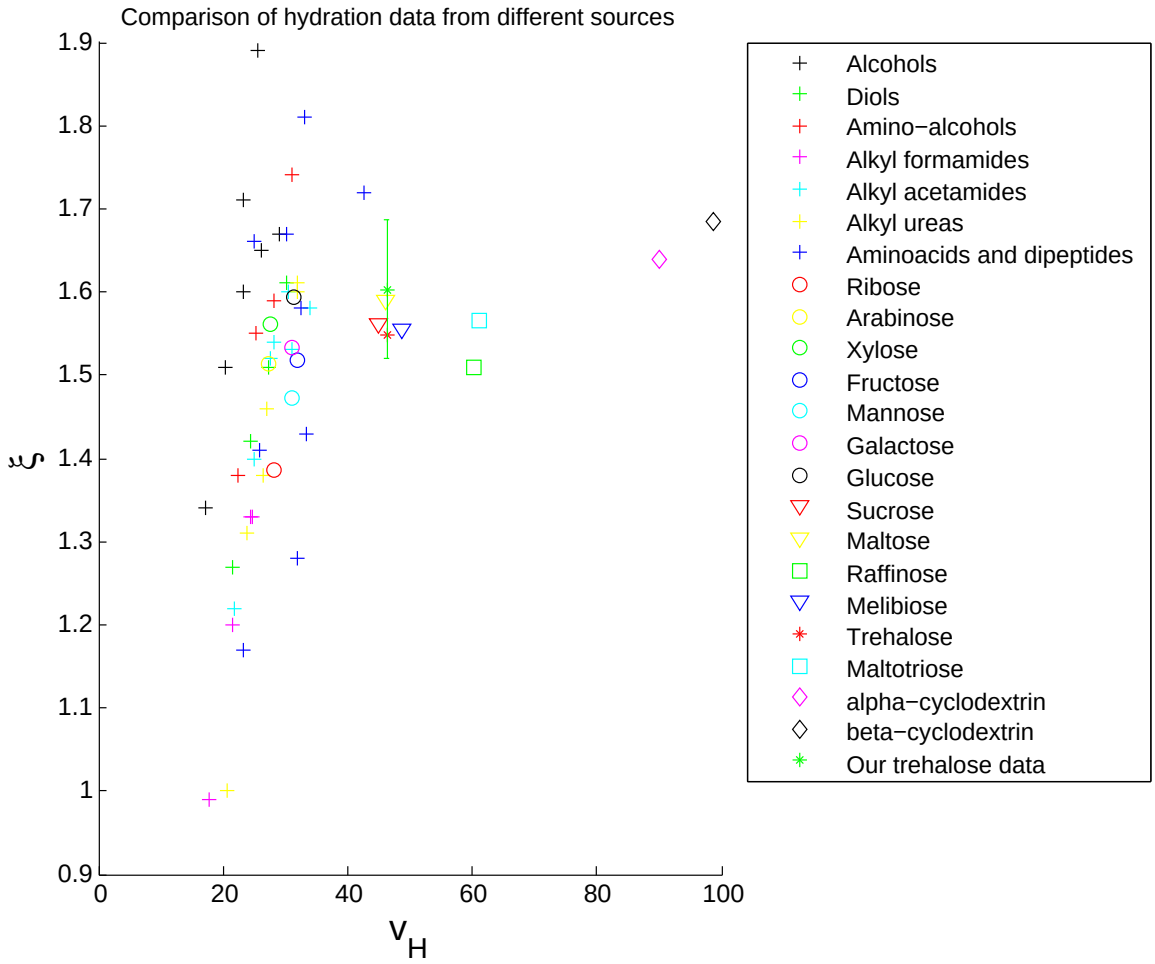

Figure 5.6: *The dynamic perturbation factor for different compounds at* 25°*C as a function of hydration number, from different sources: Sugar data: From Uedaira et al. (1990 and 1989), alcohols and diols: Ishihara (1997), amino-alcohols: Okouchi et al. (2005), formamides and acetamides: Bagno et al. (1993), alkyl-ureas: Shimizu et al. (2000) and Qvist and Halle (2008), amino acids and dipeptides (group also includes TMAO and TMU): Qvist and Halle (2008) and Ishimura et al. (1990).*

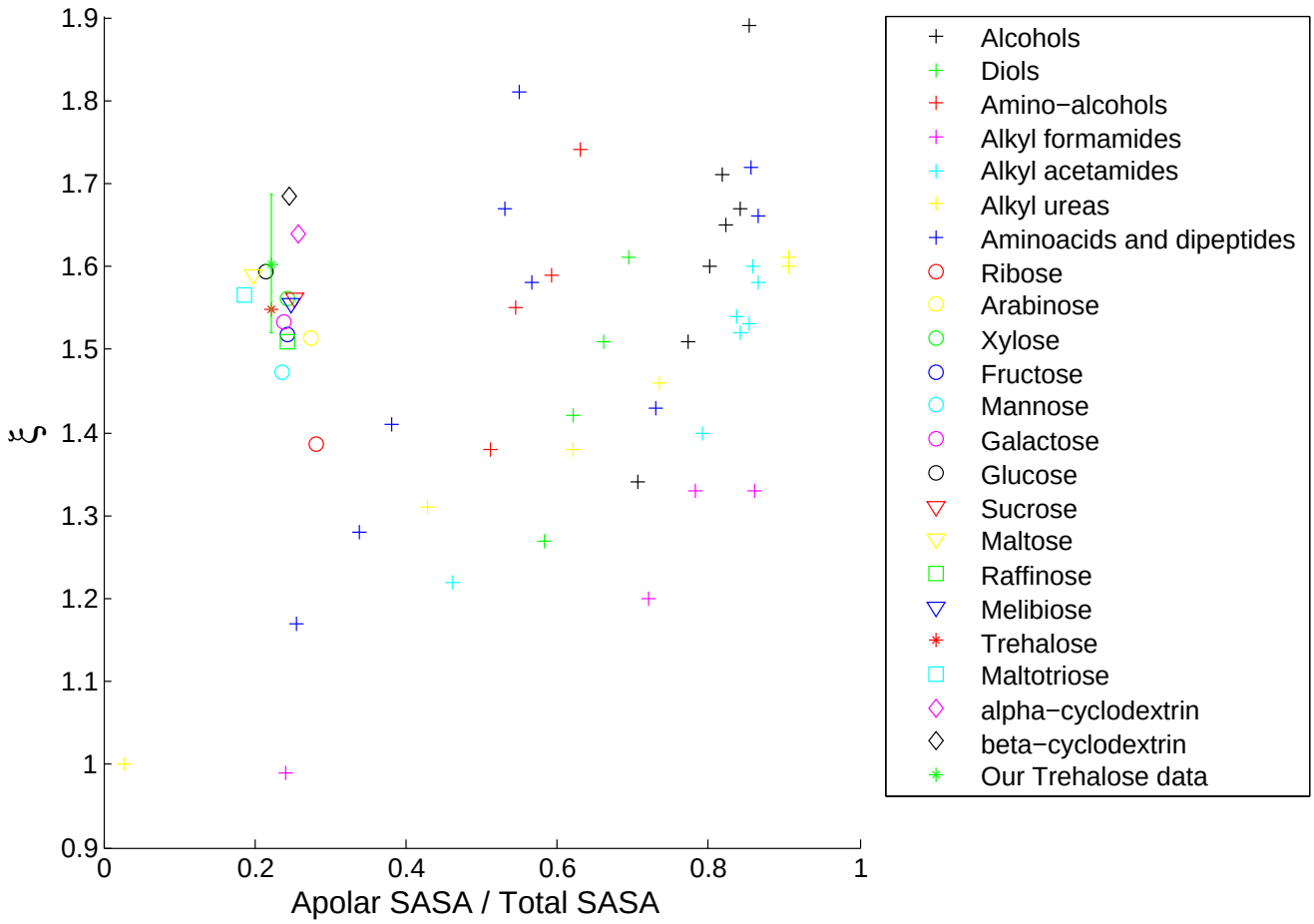

Figure 5.7: *The dynamic perturbation factor for different compounds at 25°C as a function of the fraction of apolar surface area, from different sources: Sugar data: From Uedaira et al. (1990 and 1989), alcohols and diols: Ishihara (1997), amino-alcohols: Okouchi et al. (2005), formamides and acetamides: Bagno et al. (1993), ureas: Shimizu et al. (2000) and Qvist and Halle (2008), amino acids and dipeptides (group also includes TMAO and TMU): Qvist and Halle (2008) and Ishimura et al. (1990).*

But another possible important variable is the ability of the molecule to fit into the water hydrogen bond structure, which is easiest for very small molecules that readily forms hydrogen bonds. The better it fits into the water structure, the less the water dynamics is disturbed and the smaller the dynamic perturbation factor becomes. This has been reported to perhaps be the reason why urea, which is a small, polar and potent hydrogen bond donor/acceptor, has no effect on water dynamics ($\xi = 1$).

The different sugars have comparable fractions of apolar surface areas as can be seen in figure 5.7. Recalling that sugars are polymer-like compounds built of very similar building blocks (mono-saccharides) this makes a lot of sense - adding an extra mono-saccharide does not significantly change the *fraction* of apolar surface area.
If you neglect the much larger cyclodextrins, the sugars do not vary much in ξ either. So it seems that the major part of the size effect was divided out when calculating the dynamic perturbation factor from the dynamic hydration number. And the sugars have comparable effects on water dynamics.
Figure 5.7 also shows that sugars are quite polar. Compared to the other compounds plotted, sugars have a quite high dynamic perturbation factor considering their low fraction of apolar surface area. But the other chemical groups also spread a lot along the x-axis, so it is not fair to call the sugars an outlier.

Uedaira et al. (1990) [82] found a nice linear relation between the dynamic hydration number of sugars and their number of equatorial OH groups. But again, the dynamic hydration number increases with hydration number or size, as does the number of equatorial OH groups, so this correlation is trivial.
They also tested the relation between the dynamic perturbation factor and the number of equatorial OH groups (n_{eq}), and found that for monosaccharides ξ increases linearly with n_{eq}, whereas the oligosaccharides scatter more but approach a smaller constant value as n_{eq} increases. But the hydration number used in their calculations is different from ours, instead they set the hydration number to 6, 10 and 14 for mono-, di-, and trisaccharides respectively. As this is quite crude and does not take into account the small differences in surface area within the different classes of sugars, I tested the relation ship using the dynamic perturbation factor calculated here based on SASA, see figure 5.8.

Figure 5.8 does show a slight dependence of ξ on the number of equatorial OH groups for monosaccharides. But the rest of the sugars are quite scattered and do not fall off towards a constant number, nor does glucose constitute a clear maximum, as seen in the plot by Uedaira et al. Disregarding ribose and the two cyclodextrans, the data points as a whole do not show a clear trend. But if you look at each class of saccharides individually there seems to be a correlation.

The dynamic perturbation factor as a function of the number of carbons or the number of hydrogen bonding partners, show no trend, also not for the monosaccharides (data not shown).

Figure 5.7 showed that at low concentrations, where R_{red} can be approximated to be linear with $1/N_w$, the hydration water around trehalose is not more perturbed than around a large number of other and chemically very different small molecules. But earlier it was shown that at concentrations higher than about 0.25 M linearity could no longer be assumed and the product $R_{red}N_w$ could not be taken to be constant within the error bars.
It could now be interesting to check if the hydration water probed with the quantity $R_{red}N_w$

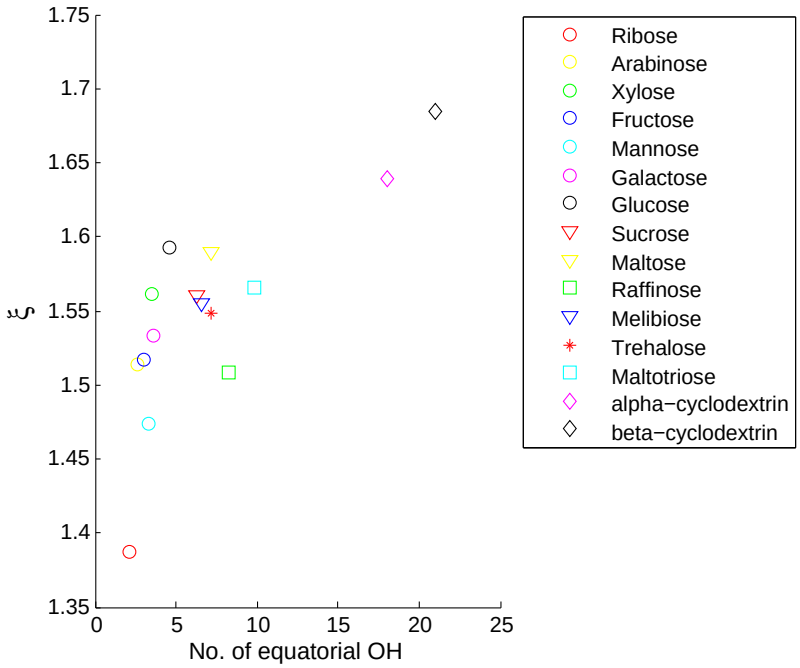

Figure 5.8: *The dependence of the dynamic perturbation factor for different sugars as a function of the number of equatorial OH groups. Based on data from Uedaira et al. (1990 and 1989).*

is affected in the same manner for other small molecules when the fraction of hydration water approaches 1.
Alcohols are like sugars quite polar and are also capable of forming hydrogen bonds with water or with other alcohols. Alcohols have not been reported to self associate at low concentrations, but according to Neutron diffraction data from Dixit et al. (2002) [84], they do form clusters in concentrated solutions (7:3 molar ratio). The simple alcohols methanol, ethanol and propanol were chosen for comparisons. It would have been interesting to also compare to eg. small peptides, but I have been unable to find experimental data that goes to concentrations high enough to give a hydration water fraction of more than 0.7-0.8 and the data scatters a lot.
Both Bagno et al. (1993) [54] and Ludwig (1995) [53] and Ishihara et al. (1997) [85] measured the ^{17}O R_1 of water in alcohol-water solutions by NMR relaxation. From the relaxation rates I calculated the product $R_{red}N_w$ seen in figure 5.9.

Before we can compare the hydration data for the alcohols to the data for trehalose, we must know how the fraction of hydration water in the two data sets compares. The fraction of hydration water for the three alcohols were calculated in the same manner as for trehalose, with hydration numbers again defined as the number of water molecules in the first solvation shell, that was taken from Qvist et al. [80]: 17.2, 20.4 and 23.3 for methanol, ethanol and (n)-propanol respectively, see figure 5.10.

Recall that the increase in $R_{red}N_w$ from about 0.25-1 M trehalose was around 30%, and from 0.25-1.5 M the product roughly doubles. In the same concentration range the fraction of hydration water increased from about 0.2-1.8.
Figure 5.10 shows that the fraction of hydration water increases up to 1.9 and 2.6 for

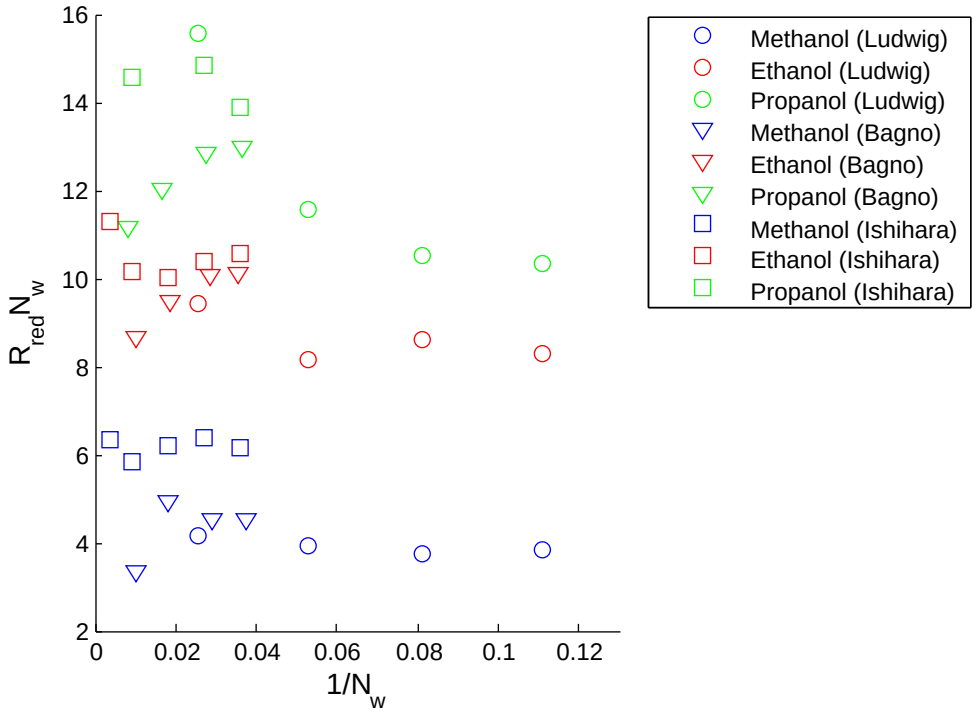

Figure 5.9: *The product of reduced relaxation rate for ^{17}O atoms and N_w for different alcohols. The circles are data from Ludwig (1995) [53] and the triangles are data from Bagno et al. (1993) [54], the squares are from Ishihara et al. (1997) [85].*

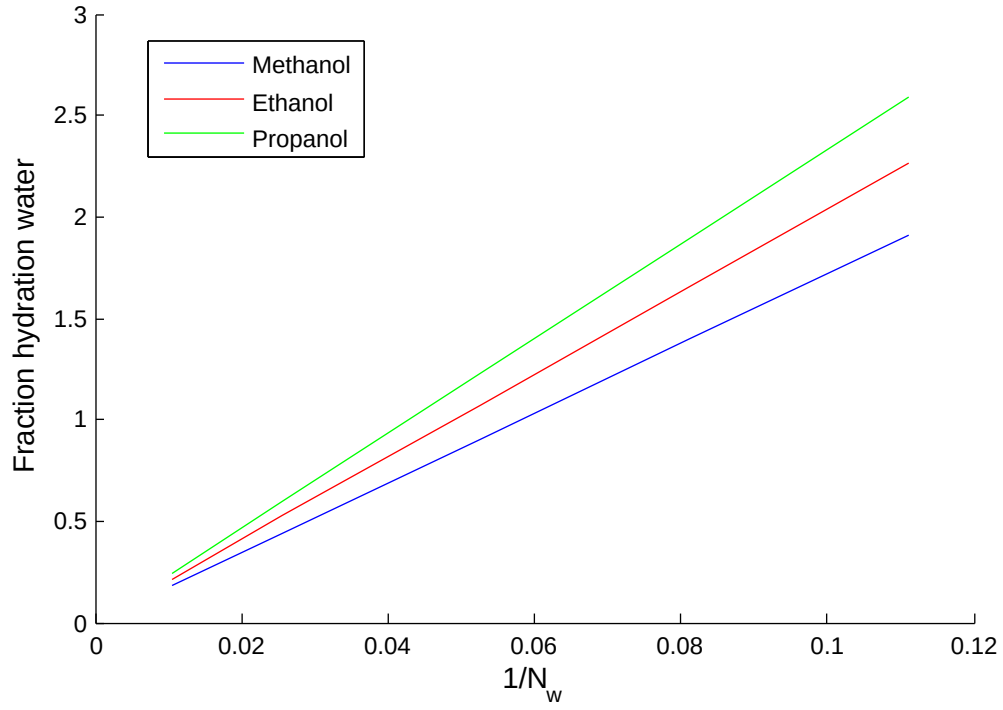

Figure 5.10: *The product of reduced relaxation rate for ^{17}O atoms and N_w for different alcohols.*

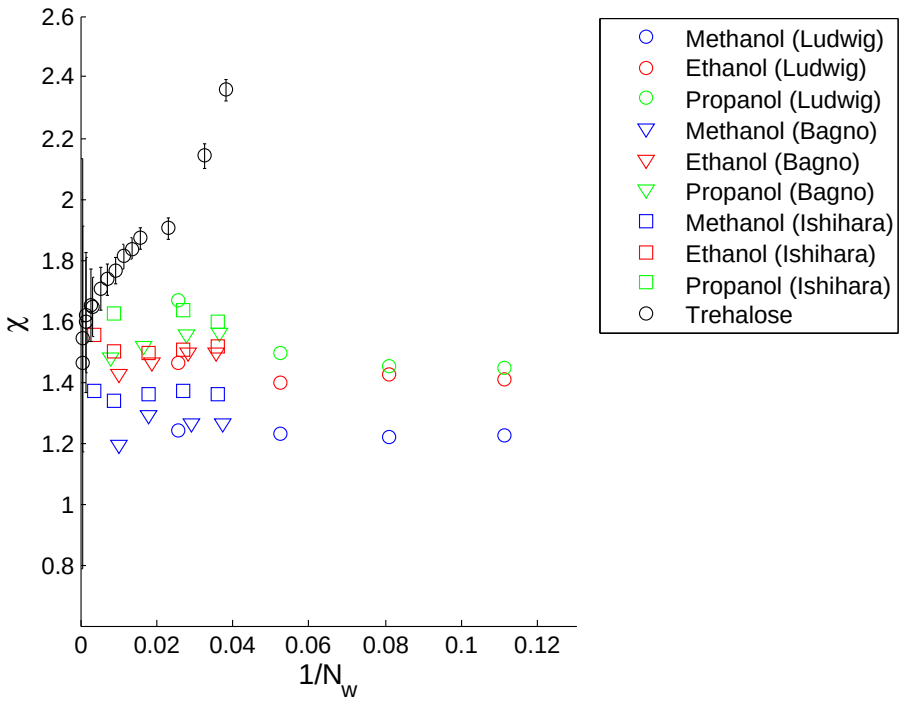

Figure 5.11: *The concentration dependence of the dynamic perturbation factor of water in solutions with different alcohols or trehalose.*

methanol and propanol respectively, in the concentration range measured. But even so the change in $R_{red}N_w$ for the alcohols is nowhere near as large as that observed for trehalose. The data from Bagno et al. shows a small increase, whereas according to Ishihara et al. (1997) there is a small decrease, but according to the data from Ludwig (1995) it levels out at higher concentrations.
$R_{red}N_w$ was converted to the dynamic perturbation factor in figure 5.11 and compared to trehalose. One could speculate that the steep increase with concentration above 1 M in $R_{red}N_w$ and ξ seen in trehalose solutions is related to the reason for the stabilizing effects of sugars, but more data from many other compounds must be taken into consideration. It might even be that the reason for the increase in ξ for trehalose solutions is simply because the molecule is larger than the small alcohols and thus disrupts the hydrogen bond pattern of water more in ways similar to other larger molecules that have no stabilizing effects. So data for fx. peptides and other larger molecules is needed.

5.3 Other experimental evidence for aggregation in aqueous sugar solutions

5.3.1 Dynamic Light Scattering

In Dynamic Light Scattering (DLS) the sample is hit by monochromatic laser light and the time dependence of the light scattered by the particles in the sample is recorded. The

technique utilizes the fact that when light hits a particle that is small compared to its wavelength, the light is scattered in all directions (Rayleigh scattering). (This is also the reason why the sky is blue.) The particles undergo Brownian motion, which causes the distance between the molecules to fluctuate. Since each molecule is also a light scatterer the light resonance will change with time, which can be seen as intensity fluctuations of the scattered light. The recorded light intensity pattern thus gives information about the dynamics/movement of the particles and from the dynamics the hydrodynamic volume can be calculated.

Sidebottom and Tran (2010) performed DLS on glucose, maltose and sucrose and got results supporting the hypothesis that sugars aggregate even at low concentrations [99]. They varied the sugar concentration from 5 to 85 wt% and temperatures from -10 to 40$^{\circ}C$. Analysis of the light intensity as a function of time gave the translational diffusion coefficient (D) as a function of temperature and concentration. Their data shows that D/T at concentrations below 30 wt% (1 M) follows (almost) the same temperature dependence as $1/\eta_{bulk}$ indicating that the temperature dependence can be explained by the temperature dependence of water viscosity and that the solution viscosity can be approximated by bulk water viscosity at these concentrations [99]:

$$D_t = \frac{kT}{6\pi\eta_{bulk}R_H} \tag{5.5}$$

DLS gives the collective diffusion coefficient, not the self-diffusion coefficient of single molecules as our NMR relaxation experiments. Thus one should not do extensive comparisons of the results from the two techniques.
But a consequence of the temperature dependence of the DLS data is that the sugar-sugar interactions cannot be largely temperature dependent below 1M, since then the temperature dependence of D/T would then not follow $1/\eta_{bulk}$. This could also be concluded from our data: When the temperature dependence of the trehalose relaxation data was compared to that of the water relaxation data, there was indications that the temperature dependence was caused only by variations in the hydration water viscosity, so the trehalose-trehalose association could not be clearly temperature dependent.

The DLS data from Sidebottom and Tran also showed a decrease in D/T with increasing concentration in the entire concentration range for both glucose and maltose (they do not show a lot of data on sucrose), so all the way down to 5-10wt% - about 0.15-0.3 M maltose [99]. Thus their data also indicates that there must be sugar-sugar interactions even down to 0.15-0.3 M. Again depending on the life time of the interactions, the decrease in D/T can be either due to viscosity or hydrodynamic volume increase. Sidebottom and Tran calculated the hydrodynamic radius of glucose and maltose at 20$^{\circ}C$ assuming bulk water viscosity and spherical geometry, and got an increase from 6.2 Å at 5wt% to 15 Å at 46 wt% (about 1.6 M) for maltose, this corresponds to 998 and $1.41 \cdot 10^4$ Å^3.

5.3.2 ^{13}C NMR relaxation of sucrose

Baraguey et al. (2002) [97] determined the concentration dependence of the rotational correlation times of sucrose in sucrose-water solutions, by measuring longitudinal relaxation times of ^{13}C in sucrose with NMR relaxation. They see an increase in the rotational

correlation time of sucrose with concentration, similar to what we found for trehalose. And by determining the relaxation rates of the individual carbons in the sugar rings, they discovered that the rotational motion of sucrose is anisotropic, and that the anisotropy is concentration dependent, which they assume is a sign of an increasing number of sucrose-sucrose interactions.

5.4 Reported effects of sugars on the H-bond network of water

The simple analysis of our relaxation data presented above, where dynamic perturbation of water is assumed to primarily take place in the first hydration shell, did not show any differences in how trehalose affects the water dynamics compared to a wide range of other small molecules, at low concentrations where aggregation is not too predominant. This means that trehalose monomers do not have extraordinary effects on water dynamics. But considering the results of Sapir et al. (2011) [77], the interpretation of water dynamics in trehalose solutions becomes far more complex. If trehalose self-associates to make large branched clusters, one should probably expect that the hydrogen bond network of water will change significantly as seen from a large scale.
NMR relaxation measures the average reorientation time of single water molecules, not the collective reorientation of water molecules. A number of research studies attempted to determine if trehalose affects the hydrogen bond network in water, with different kinds of light spectroscopy. Some examples are shown below.
In 1980 Mathlouthi et al. [89] performed Raman scattering studies on solutions of sucrose, glucose and fructose and found that the bending frequency of water increases with the concentration of glucose and sucrose. This has earlier been demonstrated to be associated with an increase in the strength of the hydrogen bonding in water. They also found a break in the increase in the frequency of one of the vibration modes of CH_2 around 20-40 wt% glucose and sucrose which they think can be associated with a transition from primarily water-sugar association to sugar-sugar association possibly leading also to the increase observed in the water-water H bond strength. If less water is sugar-bound, water clusters form more easily, thus increasing the water-water H bond strength, they speculate.

Branca et al. (1999) ([92] and [93]) performed Raman scattering measurements on aqueous solutions of trehalose. The measurements were used to investigate the effect on the hydrogen bond network of water from the intramolecular OH stretching mode in water. They conclude that the data indicates, that the addition of trehalose tends to destroy the H-bond network of water. In [93] they furthermore compared trehalose to the disaccharides sucrose and maltose and found indications that trehalose compared to these two sugars gives the largest change in the water OH stretching mode.

Later Branca et al. (2005) [90] studied the effect of sugars on the tetrahedral H bond network of water with inelastic neutron scattering measurements on trehalose and sucrose water solutions (molar fraction of 0.077 so $N_w = 12$). Again they found that trehalose strongly reduces the percentage of tetrahedral water both above and below 273K, whereas sucrose only destructures the H bond network below 273K. In the entire temperature range measured they found that the amount of tetrahedral water is lower in the

trehalose compared to the sucrose solution.

This was confirmed by Lerbret et al. (2005) [91] with Raman scattering experiments on trehalose, sucrose and maltose, all homologous disaccharides. They found that all three sugars lower the probability of tetrahedrally H bonded water and that the effect becomes stronger above 30 wt% (1 M). At this concentration trehalose also acquires a more significant effect compared to sucrose and maltose.
This finding is very consistent with the results of our ^{17}O relaxation study, which showed a steep increase in the relaxation rate and rotational correlation time of water around 1 M trehalose. This can be explained by the fact that a lower availability of hydrogen bond partners, will slow down the reorientation time of water, because reorientation becomes more restricted.

Overall what can be said is that:

- Increasing the trehalose concentration both lowers the probability of tetrahedrally bound water and increases the dynamic perturbation factor (lowers the rotational mobility) of water.
- Above about 1 M trehalose the study by Lerbret et al. [91] and our study combined shows a steep increase in the perturbation of the H bond network and the rotational mobility of water. This could well be correlated with the formation of a more extensive trehalose network, as indicated by the result from the MD study of Sapir et al. [77] who found that there might be beginning percolation around or at least formation of more extended clusters at 1.14 M trehalose. The dynamic perturbation factor calculated here for trehalose starts to increase more steeply somewhere above 1 M, see figure 4.57, as would be expected if this was true.

5.5 On the role of trehalose

Since we have shown that trehalose monomers do not perturb water mobility more than many other small molecules, one could speculate that the stabilizing effects of trehalose are related to its ability to self-associate. This is also supported by the indications in the previous section that the perturbation of water steeply increases around the same concentration where growth of infinite clusters begins.
Large branched trehalose clusters or perhaps even networks at high concentrations could possibly restrict the mobility of macromolecules in addition to disturbing the H bond network of water as shown in the previous section. Which relates the effect to the vitrification theory explained in the introduction.
It seems likely that glass formation is related to the formation of branched clusters and percolation, since the consequence of both is extreme slowing of translational mobility. If this is indeed true, then the high glass transition temperature of trehalose compared to other disaccharides could explain why trehalose is a more effective bioprotectant, because the consequence is that lower concentrations of trehalose is needed in order to approach percolation (see the phase diagram in the introduction).

But aggregation alone cannot be the explanation, because the potent protein destabilizer Tetramethylurea (TMU) both has a dynamic perturbation factor which is very close to that of trehalose [80] and has also been reported to self-associate [96]. The destabilizing effect of TMU is probably caused by its hydrophobicity: Both TMU and trehalose will at high concentrations fill out the solution with a branched network, in the case of TMU the matrix will make it difficult for the protein to avoid hydrophobic contact with TMU, thus causing the protein to unfold. Whereas trehalose is hydrophilic, so contact will not destabilize the protein.

Nonetheless most of the research done on the various bio- and cryoprotective roles of sugars, has not taken into account the fact that the sugar molecules might self-associate, and this may be the reason why a satisfactory full explanation for the effects of sugars has not been found.

5.6 Terahertz Spectroscopy Revisited

In the recent years, an experimental technique called Terahertz spectroscopy has gained more and more attention. The technique claims to be able to measure water dynamics on the sub-picosecond to picosecond scale based on the sample absorption of electromagnetic radiation with frequencies in the Terahertz range (10^{12} Hz). Water has a very high absorbance in this frequency regime compared to many solutes (including carbohydrates) and moreover, its absorbance is claimed to depend on the picosecond motions of the water molecules [49]. Thus the absorbance should be able to distinguish hydration water from bulk water.
The interpretation of the absorbance data is based on a 3 component model: The sample consists of a solute, bulk water, and hydration water that has different characteristic absorption coefficients (α) and a step transition from bulk to hydration water at a certain distance from the solute surface δR is assumed [49]. Thus the total sample absorption can be written as a volume weighted average of the 3 absorption coefficients:

$$\alpha_{tot}(\omega, \delta R, c) = \frac{V_{sol}(c)}{V_{tot}}\alpha_{sol}(\omega) + \frac{V_H(c, \delta R)}{V_{tot}}\alpha_H(\omega) + \frac{V_{bulk}(c, \delta R)}{V_{tot}}\alpha_{bulk}(\omega) \tag{5.6}$$

Where the subscripts *sol*, *H*, *bulk* and *tot* denote solute, hydration water, bulk water and total sample respectively. The bulk water term can be substituted so:

$$\alpha_{tot}(\omega, \delta R, c) = \frac{V_{sol}(c)}{V_{tot}}\alpha_{sol}(\omega) + \frac{V_H(c, \delta R)}{V_{tot}}\alpha_H(\omega) + \left(1 - \frac{V_H(c, \delta R)}{V_{tot}} - \frac{V_{sol}(c)}{V_{tot}}\right)\alpha_{bulk} \tag{5.7}$$

The reduced total absorption is defined as:

$$\alpha_{red} = \frac{\alpha_{tot}(c) - \alpha_{bulk}}{\alpha_{bulk}} \tag{5.8}$$

Combining the two previous equations gives:

$$\alpha_{red} = \frac{V_{sol}}{V_{tot}}\left(\frac{\alpha_{sol}}{\alpha_{bulk}} - 1\right) + \frac{V_H}{V_{tot}}\left(\frac{\alpha_H}{\alpha_{bulk}} - 1\right) \tag{5.9}$$

In the section about concentration measurements under Results, it was shown that the partial molar volume of trehalose only increases by 1.2% when the concentration is increased from 0 to 1.5 M, thus it can be assumed that the total volume of trehalose is proportional to the number of trehalose molecules n_{sol} (unit: moles) in the sample:

$$V_{sol} = V_{sol}^{p} n_{sol} \tag{5.10}$$

V_{sol}^{p} is the partial molar volume of the solute.
The same proportionality is assumed for hydration water, and the partial molar volume of hydration water is set equal to that of bulk water:

$$V_H = V_H^{p} n_H \approx V_w^{p} n_H \tag{5.11}$$

Also the number of hydration waters is due to the definition of the hydration number equal to the product:

$$n_H = \nu_H n_{sol} \tag{5.12}$$

Therefore:

$$V_H \approx V_w^{p} \nu_H n_{sol} \tag{5.13}$$

Inserting this into equation 5.9 gives:

$$\alpha_{red} = \frac{V_{sol}^{p} n_{sol}}{V_{tot}} \left(\frac{\alpha_{sol}}{\alpha_{bulk}} - 1 \right) + \frac{V_w^{p} \nu_H n_{sol}}{V_{tot}} \left(\frac{\alpha_H}{\alpha_{bulk}} - 1 \right) \tag{5.14}$$

Since the solute concentration $c_s = n_{sol}/V_{tot}$:

$$\alpha_{red} = c_s \left(V_s^{p} \left(\frac{\alpha_{sol}}{\alpha_{bulk}} - 1 \right) + \nu_H V_w^{p} \left(\frac{\alpha_H}{\alpha_{bulk}} - 1 \right) \right) \tag{5.15}$$

The first term in the outer parenthesis is negative since $\alpha_{sol} \ll \alpha_{bulk}$. The second term is on the other hand positive, since $\alpha_H > \alpha_{bulk}$ [49]. Because the relative difference between the two absorption coefficients in the first (negative) term is larger than in the second, the first term is numerically larger than the second, thus the reduced absorption becomes negative. What should therefore be expected from equation 5.15 is that α_{red} is negative and decreases linearly with solute concentration, because α_{red} is equal to the concentration multiplied by a negative constant.
M. Havenith et al. [49] explains this decrease with the fact that the solute has very low absorption in this frequency regime and adding more solute molecule therefore leaves more "holes" in the spectral density. But they claim to only see linearity at very dilute concentrations, and when the concentration is increased above some limit they see a deviation from linearity: α_{red} begins to decrease faster. This is what is called the "Terahertz effect" among Terahertz spectroscopists. They explain the effect by hydration shell overlap [98]. It can in principle be explained by equation 5.15: If the hydration layers start to overlap, the effective hydration number (in the positive term) will decrease, which means that the negative term dominates even more.
Thus M. Havenith and coworkers have in several publications eg. [49] and [98] calculated the thickness of the hydration shell of different small molecules from the concentration dependence of the sample absorption. More specifically they did so by first determining the volume fraction of hydration water as function of solute concentration and hydration

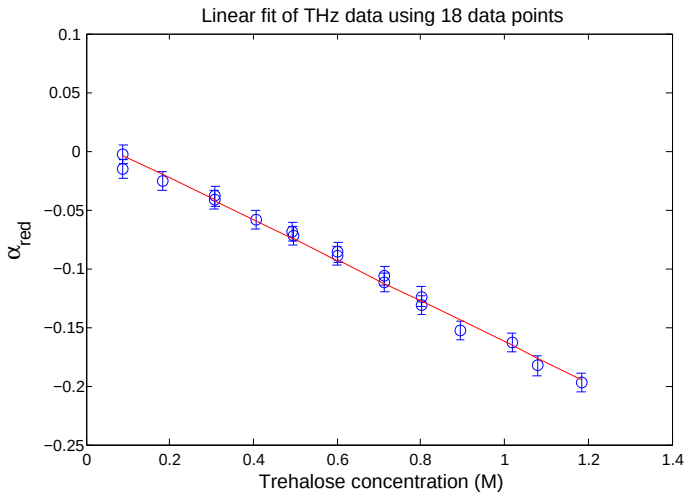

Figure 5.12: *Reduced THz absorption coefficient for trehalose at* $20^{\circ}C$ *from Heyden et al. [49]: Linear fit of all data points.*

layer thickness δR through Monte Carlo simulations that randomly insert solute molecules into water, and also takes into account hydration shell overlap [49]. Then equation 5.7 was fitted to the experimental data, in which 2 parameters: α_H and δR were fitted simultaneously. Therefore it is crucial to the outcome that the simulation is really close to reality. Furthermore the two fitted variables will have some covariance, according to Heyden et al. [49] they can still determine the statistically most likely set of parameters. Their result is that the hydration layers of disaccharides extends further than the first hydration shell: 6.46 ± 0.9 Å for trehalose, and they propose that this is a plausible explanation for their stabilizing effect.

But our relaxation study shows that trehalose self-associates at all concentrations at least down to 75 mM, which means that the assumption made in the Monte Carlo simulation, that the sugar molecules are randomly distributed is wrong. Aggregation of course gives hydration shell overlap, thus hydration shell overlap and therefore also non-linearity should be seen at least down to 75 mM trehalose. But the fraction of overlapping hydration shells increases with concentration and the effect may be too small to detect at low concentrations, so the correlation could seem linear within the error bars in the dilute end.

The reduced THz absorption coefficient for trehalose is plotted in figure 5.12, all data points were fitted to a straight line in this plot, and in fact, all data points except one fall onto a straight line within the error bars given by the authors (0.008) [49]. The fit has though not been forced to go through c=0 as it should for physical reasons. But their data analysis depends on the non-linearity of the data, so the uncertainty or the method might not be as good as required for that kind of analysis.
As one should expect that either the "THz effect" or the aggregation is minimal at the lowest concentrations, a minimal number of the lowest concentrations were also fitted to a straight line (figure 5.13). 3 different concentrations (corresponding to 5 data points) were fitted to a straight line.
The linear fit does seem to indicate what the THz spectroscopists argue: That at low concentrations, the correlation is linear, but at higher concentrations α_{red} begins to decrease

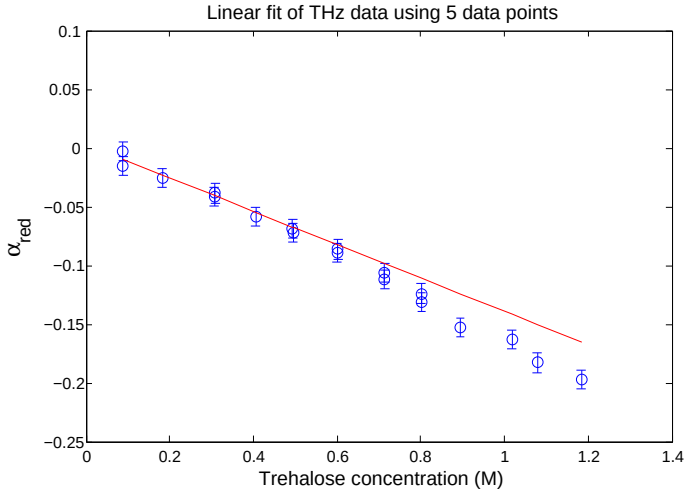

Figure 5.13: *Reduced THz absorption coefficient for trehalose at* $20^{\circ}C$ *from Heyden et al. [49]: Linear fit of the first 5 data points.*

faster. But now the real question is: Can this behavior be explained by aggregation? If this is the case, there will be a small curvature even at the lowest concentrations, so does the data rule out this possibility? In order to test this α_{red}/c was plotted as a function of concentration (fig. 5.14), since according to equation 5.15, this quantity should be constant in the concentration regimes with linearity. But as the figure shows the standard deviations are quite large at low concentrations, and in principle, α_{red}/c could both be constant and decreasing at low concentrations.
The error in α_{red}/c was calculated as:

$$\sigma_{\alpha_{red}/c} = \frac{\sigma_{\alpha_{red}}}{c} \tag{5.16}$$

As in the previous figure, the first 3 concentrations (5 points) were fitted to a straight line in fig. 5.14. This gave a slope different from zero, but with a standard deviation that makes it impossible to tell if the slope is really flat or not: -0.0521 ± 0.2494. But even though the line was only fitted to the first 3 concentrations it follows the trend of most of plot. Thus there are indications that α_{red} is not strictly linear at any concentrations, but perhaps has an increasing curvature as would be expected from increasing aggregation.
What can be said with more certainty is that at the low concentrations the data scatters quite a bit and the error bars are so large (relatively speaking), that it strongly weakens the conclusions made by a fit that depends sensitively on the location of the onset of non-linearity - which is what was done by Heyden et al. [49].

Of course one could argue that the reason why we see trehalose-trehalose interactions is because THz studies are right: There is long range effects on water dynamics. But at a concentration of 75 mM trehalose, the lowest concentration where we see aggregation, the surface-to-surface distance between adjacent trehalose molecules in a close cubic packing model would be 22.8 Å. So if there is hydration shell overlap at this concentration, the hydration shell should be at least 11.4 Å or about 4 water layers, which is significantly larger than the thickness found by THz spectroscopy (6.46 ± 0.9 Å). At 50 mM (where there are also indications of trehalose-trehalose interactions) the water layer would be even 4.9 water molecules. And the fact that trehalose aggregates is also supported by Molecular dynamics studies [77], [76].

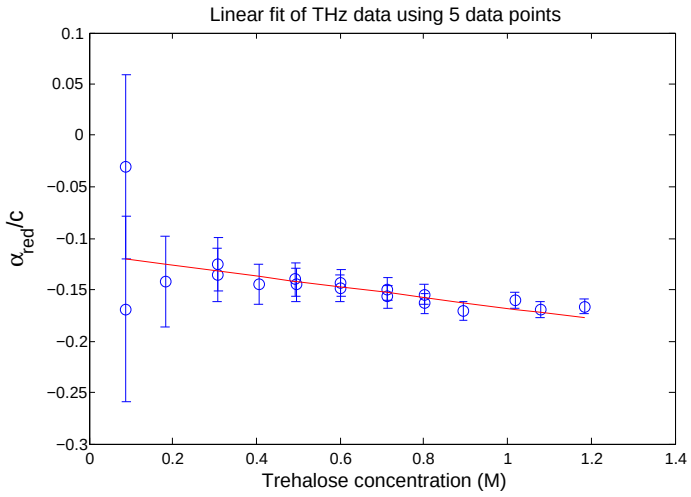

Figure 5.14: *Reduced THz absorption coefficient divided by concentration for trehalose at 20°C from Heyden et al. [49]. The first 5 data points were fitted to a linear function.*

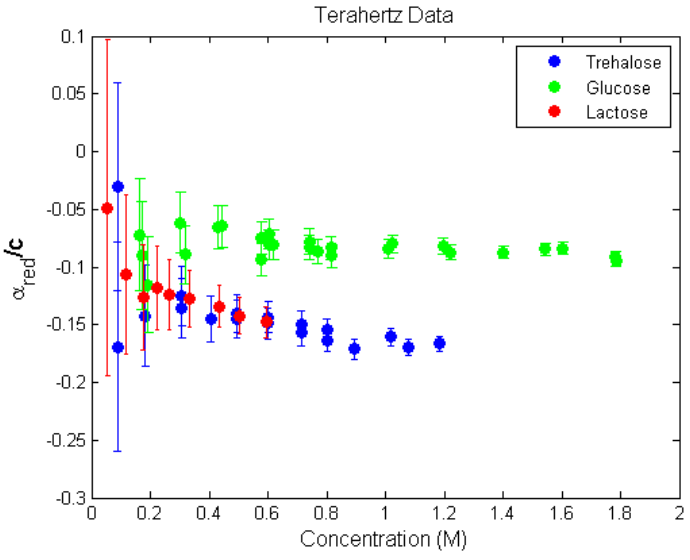

Figure 5.15: *Reduced THz absorption coefficient divided by concentration for saccharides at 20°C from Heyden et al. [49].*

5.6.1 Comparison of THz data with our ^{17}O relaxation data

The following relationship for the reduced ^{17}O relaxation rate was derived in the chapter about ^{17}O relaxation (eq. 4.46):

$$R_{red}N_w = \nu_H \left(\frac{R_{hyd}}{R_{bulk}} - 1 \right) \tag{5.17}$$

Comparing this to the equation for α_{red}/c (stems from equation 5.15):

$$\alpha_{red}/c_s = V_s^p \left(\frac{\alpha_{sol}}{\alpha_{bulk}} - 1 \right) + \nu_H V_H^p \left(\frac{\alpha_H}{\alpha_{bulk}} - 1 \right) \tag{5.18}$$

It becomes clear that the last term in equation 5.18 is very similar to eq. 5.17, and the equation can be rearranged to:

$$\nu_H \left(\frac{\alpha_H}{\alpha_{bulk}} - 1 \right) = \frac{\frac{\alpha_{red}}{c_s} - V_s^p \left(\frac{\alpha_{sol}}{\alpha_{bulk}} - 1 \right)}{V_H^p} \tag{5.19}$$

- Recall that $\alpha_H > \alpha_{bulk}$ so the result is positive.
The standard deviation was set to:

$$\sigma_{prod} = \frac{1}{V_H^p} \sigma_{\alpha_{red}/c} \tag{5.20}$$

- this is an optimistic guess of the error, since it was assumed that the error in all the constants on the right side of the equation is negligible.

Assuming that $V_H^p = V_w^p$ (partial molar volume of pure bulk water), and that all variables on the right side of the equation except for α_{red}/c can be assumed constant (shown earlier for V_s^p), the right side of the equation can easily be calculated from the values for α_{sol} and α_{bulk} in the paper by Heyden et al. [49], the result is shown in figure 5.16.

Further assuming that R_{hyd}/R_{bulk} and α_H/α_{bulk} are constant as a function of concentration, which is most likely true at low concentrations, but not at higher concentrations where a large fraction of hydration shell overlap changes the average mobility of the hydration water, means that the left side of eq. 5.19 should have a similar concentration dependence as the right side of equation 5.17. But comparison of figure 5.16 with the ^{17}O data in figure 4.40 shows that this is not the case. $\nu_H \left(\frac{R_{hyd}}{R_{bulk}} - 1 \right)$ increases with trehalose concentration, whereas $\nu_H(\alpha_H/\alpha_{bulk} - 1)$ decreases with concentration.

Taking a closer look at figure 5.16 though reveals that it does not make sense to put a lot of effort into interpreting the THz data, the error bars are extremely large, the median of the relative standard deviation of $\nu_H(\alpha_H/\alpha_{bulk} - 1)$ is 47%... This stresses the point made earlier that the conclusions that can be made from the THz data should perhaps be taken with care, since $\nu_H(\alpha_H/\alpha_{bulk} - 1)$ is exactly what must be fitted to get the hydration shell thickness.

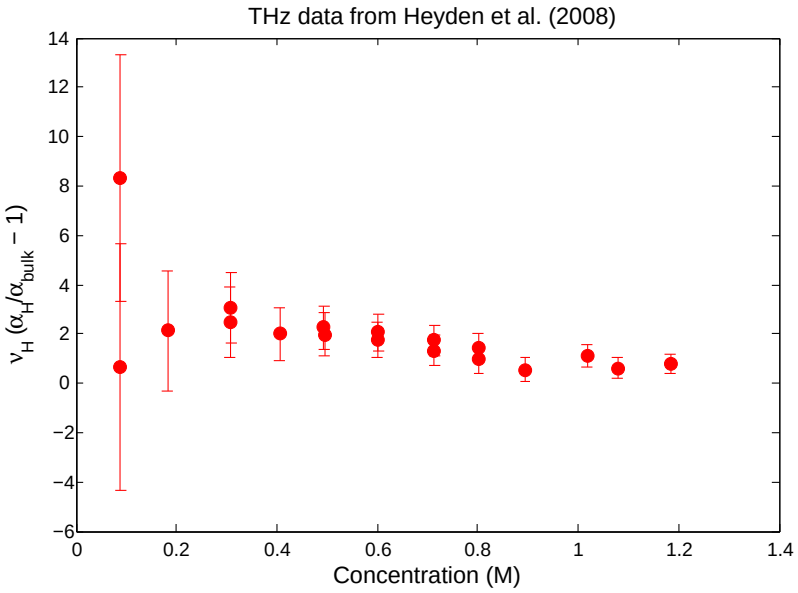

Figure 5.16: *Calculated $\nu_H(\alpha_H/\alpha_{bulk} - 1)$ for trehalose-water samples from THz data from Heyden et al. [49].*

The study by Heyden et al. [49] furthermore shows a clear difference in the concentration dependence of THz absorption of disaccharide-water samples (trehalose and lactose) compared to monosaccharide-water samples (glucose). They calculated a larger hydration shell thickness for di- than for mono-saccharides. The authors claim that the reason for this is the difference between the number of water-carbohydrate hydrogen-bonds of the two sugar classes, since they can get the absorption data to fall on the same curve when the sugar concentration is multiplied by this number. They think this is the explanation for the larger hydration shell thickness and stabilizing effect of disaccharides compared to monosaccharides. But the MD study by Sapir et al. (2011) [77] indicates that when trehalose self-associates, it often has two interaction sites and from their model it seems there is often one on each ring, therefore the resulting disaccharide "dimer" looses a significantly larger amount and fraction of hydration shell than if a mono-saccharide self-associates, see fig. 5.17.

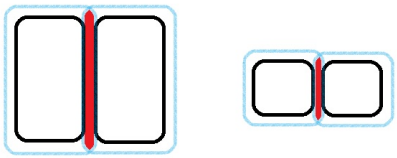

Figure 5.17: *Simplified pictures comparing the hydration shell loss when disaccharides associate (left) to when monosaccharides associate (right). The disaccharides loose a larger fraction of their hydration shell, if there is one hydrogen bonding site on each sugar ring, so it ends up looking (simplified) like the figure on the left side.*

This was not accounted for in the Monte-Carlo simulations done by Heyden et al. [49], that gave the V_H dependence on hydration shell thickness and concentration used in the data fitting, these simulations just randomly insert sugar molecules into the solution.

Furthermore the large difference in the amount of lost hydration shell upon self-association between di- and mono-saccharides might be able to explain why Heyden et al. [49] found that glucose has a hydration shell thickness of only a bit more than one water layer (3.71 Å) whereas the thickness for trehalose and lactose is almost twice as large (6.46 and 5.69 Å). The model by Heyden et al. [49] will of course give a much too large hydration shell thickness for disaccharides, because the hydration shell thickness must be increased above 1 water layer to account for the too small decrease in hydration number with concentration, that is used in their model.
This explanation is also more in line with the results from NMR relaxation, that show no significant difference between the dynamic perturbation factor of glucose and trehalose, see figure 5.7.

Chapter 6

Conclusion

The longitudinal relaxation rates and rotational correlation times of both trehalose and water in trehalose-water solutions with varying concentrations and at varying temperatures, were determined with NMR relaxation.
The rotational correlation time of trehalose showed a significant increase with concentration at least down to 75 mM trehalose. This increase could neither be explained by hydrodynamic interactions or conformational changes, but must instead be a strong indication of trehalose self-association at least down to 75 mM trehalose, a conclusion that is also supported by different Molecular Dynamics simulations [77],[76].
This made the interpretation of the concentration dependence of the rotational correlation time of water very complicated. But at concentrations below 250 mM trehalose self-association was so limited, that R_{red} was (approximatly) linearly dependent on $1/N_w$ and the dynamic perturbation factor of water could be taken to be constant. Thus it was possible to determine the temperature dependence of the dynamic perturbation factor in this concentration range. Interestingly it showed a maximum around 250-260 K, similar to what has been found for hydrophobic solutes [80]. This was shown to be the reason for the maximum in the effective hydrodynamic volume of trehalose, deduced from the trehalose correlation time.
The dynamic perturbation factor in the hydration layer of trehalose was determined to be 1.65 at 20°C, which is comparable to many other small molecules including other sugars. This means that trehalose monomers do not have extraordinary hydration characteristics. But above around 0.25 M the dynamic perturbation factor of water increases slowly with trehalose concentration, and there seems to be a limit around 1 M trehalose where both the dynamic perturbation factor of water and the rotational correlation time of trehalose/ the effective viscosity begins to increase more steeply. Lerbret et al. (2005) [91] found that the hydrogen bond network of trehalose also becomes more strongly destructured above this concentration. Furthermore the results of the MD study by Sapir et al. (2011) [77] gave indications that the growth of infinite clusters begins at 1.1 M trehalose. Thus one could speculate that the observed change in water mobility is caused by the formation of more extended clusters around 1 M.
Returning to the many theories on the reasons for the bioprotective role of trehalose, it becomes clear that most of the studies on this topic most likely should be reinterpreted with the knowledge that trehalose-water solutions are not homogeneous. But one could speculate, that since trehalose monomers were shown not to have extraordinary effects on water dynamics, the effects of trehalose are related to its tendency to self-associate.

Bibliography

[1] N.K. Jain and I. Roy (2009), *Protein Science*, Vol. 18, 24-36. Review: Effect of trehalose on protein structure.

[2] A.D. Elbein, Y.T. Pan, I. Pastuszak and D. Carroll (2003), *Glycobiology*, Vol. 13, no. 4, 17R-27R. Review: New insights on trehalose: a multifunctional molecule.

[3] www.bmrb.wisc.edu

[4] G.M. Gadd, K. Chalmers and R.H. Reed (1987), *FEMS Microbiol. Lett.*, 48, 249-254. The role of trehalose in dehydration resistance of *Saccharomyces cerevisiae*.

[5] A. Van Laere (1989), *FEMS Microbiol. Rev.*, 63, 3, 201-210. Trehalose, reserve and/or stress metabolite?

[6] A.C. Leopold, (1986), *Cornell University Press*, Ithaca, NY, 1-377. Membranes, metabolism, and dry organisms.

[7] B. Kempf, E. Bremer, (1998), *Arch Microbiol* 170, 319-330. Uptake and synthesis of compatible solutes as microbial stress responses to high-osmolality environments.

[8] J. Carpinelli, R. Kraemer, E. Agosin (2006), *Appl Environ Microbiol* 72, 1949-1955. Metabolic engineering of Corynebacterium glutamicum for trehalose over production: role of the TreYZ trehalose biosynthetic pathway.

[9] T. Duong, R. Barrangou, WM. Russell, TR. Klaenhammer (2006), *Appl Environ Microbiol* 72, 1218-1225. Characterisation of the tre locus and analysis of trehalose cryoprotection in Lactobacillus acidophilus NCFM.

[10] H.N. Murphy, G.R. Stewart, V.V. Mischenko, A.S. Apt, R. Harris, M.S. McAlister, P.C. Driscoll, D.B. Young, B.D. Robertson, (2005). *J Biol Chem* 280, 14524-14529. The OtsAB pathway is essential for trehalose biosynthesis in Mycobacterium tuberculosis.

[11] V. Rao, F. Gao, B. Chen, W.R. Jacobs, M.S. Glickman. (2006). *J Clin Invest* 116, 1660-1667. Trans-cyclopropanation of mycolic acids on trehalose dimycolate suppresses Mycobacterium tuberculosis- induced inflammation and virulence.

[12] F. Rolland, B. Moore and J. Sheen (2002). *Plant Cell* 14, s185-s205. Sugar sensing and signaling in plants.

[13] P.J. Eastmond, I.A. Graham (2003). *J Exp Bot* 54, 533-537. Is trehalose-6-phosphate a regulator of sugar metabolism in plants?

[14] J. H. Crowe, L. M. Crowe, D. Chapman (1984), *Science*, New Series, Vol. 223, No. 4637, 701-703. Preservation of Membranes in Anhydrobiotic Organisms: The Role of Trehalose.

[15] S.B. Leslie, E. Israeli, B. Lighthart, J.H. Crowe, and L.M. Crowe, (1995). *Applied and environmental microbiology* , Vol. 61, No. 10, p. 3592-3597. Trehalose and Sucrose Protect Both Membranes and Proteins in Intact Bacteria during Drying

[16] T. Hottiger, C. de Virgilio, M.N. Hall, T. Boller, A. Wiemken. (1994) *Eur J Biochem* 219: 187-193. The role of trehalose synthesis for the acquisition of thermotolerance in yeast. II. Physiological concentrations of trehalose increase the thermal stability of proteins in vitro.

[17] M. Tanaka, Y. Michida, S. Niu, T. Ikeda, N.R. Jana, H. Doi, M. Kurosawa, M. Nekooki, N. Nukina (2004), *Nat. Med.* 10, 148-154. Trehalose alleviates polyglutamine-mediated pathology in a mouse model of Huntington's disease.

[18] J.K. Kaushik and R. Bhat (2003), *Journ. Biol. Chem.*, Vol. 278, No. 29, 26458-26465. Why is trehalose an exceptional protein stabilizer?

[19] C.A. Angell, (1995) *Science*, New Series, Vol. 267, No. 5206, 1924-1935. Formation of glasses from liquids and biopolymers.

[20] J.L. Green and C.A. Angell (1989), *J. Phys. Chem.*, 93, 2880-2882. Phase relations and vitrification in saccharide-water solutions and the trehalose anomaly.

[21] J.H. Crowe, J.F. Carpenter, L.M. Crowe, (1998), *Annu. Rev. Physiol.*, 60, 73-103. The role of vitrification in anhydrobiosis.

[22] D. W. Bolen and Ilia V. Baskakov (2001), *J. Mol. Biol.* 310, 955-963. The Osmophobic Effect: Natural Selection of a Thermodynamic Force in Protein Folding

[23] P.S. Belton and A.M. Gil (1994), *Biopolymers*, Vol. 34, 957-961. IR and Raman spectroscopic studies of the interaction of trehalose with hen egg white lysozyme.

[24] M. Sola-Penna, and J.R. Meyer-Fernandes (1998), *Archives of biochemistry and biophysics*, Vol. 360, No. 1, December 1, pp. 10-14. Stabilization against Thermal Inactivation Promoted by Sugars on Enzyme Structure and Function: Why Is Trehalose More Effective Than Other Sugars?

[25] M. Paolantoni, L. Comez, M. E. Gallina, P. Sassi, F. Scarponi, D. Fioretto, and A. Morresi (2009), *J. Phys. Chem. B*, 113, 7874-7878. Light Scattering Spectra of Water in Trehalose Aqueous Solutions: Evidence for Two Different Solvent Relaxation Processes.

[26] R. Brown (1828), *Edinb. Phil. J.* 5, 358.

[27] A. Einstein (1956), Investigations on the Theory of Brownian Movement, Dover, New York, NY.

[28] G.G. Stokes (1851), *Proc. Camb. Philos. Soc.* 9, 8-106. On the Effect of the Internal Friction of Fluid on the Motion of Pendulums

[29] A. Einstein (1906), *Ann Physik* 19, 289-306. A new determination of molecular dimensions.

[30] R.J. Hunter (2001), Foundations of colloid science, Second Edition, Oxford University Press.

[31] K.L. Ngai (2011). Relaxation and Diffusion in Complex Systems. Springer.

[32] V. A. Bloomfield (2000). On-Line Biophysics Textbook, Volume: Separations and Hydrodynamics, Todd M. Schuster, editor. Chapter 1: Survey of Biomolecular Hydrodynamics.

[33] physchem.ox.ac.uk/~hill/tutorials/nm3_tutorial/nucspin/index.html

[34] www2.chemistry.msu.edu/faculty/reusch/VirtTxtJml/Spectrpy/nmr/nmr1.htm

[35] www.mikepuddephat.com/Page/1603/principles-of-magnetic-resonance-imaging

[36] B. Halle, V. P. Denisov, and K. Venu (1999). *Biological Magnetic Resonance*, Volume 17: Structure Computation and Dynamics in Protein NMR. Kluwer Academic / Plenum Publishers, New York. Multinuclear Relaxation Dispersion Studies of Protein Hydration

[37] H.J. Koch and R.S. Stuart (1977), *Carbohydr. Res.*, 59, c1-c6. A novel method for specific labelling of carbohydrates with deuterium by catalytic exchange.

[38] F. Balza and A.S. Perlin (1982), *Carbohydr. Res*, 107, 270-278, Some stereochemical characteristics of C-1H-C-2H exchange-reactions with Raney nickel catalyst in deuterium oxide.

[39] F. Balza, N. Cyr, G.K. Hamer, A.S. Perlin (1977), *Carbohydr. Res.*, 59, C7-C11. Applications of a catalytic, hydrogen-deuterium exchange in ^{13}C-n.m.r. spectroscopy.

[40] E.A. Cioffi, R.H. Bell, B. Le (2005). *Tetrahedron-assymmetry*, Vol. 16, 2, 471-495. Microwave assisted C-H bond activation using a commercial microwave oven for rapid deuterium exchange labelling (C-H -> C-D) in carbohydrates.

[41] Candy 101: http://www.baking911.com/

[42] Z. Chi, J. Liu and W. Zhang (2001), *Enzyme and Microbial Technology*, 28, 240-245, Trehalose accumulation from soluble starch by *Saccharomycopsis fibuligera* sdu.

[43] Z- Chi, J.-M. Wang, Z.-M. Chi, F. Ye (2010), *J. Ind. Microbiol. Biotechnol.*, 37, 19-25. Trehalose accumulation from corn stach by *Saccharomycopsis fibuligera* A11 during 2-l fermentation and trehalose purification.

[44] N. Asano, K. Matsui, S. Takeda, Y. Kono, *Carbohydrate Research*, 243, 1993, 71-78. Microbial preparation of α,α'-[1,1'-^{13}C] trehalose.

[45] Preparation of Chelex: http://structbio.vanderbilt.edu/chazin/wisdom/labpro/chelex.html

[46] B. Bose-Basu, J. Zajicek, G. Bondo, S. Zhao, M. Kubsch, I. Carmichael, and A. S. Serianni (2000), *Journal of Magnetic Resonance* 144, 207-216. Deuterium Nuclear Spin-Lattice Relaxation Times and Quadrupolar Coupling Constants in Isotopically Labeled Saccharides

[47] R. Ludwig, F. Weinhold, and T. C. Farrar (1995), *J. Chem. Phys.*, Vol. 103, No. 16, 6941-6950. Experimental and theoretical determination of the temperature dependence of deuteron and oxygen quadrupole coupling constants of liquid water.

[48] J. Qvist, H. Schober and B. Halle (2011), *J. Chem. Phys.*, 134, 144508-1 - 144508-20, Structural dynamics of supercooled water from quasielastic neutron scattering and molecular simulations

[49] M. Heyden, E. Bründermann, U. Heugen, G. Niehues, D.M. Leitner and M. Havenith (2008), *J.Am.Chem.Soc.*, 130, 5773-5779. Long-range influence of carbohydrates on the solvation dynamics of water - Answers from Terahertz absorption measurements and molecular modeling simulations.

[50] P.K. Banipal, T.S. Banipal, B.S. Lark and J.C. Ahluwalia (1997) *J.Chem. Soc., Faraday Trans.*, 93 (1), 81-87. Partial molar heat capacities and volumes of some mono-, di- and tri-saccharides in water at 298.15, 308.15 and 318.15 K.

[51] T.A. Schmedake and L.E. Welch (1996) *Journ. of Chemical Education*, Vol. 73, No. 11. The quantitative analysis of an analgesic tablet.

[52] NMR tutorial: http://chem.ch.huji.ac.il/nmr/techniques/1d/1d.html

[53] R. Ludwig (1995), *Chemical Physics* 195 329-337, NMR relaxation studies in water-alcohol mixtures: the water-rich region.

[54] A. Bagno, G. Lovato, G. Scorrano and J.W. Wijnen (1993). *J. Phys. Chem.*, 97, 4601-4607. Solvation of nonelectrolytes in water probed by ^{17}O NMR relaxation of the solvent.

[55] B. Halle and V.P. Denisov (2001). *Academic Press*. Magnetic Relaxation Dispersion studies of biomolecular solutions.

[56] P. J. Rossky, M. Karplus (1979), *J. Am. Chem. Soc.*, 101, 1913-1937. Solvation - Molecular-Dynamics study of a dipeptide in water.

[57] I.I. Vaisman, F. K. Brown, A. Tropsha (1994), *J. Phys. Chem.*, 98, 5559-5564. Distance dependence of water-structure around model solutes.

[58] D. Paschek (2004). *J. Chem. Phys.*, 120, 22, 10605-10617. Heat capacity effects associated with the hydrophobic hydration and interaction of simple solutes: A detailed structural and energetical analysis based on molecular dynamics simulations.

[59] D. B. Bechtold, G. Liu, H. W. Dodgen, and J.P. Hunt (1978). *J Phys Chem*, **82**, 333. An Oxygen-I 7 Nuclear Magnetic Resonance Study of the Aquo Nickel(I1) Sulfate System.

[60] G. Batta, K. E. Kövér, J. Gervay, Miklós Hornyá and G. M. Roberts (1997). *J. Am. Chem. Soc.*, 119, 1336-1345. Temperature Dependence of Molecular Conformation, Dynamics, and Chemical Shift Anisotropy of α,α-Trehalose in D_2O by NMR Relaxation.

[61] M.P. Longinotti and H.R. Corti (2008). *J. Phys. Chem. Ref. Data*, Vol. 37, No. 3, Viscosity of concentrated sucrose and trehalose aqueous solutions including the supercooled regime.

[62] R. Fraczkiewicz, and W. Braun (1998). *J. Comp. Chem.*, 19, 319-333. Exact and Efficient Analytical Calculation of the Accessible Surface Areas and Their Gradients for Macromolecules

[63] T. Chen, A. Fowler and M. Toner (2000). *Cryobiology* 40, 277-282. Literature review: Supplemented Phase Diagram of the Trehalose-Water Binary Mixture.

[64] T. Uchida, M. Nagayama and K. Gohara (2009). *Journal of Crystal Growth*, 311, 4747-4752. Trehalose solution viscosity at low temperatures measured by dynamic light scattering method: Trehalose depresses molecular transportation for ice crystal growth

[65] J. Keeler (2010), *Wiley*, 2nd edition, Understanding NMR Spectroscopy.

[66] D.P. Miller, J.J. De Pablo and H.Corti (1997), *Pharm.Res.*, Vol 14, No 5. Thermophysical properties of trehalose and its concentrated aqueous solutions.

[67] Pictures from Wikipedia.org

[68] M.E. Elias, A.M. Elias (1999). *Journal of Molecular Liquids*, 83, 303-310, Trehalose + water fragile system: properties and glass transition.

[69] S. Magazú P. Migliardo, A.M. Musolino and M.T. Sciortino (1997). *J.Phys.Chem.*, 2348-2351, α,α-Trehalose-Water solutions. 1. Hydration phenomena and anomalities in the acoustic properties.

[70] S. Magazù, G. Maisano, P. Migliardo, and V. Villari, (1999), *J. Chem. Phys.* 111, 9086. Experimental simulation of macromolecules in trehalose aqueous solutions: A photon correlation spectroscopy study

[71] D. P. Miller, J. J. de Pablo, and H. R. Corti, *J. Phys. Chem. B* (1999), 103, 10243. Viscosity and glass transition temperature of aqueous mixtures of trehalose with borax and sodium chloride

[72] M. Rampp, C. Buttersack, and H. D. Lüdemann (2000). *Carbohydr. Res.* 328, 561. c,T-Dependence of the viscosity and the self-diffusion coefficients in some aqueous carbohydrate solutions

[73] C. Branca, S. Magazú, G. Maisano, P. Migliardo, V. Villari and A.P. Sokolov (1999). *J. Phys.: Condens. Matter*, 11, 3823-3832. The fragile character and structure-breaker role of trehalose: viscosity and Raman scattering findings

[74] B. Halle and M. Davidovic (2003), *PNAS*, 21, 12135-12140, Biomolecular hydration: From water dynamics to hydrodynamics.

[75] T. Uchida, M. Nagayama, T. Shibayama, K. Gohara (2007). *Journal of Crystal Growth*, 299, 125-135, Morphological investigations of disaccharide molecules for growth inhibition of ice crystals.

[76] A. Lerbret, P. Bordat, F. Affouard, M. Descamps, and F. Migliardo (2005). *J. Phys. Chem. B*, 109, 11046-11057, How Homogeneous Are the Trehalose, Maltose, and Sucrose Water Solutions? An Insight from Molecular Dynamics Simulations.

[77] L. Sapir and D. Harries (2011), *J. Phys. Chem. B*, 115, 624-634, Linking Trehalose Self-Association with Binary Aqueous Solution Equation of State

[78] Valeria Molinero, Tahir Çağin, William A. Goddard III (2003). *Chemical Physics Letters* 377, 469-474. Sugar, water and free volume networks in concentrated sucrose solutions.

[79] Milton T. Sonoda and Munir S. Skaf (2007), *J. Phys. Chem. B*, 111, 11948-11956. Carbohydrate Clustering in Aqueous Solutions and the Dynamics of Confined Water.

[80] J. Qvist and B. Halle (2008), *JACS*, Thermal signature of hydrophobic hydration dynamics, 130, 10345-10353.

[81] H. Uedaira, M. Ikura, H. Uedaira (1989), *Bull. Chem. Soc. Jpn.*, 62, 1-4. Natural-abundance Oxygen-17 magnetic relaxation in aqueous solutions of carbohydrates.

[82] H. Uedaira, M. Ishimura, S. Tsuda and H. Uedaira (1990), *Bull. Chem. Soc. Jpn.*, 63, 3376-3379. Hydration of oligosaccharides.

[83] R.B. Jones, (1989), *Physica A*, 157, 752-768. Rotational diffusion of a tracer colloid particle.

[84] S. Dixit, J. Crain, W. C. K. Poon, J. L. Finney and A. K. Soper. (2002) *Nature*, Vol. 416, 829-832. Molecular segregation observed in a concentrated alcohol-water solution

[85] Y. Ishihara, S. Okouchi, H.Uedaira, (1997) *J.Chem.Soc. Faraday Trans.*, 93, 3337-3342. Dynamics of hydration of alcohols and diols in aqueous solutions

[86] S. Okouchi, K. Tsuchida, S. Yoshida, Y. Ishihara, S. Ikeda, H. Uedaira (2005), *Bull. Chem. Soc. Jpn.*, 78, 424-429.

[87] A. Shimizu, K. Fumino, K. Yukiyasu, Y. Taniguchi, (2000), *J. Mol. Liq.*, 85, 269-278.

[88] M. Ishimura, H. Uedaira, (1990) *Bull. Chem. Soc. Jpn.*, 63, 1-5.

[89] M. Mathlouthi, C. Luu, A.M. Meefroy-Biget and D.V. Luu, (1980) *Carbohydrate Research*, 81, 213-223. Laser-Raman study of solute-solvent interactions in aqueous solutions of D-fructose, D-glucose, and sucrose.

[90] C. Branca, S. Maccarrone, S. Magazù, and G. Maisano, (2005). *Journ. Chem. Phys.*, 122, 174513-174513-6, . Tetrahedral order in homologous disaccharide-water mixtures.

[91] A. Lerbret, P. Bordat, F. Affouard, Y. Guinet, A. Hédoux, L. Paccou, D. Prévost and M. Descamps. (2005), *Carbohydrate Research*, 340 881-887. Influence of homologous disaccharides on the hydrogen-bond network of water: complementary Raman scattering experiments and molecular dynamics simulations.

[92] C. Branca, S. Magazu, G. Maisano and P. Migliardo, (1999) *J. Chem. Phys.*, 111, 1, 281-287, Anomalous cryoprotective effectiveness of trehalose: Raman scattering evidences.

[93] C. Branca, S. Magazu, G. Maisano and P. Migliardo, (1999) *J. Phys. Chem. B*, 103, 1347-1353. α,α- Trehalose-water solutions. 3. Vibrational dynamics studies by inelastic light scattering.

[94] S. Magazu V. Villari, P. Migliardo, G. Maisano, and M. T. F. Telling, (2001) *J. Phys. Chem. B* , 105, 1851-1855. Diffusive Dynamics of Water in the Presence of Homologous Disaccharides: A Comparative Study by Quasi Elastic Neutron Scattering. IV.

[95] A. Lerbret, F. Affouard, P. Bordat , Y. Hédoux A., Guinet, M. Descamps (2011), *Journ. Non-crystalline solids*. 357, 695-699. Slowing down of water dynamics in disaccharide aqueous solution.

[96] G. Stirnemann, F. Sterpone, and D. Laage. (2011), *J. Phys. Chem. B*., 115, 3254-3262. Dynamics of Water in Concentrated Solutions of Amphiphiles: Key Roles of Local Structure and Aggregation.

[97] C. Baraguey, D. Mertens, and A. Dölle, (2002) *J. Phys. Chem. B*, 106, 6331-6337 Anisotropic Reorientation and Intermolecular Interactions of Sucrose Molecules in Aqueous Solution. A Temperature and Concentration-Dependent 13C NMR Relaxation Study

[98] U. Heugen, G. Schwaab, E. Bründermann, M. Heyden, X. Yu, D.M. Leitner, and M. Havenith, (2006), *PNAS*, 103, 33, 12301-12306. Solute-induced retardation of water dynamics probed directly by terahertz spectroscopy.

[99] D.L. Sidebottom and T.D. Tran (2010), *Physical Review E*, 82, 051904-1 - 051904-7, Universal patterns of equilibrium cluster growth in aqueous sugars observed by dynamic light scattering.

Appendix A

Data from emulsified trehalose-water solutions

A.1 Deuterium relaxation

T	c (mM)	T_1 (ms)	No of measurements	Relative σ of T_1
236.302 K	249.269	8.677 8.924	2	0.0198
	199.415	8.606 8.685	2	0.0065
	149.561	8.994 9.061	2	0.0052
	99.708	8.232 8.020	2	0.0184
238.204 K	249.269	7.768 7.782 7.809	3	0.0027
	199.415	7.632 7.669	2	0.0034
	149.561	7.709 7.661	2	0.0044
	99.708	7.283 7.253	2	0.0029
239.904 K	249.269	6.949 7.036 6.984 6.961	4	0.0055
	199.415	6.734 6.794 6.789	3	0.0049
	149.561	6.777	1	-
	99.708	6.507 6.653 6.691	3	0.0147
243.121 K	249.269	6.289	1	-
	199.415	6.167	1	-
	149.561	6.067	1	-
	99.708	6.021	1	-
	49.854	6.182	1	-
248.110 K	249.269	5.729	1	-
	199.415	5.716	1	-
	149.561	5.687	1	-
	99.708	5.706	1	-
	49.854	5.532 5.600	2	0.0086
253.223 K	249.269	5.864	1	-
	199.415	5.920	1	-
	149.561	5.990 5.912	2	0.0093
	99.708	5.963	1	-
	49.854	6.182	1	-
263.025 K	249.269	7.272	1	-
	199.415	7.510	1	-
	149.561	7.725	1	-
	99.708	7.973	1	-
	49.854	8.292	1	-
273.176 K	249.269	10.09	1	-
	199.415	10.66	1	-

T	c	T_1 (ms)	No of measurements	Relative σ of T_1
293.181 K	249.269	19.71	1	-
	199.415	20.65	1	-
	149.561	21.43 21.65	2	0.0072
	99.708	22.54	1	-
	49.854	23.61	1	-

A.2 ^{17}O relaxation

T	c (mM)	T_1 (ms)	No of measurements	Relative σ of T_1
236.302 K	249.269	0.2621 0.2554	2	0.0183
	199.415	0.2689 0.2657 0.2701	3	0.0085
	149.561	0.2751 0.2781 0.2858	3	0.0197
	99.708	0.2793 0.2822 0.2822 0.2839 0.2714	5	0.0178
	0	0.3007 0.2887 0.2719	3	0.0504
238.204 K	249.269	0.3234	1	-
	199.415	0.336 0.3383	2	0.0067
	149.561	0.3447 0.3419	2	0.0161
	99.708	0.3445 0.3288	2	0.0148
	49.854	0.3494	1	-
	0	0.3461	1	-
239.904 K	249.269	0.3954 0.3931 0.3966	3	0.0045
	199.415	0.4122 0.4114 0.4078	3	0.0057
	149.561	0.4263 0.4370	2	0.0175
	99.708	0.4260 0.4168 0.4200	3	0.0111
	0	0.4522 0.4443 0.4434	3	0.0108
243.121 K	249.269	0.5142	1	-
	199.415	0.5273	1	-
	149.561	0.5640	1	-
	99.708	0.5638	1	-
	49.854	0.5845 0.5942	2	0.0116
	0	0.5920 0.5971	2	0.0061
248.110 K	249.269	0.7635	1	-
	199.415	0.8009	1	-
	149.561	0.8261	1	-
	99.708	0.8546	1	-
	49.854	0.9076	1	-
	0	0.908	1	-
253.223 K	249.269	1.061	1	-
	199.415	1.115	1	-
	149.561	1.154 1.153	2	6.1301e-004
	99.708	1.202 1.202	2	0
	49.854	1.259	1	-
	0	1.288 1.304	2	0.0087
263.025 K	249.269	1.826	1	-
	199.415	1.885	1	-
	149.561	1.933	1	-
	99.708	2.017	1	-
	49.854	2.076	1	-
	0	2.137	1	-
273.176 K	249.269	2.845	1	-
	199.415	2.89	1	-
	149.561	2.981	1	-
	99.708	3.123	1	-
	49.854	3.219	1	-
	0	3.352	1	-

T	c (mM)	T_1 (ms)	No of measurements	Relative σ of T_1
283.267 K	249.269	4.062	1	-
	199.415	4.189	1	-
	149.561	4.277	1	-
	99.708	4.45	1	-
	49.854	4.606	1	-
293.181 K	249.269	5.470	1	-
	199.415	5.650	1	-
	149.561	5.819	1	-
	99.708	6.011	1	-
	49.854	6.103	1	-

Appendix B

Data from trehalose-water solutions at 20°C

Trehalose concentration (M)	O^{17} R_1 (s^{-1})	Deuterium R_1 (s^{-1})
0	158.5791	-
0.0253	160.1281	42.4646
0.0460	161.9171	42.9074
0.0758	164.6633	44.0451
0.0921	166.3063	45.0106
0.1517	172.1170	46.4188
0.1842	174.9475	48.6121
0.2762	186.0119	52.9157
0.3683	197.4724	57.2574
0.4604	210.2165	62.2161
0.5525	225.7336	68.0735
0.6445	241.1382	74.0466
0.7366	259.0003	81.2480
1.0112	311.8665	100.6340
1.3146	432.1521	129.5169
1.4732	540.5405	145.0326